ISSN 0972 - 2955

# RATIONAL DISCOURSE

Vol. 31 No.1 December 2025

**A Multidisciplinary Journal of Current Research and Studies**

Mar Thoma College, Tiruvalla
Kerala - 689103, India

# Rational Discourse

*A Multidisciplinary Refereed Journal of Current Research and Studies*

December 2025

© Mar Thoma College, Tiruvalla

ISSN 0972 – 2955

*Edited by*
Dr. Remi Cherian George
Chief Editor of Rational Discourse on behalf of
Mar Thoma College, Tiruvalla.

*Typesetting and Printing:*
Mar Thoma Press, Tiruvalla.
Mob: 9447641191

***Chief Editor***

Dr. Remi Cherian George
Associate Professor
Department of English
Mar Thoma College
Tiruvalla - 689103
Email: remi@mtct.ac.in

***Associate Editor***

Dr. Mathew Sam
Assistant Professor
Department of History
Mar Thoma College, Tiruvalla

***Editorial Board***

Dr. Noble P. Abraham
Assistant Professor
Department of Physics
Mar Thoma College, Tiruvalla

Dr. Liji Samuel
Assistant Professor
Department of Economics
Mar Thoma College, Tiruvalla

Dr. Reenamole G.
Assistant Professor
Department of Chemistry
Mar Thoma College, Tiruvalla

***Editorial Advisors***

Dr. Mathew Varkey T.K.
Principal
Mar Thoma College
Tiruvalla, Kerala.

Dr. Jayakrishnan R.
Professor and Head
Department of Physics
University of Kerala
Kariavattom Campus
Thiruvananthapuram, Kerala.

Dr. Raji B. Nair
Department of English
Sree Sankaracharya
University of Sanskrit
P.O. Kalady
Ernakulam, Kerala

Dr. Rayson K. Alex
Associate Professor
Department of Humanities
and Social Sciences
Birla Institute of Technology
and Science, Pilani, Goa, India.

Dr. Sooraj K.
Assistant Professor
Department of Chemistry
Indian Institute of Technology
Madras, Tamil Nadu, India.

**Rational Discourse**
National Reg. No. 2493/96
ISSN: 0972-2955

**RATIONAL DISCOURSE** is a peer-reviewed, multidisciplinary research journal of Mar Thoma College, Tiruvalla, which has been re-accredited with an A grade by NAAC. Original research articles adhering to the latest APA guidelines are invited from faculty members and research scholars of university departments and affiliated colleges.

# Contents

# Chemical and Biosynthetic Perspectives on the Bioactive Constituents of Ginger *(Zingiber officinale)*

**[1]Rani R. Nair**

[1]Associate Professor, Post Graduate and Research Department of Chemistry, Bishop Abraham Memorial College, Thuruthicad, Kerala, India. E-mail: drrani2001@gmail.com.

**Abstract:** Ginger *(Zingiber officinale Roscoe)*, a widely used medicinal plant belonging to the family Zingiberaceae, has attracted significant scientific interest due to its diverse bioactive constituents and therapeutic potential. This review provides a comprehensive overview of the major phytochemicals present in ginger, particularly gingerols, shogaols, zerumbone, and zingiberene, emphasizing their biosynthesis, total synthesis, and applications as synthons in organic chemistry. The biosynthetic pathways of key compounds such as [6]-gingerol are discussed, highlighting both classical and enzyme-mediated mechanisms. Various synthetic strategies, including aldol reactions, isoxazole intermediates, and chemoenzymatic approaches, are examined to demonstrate advancements in the laboratory synthesis of these bioactive molecules. Additionally, the role of ginger-derived compounds as versatile building blocks in the synthesis of complex natural products and pharmacologically active molecules is explored. Special attention is given to zerumbone due to its unique structural features and wide range of biological activities, including anti-inflammatory, anticancer, and antimicrobial properties. The review also integrates traditional knowledge with modern scientific findings, underscoring ginger's longstanding medicinal relevance. Overall, this work aims to provide insights into the chemical diversity and synthetic accessibility of ginger constituents, encouraging further research in natural product chemistry and drug development.

**Keywords:** *Zingiber officinale,* gingerol, zerumbone, bioactive compounds, biosynthesis, total synthesis

## Introduction

Ginger *(Zingiber officinale)* belongs to the family Zingiberaceae, which also includes important plants such as turmeric and cardamom. It is a perennial herb that typically grows up to 1 m in height, characterized by long, narrow leaves (approximately 20 cm in length and 1.5–2 cm in width) and a thick, branched (Ross, I. A. 2005), horizontal rhizome that is yellowish to brown in color. Ginger is well known for its characteristic pungent aroma and flavor. Indigenous to Southeast Asia, it is now cultivated widely across tropical and subtropical regions of the world. It is extensively used in various forms such as gingerbread, candies, biscuits, beverages, and herbal teas, and holds a significant position as a nutraceutical, spice, flavoring agent, and food additive (Pour, H. A. 2014).

Major ginger-producing countries include India, China, Japan, Indonesia, Australia, Nigeria, and the West Indies. Among these, India is the largest producer and consumer, contributing approximately 30–40% of global production. The quality, aroma, and pungency of ginger are influenced by geographical and environmental factors, with Indian and Jamaican varieties regarded as superior, followed by African varieties. Within India, Kerala is the leading producer, accounting for nearly one-third of total production. A significant portion of this yield is processed into dried ginger, a large fraction of which is exported, with Cochin and Calicut varieties being particularly valued in international markets.

Historically, ginger has been documented in *Hortus Indicus Malabaricus* (Vol. 11) by Hendrik van Rheede in 1692, marking one of the earliest records of cultivated Zingiber species in India. Although the plant was botanically described by William Roxburgh in 1810, it was earlier named *Zingiber officinale* by William Roscoe in 1807. The term "Zingiber" is believed to have originated from the Greek word *zingiberis,* derived from

the Sanskrit *shringavera,* referring to the antler-like shape of the rhizome, though alternative linguistic origins from Tamil have also been proposed. Historical trade routes suggest that ginger was introduced to the Greeks through Arab traders who sourced it from Kerala (Nair, K. P. P. 2013).

The rhizome of ginger has been utilized for thousands of years as both a culinary spice and a medicinal agent. Its extensive therapeutic applications have earned it the title "Maha Aushadhi" (the great medicine) in ancient Indian literature, reflecting its prominent role in Ayurvedic formulations. Traditional systems of medicine have long recognized ginger for its efficacy in treating a wide range of ailments. In recent years, scientific interest in ginger has grown substantially, as evidenced by the vast number of publications and patents related to its bioactive compounds. This increasing body of research highlights the continued relevance of ginger and its constituents in modern pharmacology, nutraceutical development, and natural product chemistry.

## TRADITIONAL KNOWLEDGE

The rhizome of ginger is one of the most widely used spice and condiment and has a long and rich history of medicinal applications intertwined between different cultures and civilization. The Indian, Chinese, Arabic, Roman, Greek alternative medicines are heavily influenced by both the fresh and dried rhizome of ginger. It is also an integral part of many traditional medicines and has been extensively used in Ayurvedic, Chinese, Tibb-Unani, Srilankan, Arabic, and African traditional medicines.

The characteristic pleasant fresh aroma and pungency has made its use as a spice and food additive very popular in different cultures. The Chinese use ginger extensively and ginger tea is used as a health drink for centuries. The Shang dynasty popularized the use and proper cultivation of ginger in China. Indians consume ginger in large amounts and because of its non-toxicity about 8-10 grams of ginger- as paste, fresh, dried, or as

tea –is consumed on a daily basis. The distinct flavor makes it an indispensable component of the curry powder and sauces.

Description of the plant can be found in ancient Indian medical texts like Charaka, Susrutha, Vagbhatta and Chakra-Dutta. In ASTANGA HRIDAYA mention for use against arthritis can be found. Ayurvedic, Chinese, and traditional medicinal systems have recommended ginger as a sole remedy or in combination with other herbs for numerous ailments including common cold, fever, sore throats, vomiting, nausea, sea or motion sickness, nausea related to pregnancy, loss of appetite, gastrointestinal complications, indigestion, constipation, diarrhea, infectious diseases, heartburn, colic, flatulence, influenza, cough, arthritis, rheumatic disorders, migraines, headaches, cardiac palpitations, hypertension, muscular pains and cramps, helminthiasis, dementia and impotence.

**Table: 1**

The traditional medicinal use of ginger in different countries. (Ross, I. A. 2005)

| Country | Traditional medicinal application |
|---|---|
| Arab countries | • Dried seeds are used externally in the form of a plaster as a contraceptive in Unani medicine. |
| China | • The seed oil is applied on the glans penis before coitus to prevent conception. |
| Europe | • Hot water extract of dried plant was used as a contraceptive in the 13th century |
| India | • Hot water extract of seed is taken orally for impotence. |
| | • Seed oil is taken orally for tuberculosis |
| | • Scrambled egg with powdered ginger is taken for coughing. |
| | • Seed oil taken orally is used as an emmenagogue. |

| | |
|---|---|
| | • Seed oil is taken orally as a purgative |
| | • A mixture of dried fruits of *Sesamumindicum Clerodendrumindicum, Moringapterygosperma,* and *Piper nigrumis* mixed with crude sugar and taken orally for20 days to produce sterility. |
| | • Leaves are ground with jaggery and taken orally with coconut milk to treat rabies. |
| | • Ginger mixed withlemon and black salt is extensively used to combat nausea. |
| | • Hot water extract of the dried seed is taken orally as an abortifacient, an emmenagogue, a tonic, a diuretic, and an aphrodisiac; to pro mote hair growth; for ulcers, piles, eye diseas es, and biliousness; and as a galactagogue. |
| | • A paste of *Brideliascandens* prepared in *Sesa mumindicumoil* is applied externally to wounds caused by dog bites. |
| | • A decoction of the leaf of *Gymnemasilvestreis* heated with sesame seed oil until an emulsion is formed and then used as a drop for the eyes several times a day. |
| Ivory coast | • Fresh seed oil is used for eye diseases |
| Jordan | • The juice of new leaves is drunk to expel placenta |
| Malaysia | • Seed oil is taken orally to induce lactation and as an antitussive |
| | • Hot water extract of seeds is taken orally as an emmenagogue and in a large dose as an abor tifacient. |

| | |
|---|---|
| Mozambique | • Seed oil is taken orally as an emmenagogue and used by males as a tonic for sexual neur asthenia |
| | • Juice of the entire plant is taken orally as an aphrodisiac. |
| Peru | • Hot water extract of the seed is taken orally as emmenagogue and abortifacient. |
| South Africa | • Hot water extract of the dried bark is taken orally for dislocations, chest pains,and contu sions |
| South Korea | • Hot water extract of aerial parts is taken orally by the Bantu as an aphrodisiac. |
| | • Hot water extract of leaves is taken orally by the Transvaal Sotho as a remedy for malaria |
| | • Hot water extract of seed is taken orally to in duce menstruation. |
| | • Hot water extract of dried seed is taken orally as an abortifacient and emmenagogue. |

Gingerol is also reported to be found in other species and families outside of *Zingiberaceae*. Apart from the extractable oleoresins ginger also contains a potent proteolytic enzyme, zingibain. 45 compounds were isolated from the n-hexane extract of the ginger rhizome including fatty acids (Marrelli, M., 2015). It is not our intention to discuss the chemistry of each and every compound that has ever been isolated from ginger, but to discuss a selected few and to inspire the readers to further pursue research into the chemistry of the plant and it's isolable.

## BIOSYNTHESIS

### Biosynthetic Pathway Proposed by Denniff *et al.*

The biosynthesis of [6]-gingerol was first investigated by Denniff and Whiting through radiolabeling studies reported in 1976 and 1980 (Denniff, P. 1976, & 1980). In their initial

proposal, dihydroferulate derived from phenylalanine underwent Claisen condensation with malonate and hexanoate, producing a β-diketone intermediate that was subsequently reduced to form [6]-gingerol. In the revised pathway, phenylalanine was first converted to ferulic acid, which then participated in Claisen condensation with malonate and hexanoate to generate [6]-dehydrogingerdione. This intermediate was further reduced in two successive steps to yield [6]-gingerol. Although these studies provided important insights into the biosynthetic route, they did not identify the specific enzymes involved, relying instead on the distribution patterns of radiolabeled atoms to support the proposed mechanisms (Kubra, I. R. 2012).

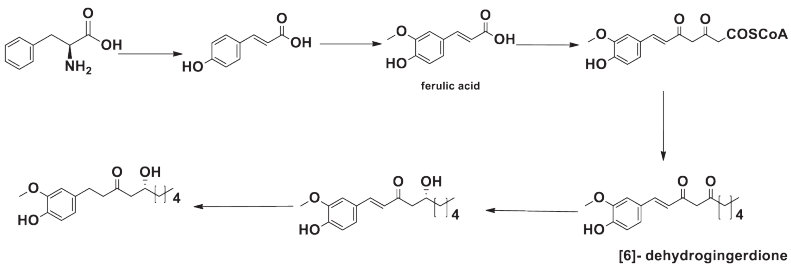


**Biosynthetic Pathway by Ramirez-Ahumada *et al.***

Ramirez-Ahumada et al. (2006) proposed an alternative biosynthetic pathway for gingerol formation based on enzyme assays conducted on protein extracts associated with the phenylpropanoid pathway in ginger. Their investigation highlighted the significant roles of several enzymes, including phenylalanine ammonia-lyase (PAL), polyketide synthases, p-coumaroyl shikimate transferase, p-coumaroyl quinate transferase, caffeic acid O-methyltransferase, and caffeoyl-CoA O-methyltransferase, in the biosynthesis of gingerol. However, the authors were unable to conclusively differentiate between the two proposed biosynthetic routes illustrated in their study. Specifically, it remained unclear whether the methoxy groups on the aromatic ring are introduced before or after the condensation

reactions leading to the gingerol backbone. Consequently, both pathways continue to be considered plausible, and the authors suggested that future genomics-based investigations may help to elucidate the precise biosynthetic mechanism (Kubra, I. R. 2012).

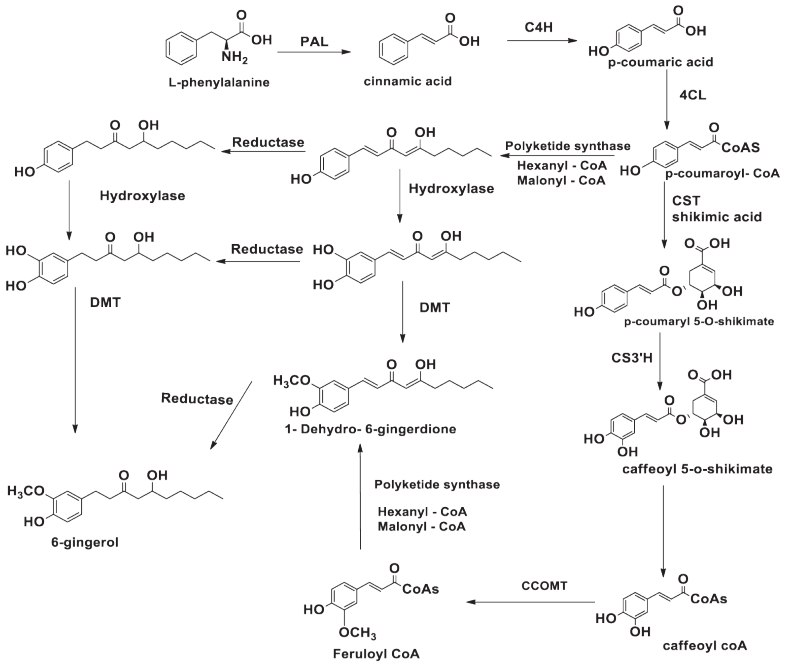


Enzymes: PAL = phenylanalineammonialyase; C4H = cinnamate 4-hydroxylase; 4CL = 4 coumara-te: CoA ligase; CST = p-coumaroylshikimatetransferase; CS3'H = p-coumaroyl 5-O-shikimate 3'-hydroxylase; OMT = O-methyltransferase; CCOMT = caffeoyl-CoA O-methyltransferase.

The essential oil of ginger is predominantly composed of terpenoids, which constitute the largest class of natural products, comprising more than 30,000 known compounds. Terpenoids are structurally derived from repeating isoprene units and are biosynthesized through the sequential condensation of isopentenyl diphosphate (IPP) and dimethylallyl diphosphate (DMAPP). Their initial condensation yields geranyl diphosphate (GPP), which

upon further addition of IPP forms farnesyl diphosphate (FPP), with continued elongation producing larger terpenoid precursors as required. Monoterpenes, sesquiterpenes, and diterpenes contain C10, C15, and C20 carbon skeletons, respectively. These basic structures subsequently undergo a variety of biochemical transformations, including oxidation, reduction, isomerization, and hydration, resulting in the vast structural diversity of terpenoids. Two principal biosynthetic pathways are involved in the formation of IPP: the acetate–mevalonate pathway, which primarily operates in the cytoplasm and mitochondria, and the deoxyxylulose phosphate pathway, which occurs predominantly in plastids (Dewick, P. M. 2002 & Dubey, V. S. 2003).

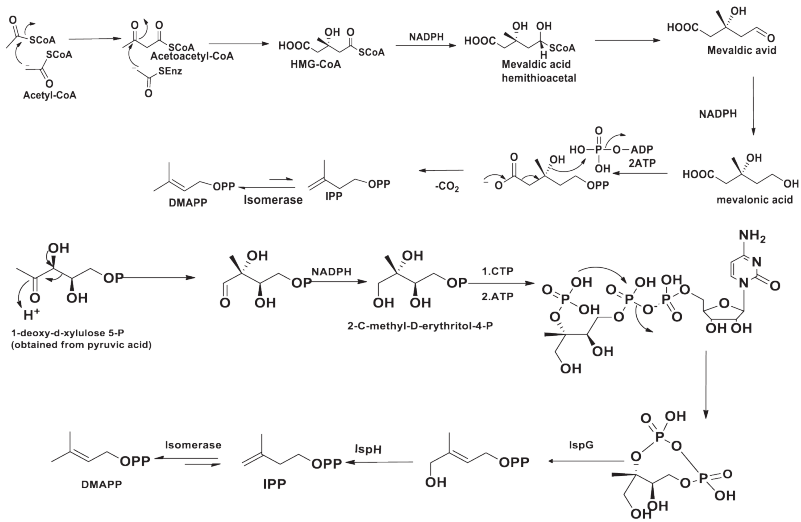


## Total Synthesis

The first isolation of gingerol as a volatile yellow oil was reported by Thresh *et al.*(1879). Subsequently, Garnett and Grier (1907) improved the isolation procedure, and the structure of gingerol was initially proposed by Lapworth (1917) based on chemical degradation studies, which were later supported by investigations conducted by Nelson (1917). The isolated pungent yellow oil was found to be optically active; however,

upon distillation, it lost this property and produced a less pungent compound. Lapworth originally assigned the structure as [7]-gingerol, but this was later corrected by Connell *et al.* (1969), who identified [6]-, [8]-, and [10]-gingerols and successfully isolated [6]-gingerol as a crystalline solid with a reported melting point of approximately 5–15 °C. Nevertheless, subsequent studies have reported varying melting points for [6]-gingerol, generally ranging between 20 and 32 °C. Connell also established the absolute stereochemistry of [6]-gingerol as the S-configuration by comparing the heptane-1,2-diol obtained through Baeyer–Villiger oxidation of gingerol with the stereochemical data reported by Levene and Walti (1931). Nomura (1917) isolated zingerone in the form of its bisulfite adduct, and later, in 1918, isolated shogaol (Connell, D. W. 1983). Due to the challenges associated with the large-scale isolation of these bioactive constituents from natural sources, considerable efforts have been directed toward their total synthesis (Semwal, R. B., 2015). Consequently, numerous synthetic methodologies for ginger-derived compounds have been developed and are discussed in this section.

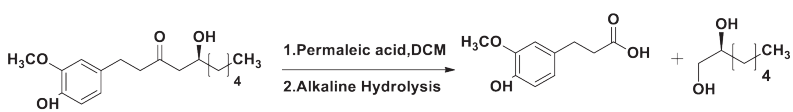


## Gingerol

[6]-Gingerol is the major pungent constituent of ginger and has attracted considerable attention due to its diverse biological activities and synthetic importance. Owing to the difficulties associated with its large-scale isolation from natural sources, several synthetic approaches have been developed for the preparation of gingerol and its analogues.

The first synthesis of racemic [(±)]- and (−)-[6]-gingerol was reported by Hirao *et al* (1973). through the condensation of benzyl zingerone with caproic aldehyde, followed by deprotection. In 1979, Enders et al. (1979) achieved the enantioselective synthesis of (+)- and (−)-gingerol in nine steps using an aldol reaction

between the anion of a chiral hydrazone derived from vanillin and n-hexanal. This method afforded optical yields of 33–39% with an overall yield of 26.4%.

Denniff *et al.*, (1976 & 1981) extensively investigated the synthesis of gingerol and its derivatives. Their strategy involved the condensation of trimethylsilyl zingerone with alkanals and acylimidazoles to produce [2]-, [4]-, [6]-, [8]-, [10]-, and [12]-gingerols along with the corresponding gingerdiones. In the same period, Banno and Mukaiyama (1976) employed a Lewis acid-catalyzed cross-aldol reaction for the synthesis of zingerone, shogaol, and gingerol derivatives.

Kato *et al.* (1984) introduced an alternative synthetic route for racemic gingerol through the direct C-acylation of ferulic acid using phosphorocyanidate, thereby providing a novel and efficient approach toward gingerol synthesis.

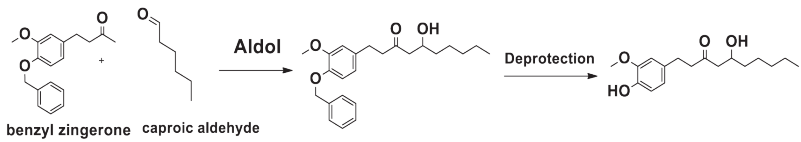


Hirao et al 1973

The isoxazole moiety has emerged as one of the most widely employed intermediates in the synthesis of gingerol and its analogues, primarily because it functions as a masked β-hydroxy ketone. Barco *et al.* (1981) utilized 3,5-disubstituted isoxazoles in the synthesis of gingerol through a Wittig reaction involving benzyl-protected vanillin, followed by transformation of the resulting isoxazole intermediate into gingerol.

Subsequently, Baraldi Giovanni *et al.* (1982) adopted a similar synthetic strategy but introduced N-tosyl-L-prolyl chloride for the preparation of a chiral vinylogous imide and employed K-Selectride as the reducing agent. This approach enabled the enantioselective synthesis of gingerol in nine steps with an optical yield of 30–40% and an overall yield of approximately 20%.

Tsuge *et al.* (1987) further modified the isoxazole-based approach by incorporating the Horner–Emmons olefination methodology for the synthesis of racemic gingerol. This strategy was later extended to the synthesis of several other natural products as well.

Le Gall *et al.* (1989) developed a highly stereoselective route involving the diastereoselective cycloaddition of nitrile oxides with a chiral acyclic iron-complexed triene to generate a chiral isoxazole intermediate. This intermediate was subsequently converted into (S)-[6]-gingerol in nine steps with an excellent enantiomeric excess of 96%, although the overall yield was relatively low (10%).

Cinquini *et al.* (1984) synthesized (S) - [6] - gingerol with greater than 96% enantiomeric excess using 4, 5 - dihydroisoxazolines and benzyl - protected vanillin in the presence of menthyl p-toluenesulfinate as a chiral auxiliary. Building upon this methodology, Martin and Guibet (1991) successfully synthesized both (R) - and (S)-[8]-gingerol with similarly high enantiomeric purity (>96% ee).

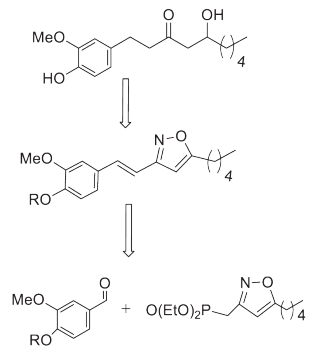


Retrosynthesis of the isoxazole strategy

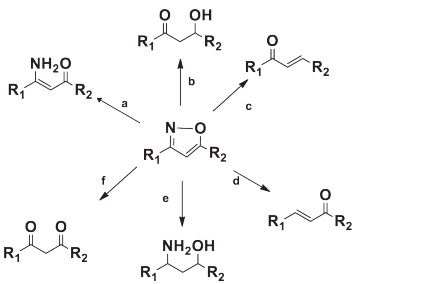


Reagents: a) $H_2$, $PtO_2$; b) $H_2$, $PtO_2$; PhCOCl, Py; $NaBH_4$; 90% AcOH; c) $H_2$, $PtO_2$; PhCOCl, Py; $NaBH_4$; $H^+$; d) Na, $NH_3$(l); $SiO_2$; e) Na, n-$C_3H_{11}OH$; f) $H_2$, $PtO_2$, $H^+$

Different transformations of isoxazoles in synthesis

Solladié and Cherif (1993) synthesized (S)-[6]-, [8], and [10]-gingerols starting from ferulic acid using a chiral β-ketosulfoxide as the asymmetric reagent. Sharma *et al.* (1998) later reported a chemoenzymatic synthesis of (S)-[8]-gingerol in 1998, employing enantioselective lipase-catalyzed esterification

of a 2-hydroxy acid to prepare the chiral precursor. Earlier, Annunziata *et al.* (1984) synthesized the antipode of natural gingerol with 60% optical purity from zingerone using (−)-(S)-menthyl p-toluenesulfinate as the chiral auxiliary, motivated by the limited natural availability and potential biological activity of the antipode.

Racemic gingerols were also synthesized through one-pot addition of the dianion of zingerone to various aldehydes, affording gingerols in 75–95% yield. The corresponding shogaols were obtained by acid-catalyzed dehydration. The dianion intermediate was generated by treating zingerone with 1 equivalent of n-BuLi at −78 °C followed by 1 equivalent of LDA.

Due to the poor thermal stability and water solubility of gingerol, Ojima *et al.*(2012) converted it into 5-α-Glc-gingerol using α-glucosidase from Halomonas sp. H11. Selective glucosylation occurred at the β-hydroxy group while the phenolic hydroxyl group remained unaffected, resulting in enhanced stability toward heat and acidic conditions.

Morera *et al.* (2012) investigated the agonistic activity of racemic gingerols and their analogues toward TRPV1 and TRPA1 receptors, important targets in analgesic research, and identified seven active compounds including [6]-shogaol. Sabitha *et al.* (2011), in two separate studies, reported the synthesis of gingerols, gingerdiols, and diarylheptanoid derivatives using key reactions such as Keck allylation, Crimmins aldol condensation, aldehyde–acetylene coupling, and chelation-controlled reductions.

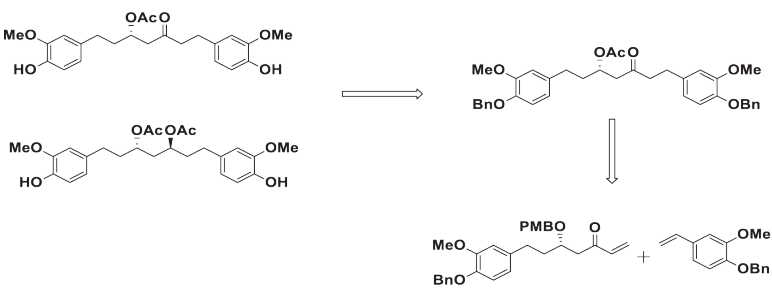


Retrosynthetic analysis of Diarylheptanoids; Sabitha et al

Fukuda *et al.* (1996) reported the synthesis of S and R [6]-α-difluro-gingerol using anenzymatic resolution with olipase/4S (Rhizopusjaponicus)as the key step. β-hydroxycarbonyl structure with α-fluoro substitution shows biological activity as well as ferroelectric liquid crystals.An enantioselective synthesis of (+)-(S)-[n]-gingerols via theL-proline-catalyzed aldol reaction was achieved by Ma *et al* (2009). The 5 step synthesis had an overall yield of 14-19%, employed Mukayama synthesis (1976) as a key step, but it is to be noted that only 74% ee could be achieved.

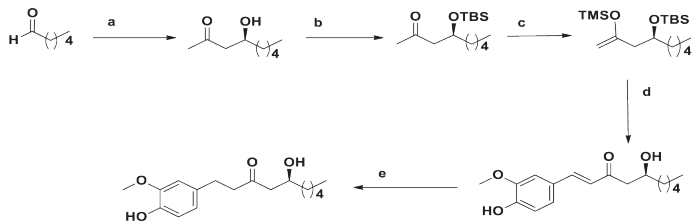


**Reagents: a) acetone, L-proline, 30 $^0$C, 3 d; (b) TBSCl, imidazole, $CH_2Cl_2$, rt, overnight; (c) TMSOTf, i-$Pr_2$NEt, $CH_2Cl_2$, 0 $^0$C, 3h; (d) vanillin, $BF_3OEt_3$, $CH_2Cl_2$, 0 $^0$C, 3h; (e) $H_2$ (1 atm), 10% Pd/C, $Et_3N$/EtOAc (v/v) = 1/ 20, rt, 4h.**

Vijender *et al.* (2012) did a scalable and eco-friendly synthesis of racemic gingerols in 24-28 % yield and in 2015 improved the procedure. The primary alcohol formed by the hydroboration-oxidation of benzyl protected eugenol was oxidized to the corresponding aldehyde and was converted to the oxime which then underwent 1,3 dipolar cycloaddition to yield the isoxazolines, which was then converted to gingerol by reductive cleavage and deprotection.

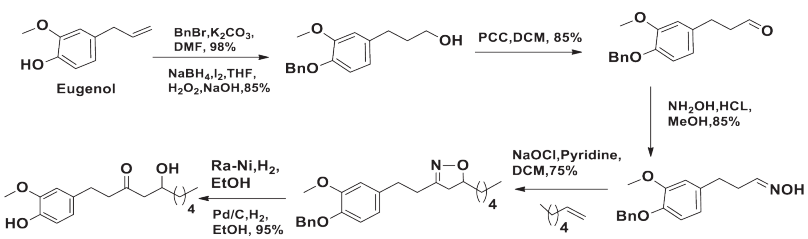

## CONCLUSION

In conclusion, *Zingiber officinale* continues to stand as a remarkable source of structurally diverse and biologically potent phytochemicals, with compounds such as gingerols, shogaols, zerumbone, and zingiberene playing central roles in its pharmacological significance. This review highlights that both biosynthetic and total synthetic approaches have significantly advanced our understanding of these molecules, revealing intricate pathways and innovative strategies for their preparation. The evolution of synthetic methodologies—from classical aldol reactions to modern chemoenzymatic and stereoselective techniques—demonstrates the growing efficiency and versatility in accessing these bioactive compounds. Such advancements not only address challenges associated with natural extraction but also enable structural modification and large-scale production. Moreover, the utility of ginger-derived compounds as synthons underscores their importance in organic synthesis and drug development, particularly in designing molecules with enhanced therapeutic potential.

By bridging traditional medicinal knowledge with contemporary chemical research, this work emphasizes the enduring relevance of ginger in both natural product chemistry and modern pharmacology. Future research focusing on genomic insights, greener synthetic routes, and detailed structure–activity relationships will further unlock the potential of these compounds, paving the way for novel applications in medicine and industry.

## References

Annunziata, R., Cinquini, M., Gennari, C., & Poli, G. (1984). Enantioselective synthesis of (−)-(R)-[6]-gingerol. *Synthesis,* 702–703.

Banno, K., & Mukaiyama, T. (1976). New synthesis of the pungent principles of ginger: Zingerone, shogaol, and gingerol. *Bulletin of the Chemical Society of Japan,* 49, 1453–1454.

Baraldi, P. G., Fruttarolo, F., Pollini, G. P., & Simoni, D. (1982). Asymmetric synthesis of a β-ketol moiety via 3,5-disubstituted isoxazoles: Application to (+)-(S)-[6]-gingerol. *Journal of the Chemical Society, Perkin Transactions* 1, 2983–2987.

Barco, A., Benetti, S., Baraldi, P. G., Guarneri, M., Pollini, G. P., & Simoni, D. (1981). 3,5-Disubstituted isoxazoles as a latent aldol moiety: Application to the synthesis of (±)-[6]-gingerol. *Journal of the Chemical Society, Chemical Communications,* 599–600.

Cinquini, M., Frignani, F., & Grasselli, A. (1984). Synthesis of enantiomerically pure Δ2-isoxazolines via sulphinyl derivatives. *Journal of the Chemical Society, Chemical Communications,* 551–552.

Denniff, P., & Whiting, D. A. (1976). Biosynthesis of [6]-gingerol, pungent principle of Zingiber officinale. *Journal of the Chemical Society, Chemical Communications,* (18), 711–712.

Denniff, P., & Whiting, D. A. (1976). Synthesis of (±)-[6]-gingerol and relatives via directed aldol reactions. *Journal of the Chemical Society, Chemical Communications,* 712–713.

Denniff, P., Macleod, I., & Whiting, D. A. (1980). Studies in the biosynthesis of [6]-gingerol, pungent principle of ginger (Zingiber officinale). *Journal of the Chemical Society, Perkin Transactions* 1, 2637–2644.

Denniff, P., Macleod, I., & Whiting, D. A. (1981). Syntheses of the (±)-[n]-gingerols and related compounds through regioselective aldol condensations. *Journal of the Chemical Society, Perkin Transactions* 1, 82–87.

Dewick, P. M. (2002). The biosynthesis of C5–C25 terpenoid compounds. *Natural Product Reports,* 19, 181–222.

Dubey, V. S., Bhalla, R., & Luthra, R. (2003). An overview of the non-mevalonate pathway for terpenoid biosynthesis in plants. *Journal of Biosciences,* 28(5), 637–646.

Enders, D., Eichenauer, H., & Pieter, R. (1979). Enantioselective synthesis of (−)-(R)- and (+)-(S)-[6]-gingerol. *Chemische Berichte,* 112, 3703–3714.

Fukuda, H., Takahashi, M., & Kitazume, T. (1996). Synthesis of chiral difluorinated [6]-gingerol. *Tetrahedron,* 52(1), 157–164.

Garnett, G., & Grier, G. (1907). Studies on ginger constituents. *Pharmaceutical Journal,* 25, 118.

Govindarajan, V. S., & Connell, D. W. (1983). Ginger—Chemistry, technology, and quality evaluation: Part 1. CRC Critical *Reviews in Food Science and Nutrition,* 17(1), 1–96.

Hirao, N., Kawachi, J., & Yasui, B. (1973). Synthesis of natural gingerol. *Chemical and Pharmaceutical Bulletin,* 21, 2569–2571.

Kato, N., Hayashi, Y., & Shioiri, T. (1984). Direct C-acylation approach toward gingerol synthesis. *Chemical and Pharmaceutical Bulletin,* 32, 1679–1682.

Kubra, I. R., & Rao, L. J. M. (2012). An impression on current developments in the technology, chemistry, and biological activities of ginger *(Zingiber officinale Roscoe). Critical Reviews in Food Science and Nutrition,* 52(8), 651–688.

Kumar, N. V., Srinivas, N. S., & Bettadaiah, B. K. (2012). New scalable and eco-friendly synthesis of gingerols. *Tetrahedron Letters,* 53(24), 2993–2995.

Kumar, N. V., Srinivas, S. C., Srinivas, P., & Bettadaiah, B. K. (2016). An improved route to the preparation of 6-, 8-, and 10-gingerols. *Organic Preparations and Procedures International,* 47(6), 443–448.

Lapworth, A., Pyman, F. L., & Royle, F. A. (1917). The pungent principle of ginger. Part I. The chemical characters and decomposition products of Thresh's "gingerol." *Journal of the Chemical Society, Transactions,* 111, 777–790.

Le Gall, T., Lellouche, J. P., & Beaucourt, J. P. (1989). An organoiron-mediated chiral synthesis of (+)-(S)-[6]-gingerol. *Tetrahedron Letters,* 30, 6521–6524.

Levene, P. A., & Walti, A. (1931). Configurational relationship of alpha-hydroxy-heptanoic acid to other alpha-hydroxy acids. *Journal of Biological Chemistry,* 94, 593–598.

Ma, S., Zhang, S., Duan, W., & Wang, W. (2009). An enantioselective synthesis of (+)-(S)-[n]-gingerols via the L-proline-catalyzed aldol reaction. *Bioorganic and Medicinal Chemistry Letters,* 19, 3909–3911.

Marrelli, M., Menichini, F., Conforti, F., et al. (2015). A comparative study of *Zingiber officinale Roscoe* pulp and peel: Phytochemical composition and evaluation of antitumour activity. *Natural Product Research,* 29(21), 2045–2049.

Martin, M., & Guibet, P. (1991). Synthesis of the [8]-gingerol enantiomers. *Chirality,* 3(2), 151–155.

Morera, E., De Petrocellis, L., Morera, L., Moriello, A. S., Nalli, M., Di Marzo, V., & Ortar, G. (2012). Synthesis and biological evaluation of [6]-gingerol analogues as TRPV1 and TRPA1 modulators. *Bioorganic and Medicinal Chemistry Letters,* 22, 1674–1677.

Nair, K. P. P. (2013). *The agronomy and economy of turmeric and ginger.* Elsevier.

Nelson, E. K. (1917). Gingerol and paradol. *Journal of the American Chemical Society,* 39, 1466.

Nomura, H. (1917). The pungent principles of ginger. Part I. A new ketone, zingerone (4-hydroxy-3-methoxyphenylethyl methyl ketone) occurring in ginger. *Journal of the Chemical Society, Transactions,* 111, 769–776.

Ojima, T., Arai, K., Saburi, W., & Yamamoto, T. (2012). α-Glucosylated 6-gingerol: Chemoenzymatic synthesis using α-glucosidase from Halomonas sp. H11 and its physical properties. *Carbohydrate Research,* 354, 59–64.

Pour, H. A., Norouzzadeh, R., Heidari, M. R., Ogut, S., Yaman, H., & Gokce, S. (2014). Therapeutic properties of Zingiber officinale Roscoe: A review. *European Journal of Medicinal Plants,* 4(12), 1431–1446.

Ramirez-Ahumada, C., Timmermann, B. N., & Gang, D. R. (2006). Biosynthesis of curcuminoids and gingerols in turmeric (Curcuma longa) and ginger (Zingiber officinale): Identification of curcuminoid synthase and hydroxycinnamoyl-CoA thioesterases. *Phytochemistry,* 67, 2017–2029.

Ross, I. A. (2005). Medicinal plants of the world (Vol. 3). *Humana Press*.

Sabitha, G., Chandra, G., Yadagiri, K., & Yadav, J. S. (2011b). Synthesis of diarylheptanoids and related derivatives. Tetrahedron: *Asymmetry,* 22, 1729–1735.

Sabitha, G., Reddy, T. R., Yadagiri, K., & Yadav, J. S. (2011a). Synthesis of gingerol and diarylheptanoids. *Tetrahedron: Asymmetry,* 22(24), 2124–2133.

Semwal, R. B., Semwal, D. K., Combrinck, S., & Viljoen, A. M. (2015). Gingerols and shogaols: Important nutraceutical principles from ginger. *Phytochemistry,* 117, 554–568.

Sharma, A., Sankaranarayanan, S., & Chattopadhyay, S. (1998). A chemoenzymatic synthesis of (R)-[8]-gingerol. *Enantiomer,* 3(1), 45–50.

Solladié, G., & Ziani-Cherif, C. (1993). Total synthesis of natural gingerols, the three active principles of ginger. *Journal of Organic Chemistry,* 58(8), 2181–2185.

Thresh, J. C. (1879). Proximate analysis of the rhizome of Zingiber officinale and comparative examination of typical specimens of commercial gingers. *Pharmaceutical Journal,* 10, 171.

Tsuge, O., Kanemasa, S., Nakagawa, N., & Suga, H. (1987). Horner–Emmons olefination of 4-hydroxy - 2 - oxoalkylphos phonates and related compounds: Applications to the syntheses of (±)-gingerol and related compounds. *Bulletin of the Chemical Society of Japan,* 60, 4091–4098.

# Study on the Structural and DC Conductivity of Polypyrrole Synthesized via Chemical and Ultrasonication Methods

**[1]Lincy K Alex and [2]Lakshmi Vijayan**

[1, 2] Department of Physics, St. Aloysius College, Edathua, Kuttanad Thaluk, Alappuzha-689573, Kerala, India.
[1]Email: lincyalex93@gmail.com
[2]Email: lakshmivijayan@gmail.com

**Abstract:** Polypyrrole (Ppy) was synthesized via chemical oxidation and ultrasonication-assisted polymerization. Structural, optical, and electrical properties were systematically studied using UV–Vis, FTIR, XRD, and conductivity measurements. Ultrasound assisted synthesis showed uniform thickness and superior performance of films. UV–Vis confirmed π–π* and polaron transitions, with band gap variation dependent on oxidant-to-monomer ratio. XRD confirmed an amorphous packing structure favorable for charge transport. Conductivity increases with oxidant concentration in chemically synthesized films, reflecting an increase in charge-carrier density. Overall, ultrasonication proved to be more effective, yielding high-quality PPy films suitable for advanced electronic and sensing applications.

**Keywords:** Polypyrrole Films, ultrasonication-assisted polymeri zation, optical and electrical properties, conductive polymers

## Introduction

The study of conjugated conducting polymers gained significant attention following the discovery of polyacetylene in 1977 by Hideki Shirakawa, Alan MacDiarmid, and Alan Heeger. Researchers have since extensively explored various important conjugated polymers (CPs). Over the past two decades, researchers have made significant progress in developing polymers with high electrical conductivity (intrinsic conducting polymers (ICPs) or synthetic metals) by implementing a simple change in traditional conjugated polymers. Unlike other conducting polymers, which rely on the dispersion of metal or carbon powder within an insulating polymer, ICPs can conduct electricity independently.

Over time, several other conjugated polymeric materials and their derivatives have been found to possess electrical conductivity. Extensive research on various conjugated polymers, including poly(p-phenylene), polyaniline (PANI), polypyrrole, polythiophene, polycarbazole, polyfluorene, polyvidone, poly (p-phenylene vinylene), and their substituted derivatives, has led to their applications in rechargeable batteries, microelectronics, sensors, electrochromic displays, and light-emitting and photovoltaic devices. They are attractive materials used in various fields, including energy storage, corrosion protection, gas sensors, supercapacitors, aeronautics, space, and electronics. A key property that distinguishes polymers from metals is their electrical conductivity.

Among these, polyaniline (PANI), polypyrrole (PPy), and polythiophene (PTh) have attracted considerable interest from researchers. These polymers are valued for their lightweight nature, enhanced functionality, corrosion resistance, ease of synthesis, cost-effectiveness, stability, unique redox properties, and a wide range of electrical conductivity, which can vary from insulating to metallic. Polypyrrole (Ppy) is a conducting polymer that has attracted significant attention due to its unique combination of electrical, optical, and mechanical properties.

In this study, we explored the chemical oxidative polymerization and ultrasonics-assisted polymerization of pyrrole. Synthesized samples are characterized using methods such as XRD, FTIR, UV-Vis, and DC conductivity. As a member of the polyheterocycle family, polypyrrole (Ppy) features a conjugated backbone that enables efficient charge transport and contributes to its remarkable conductivity.

## Materials and methods

### 1. Reagents

Pyrrole monomer (98%) and AR-grade ammonium persulfate (APS) were obtained from Sigma-Aldrich Chemicals Pvt. Ltd. All solutions and reactions were performed using

deionized water. Precleaned glass slides were utilized as the substrate.

## 2. Preparation of PPy thin films

Polypyrrole was synthesized via chemical oxidative polymerization using ammonium persulfate (APS) as the oxidant. The pyrrole solution was slowly added to the APS solution, which was stirred with a magnetic stirrer at room temperature. The oxidant-to-monomer ratio was varied by adjusting the amount of APS added, and the reaction was allowed to proceed for 2 to 4 hours or until the desired level of polymerization was achieved. A polypyrrole thin film was deposited on a pre-cleaned glass substrate by immersing the substrate in the oxidant solution. This deposition reaction was carried out for 150 minutes. Afterward, the film was washed with deionized water to remove any residual oxidant and unreacted monomer. [3]. Black-colored thin films were coated on a glass substrate, as shown in Fig. 1. Chemical oxidative polymerization of Ppy using $(NH_4)_2S_2O_8$ is shown below (Fig. 2).

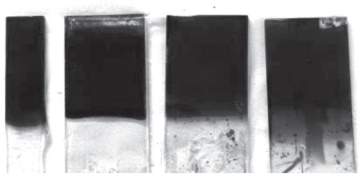

Figure 1. Polypyrrole thin films of various o/m ratios

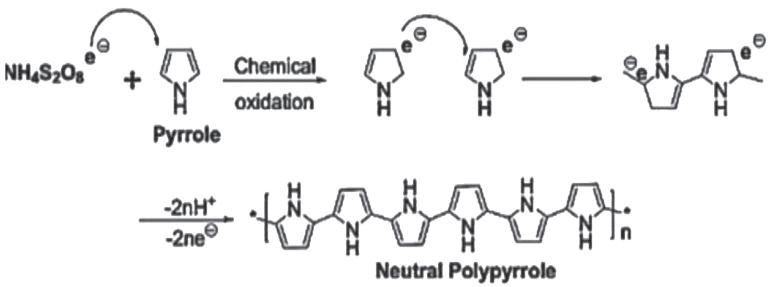


Figure 2. Chemical oxidative polymerization of pyrrole using APS

## Results and Discussions

### X-ray diffraction analysis

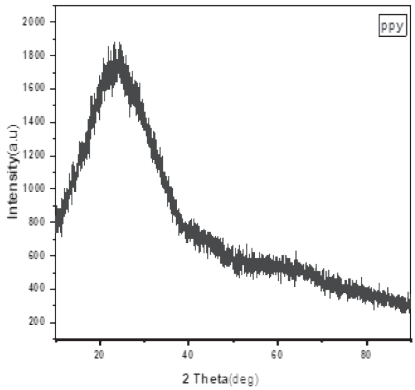


Figure 3: XRD of polypyrrole

X-ray diffraction studies reveal a broad peak at approximately $2\theta = 24.35°$, indicating the polymer's amorphous nature. This peak arises from the scattering of the polypyrrole (Ppy) chains at the interplanar spacing. The average chain separation can be calculated using the appropriate formula $S = 5\lambda/8\sin\theta$ ……. (1) where S is the polymer chain separation, $\lambda$ is the X-ray wavelength, and $\theta$ is the diffraction angle at the maximum intensity of the amorphous halo. The average chain separation (R) is found to be 4.5 Å for Ppy.

### FTIR Spectroscopy

The FTIR spectra of polypyrrole with varying monomer-to-oxidant (M/O) ratios were recorded using an FTIR spectrometer in the range of 500–4000 $cm^{-1}$, as shown in Figures 4 and 5. For both spectra, the peaks at 608 $cm^{-1}$ and 611 $cm^{-1}$ indicate the presence of skeletal vibrations. The peaks at 788 $cm^{-1}$, 929 $cm^{-1}$, and 924 $cm^{-1}$ correspond to C–H out-of-plane deformations, whereas the peaks at 1042 $cm^{-1}$ and 1200 $cm^{-1}$ are attributed to C–H in-plane deformations. As the O/M ratio increases, the peaks initially shift toward lower wavenumbers up to a certain point; beyond that, further increases in the M/O ratio shift the peaks toward higher wavenumbers. The peaks at 1560 $cm^{-1}$ and 1561 $cm^{-1}$ are associated with C=C stretching vibrations. Thus, the FTIR spectra confirm the formation of polypyrrole and show that, with a change in the M/O ratio, the vibrational band frequencies shift. Changes in vibrational frequencies match with UV-Vis trends in band gap and XRD's indication of amorphous nature.

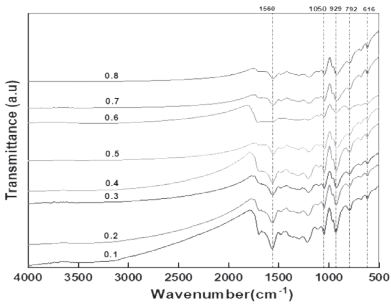


Figure 4: FTIR of the Chemical method

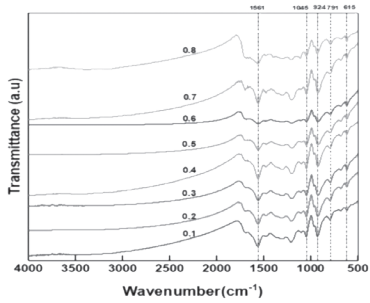


Figure 5: FTIR of the Ultrasound-assisted method

## UV-Vis Spectroscopy

The optical absorption spectra of the polymer samples were recorded using Thermo Fisher equipment, covering a wavelength range from 300 nm to 700 nm (Fig. 6). A strong absorption peak observed around 400-500 nm corresponds to the π-π transition from the highest occupied molecular orbital (HOMO) to the lowest unoccupied molecular orbital (LUMO). This peak indicates the presence of a conjugated backbone in PPy. A weaker absorption peak around 550-600 nm is also attributed to the n-π transition, which occurs from non-bonding orbitals (n) to the LUMO. This peak is linked to the nitrogen atoms within the PPy chain. Furthermore, small humps appearing at wavelengths greater than 600 nm indicate polaron-bipolaron transitions in all samples. Notably, the intensity of these peaks increases as the O/M ratio decreases.

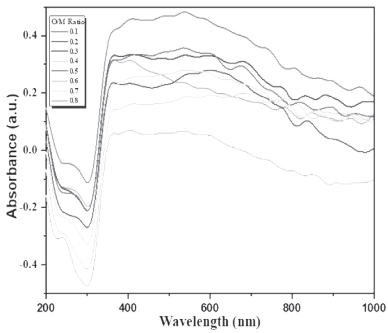


Figure 6: UV -VIS Spectra chemical method

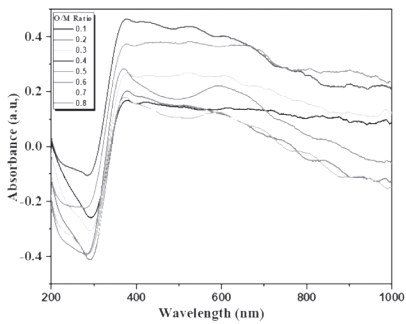


Figure 7:: UV- VIS Spectra Ultrasound-assisted

## Optical band gap

The optical band gap has been calculated using formula (2). In a graph of $(\alpha h\nu)^2$ versus $h\nu$, the extrapolation of the straight line to the $(\alpha h\nu)^2 = 0$ axis yields the optical band gap. Fig. 8 shows the bandgap for both methods.

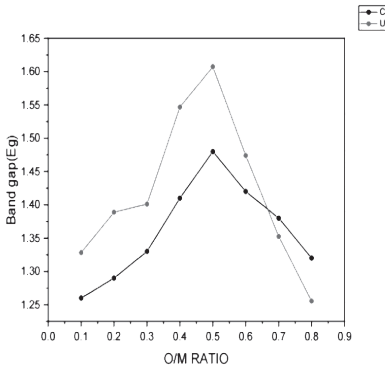


**Figure 8:** *Bandgap vs O/M ratio*

$$\propto h\vartheta = A[h\vartheta - E_g)]^n \quad \ldots\ldots\ldots\ldots (2)$$

where '$E_g$' is an optical band gap, 'α' is the absorption of the thin film, 'A' is a constant, '$h\vartheta$' is the photon energy, and 'n' is a constant.

## DC Conductivity

Electrical conductivity was measured at room temperature using a four-probe system. I-V characteristics of polypyrrole samples for different O/M ratios are shown in figure 9. Resistance values for samples with different O/M ratios were obtained from the slopes of the I-V characteristics. From the values of resistances, conductivity has been calculated for all polypyrrole samples using the formula given below.

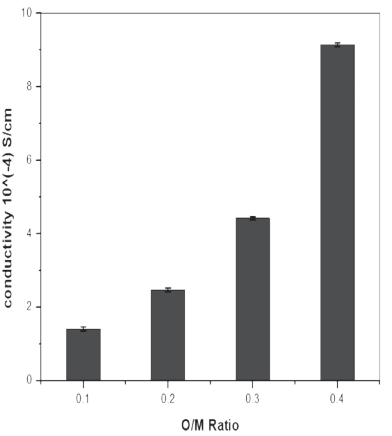


**Figure 9: Conductivity vs o/m ratio**

$$\sigma = \ln(2)/(R*\pi*t) \quad \ldots\ldots\ldots (3)$$

Where σ is the conductivity, R is the resistance, and t is the thickness of the thin films. It is observed that the resistance of the polypyrrole samples decreases with increasing O/M ratio. It may be due to an increase in the number of cation formations resulting from a higher oxidant concentration, leading to more charge carriers per unit volume and, consequently, more current through the sample and, hence, lower resistance.

## Scanning Electron Microscopy (SEM)

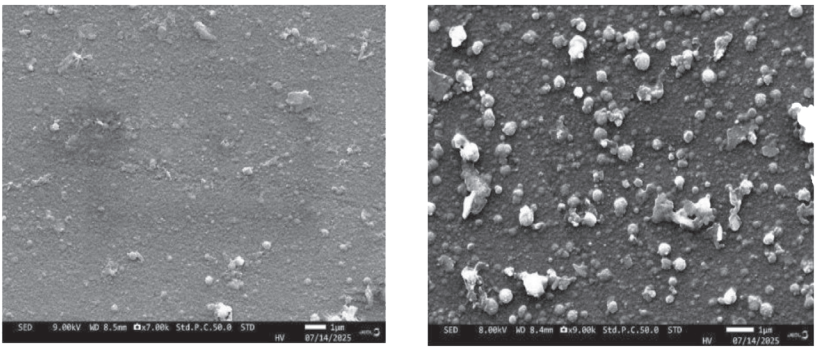


**Figure 10: SEM micrographs of chemically synthesised samples a) 0.1 O/M ratio, b) 0.3 O/M ratio**

Scanning electron microscopy micrographs of chemically synthesized polypyrrole samples are shown in the figure. All the samples exhibit a spherical, agglomerated structure. Different O/M ratios show grains of different sizes.

## Conclusion

In this work, polypyrrole (Ppy) thin films were successfully synthesized via chemical oxidative polymerization and ultrasonication-assisted polymerization, both using ammonium persulfate as the oxidant. A systematic investigation of structural, optical, morphological, and electrical properties was carried out using XRD, FTIR, UV–VIS spectroscopy, SEM, and DC conductivity measurements.

XRD analysis confirmed the predominantly amorphous nature of the synthesized PPy films, which is favorable for charge transport through disordered π-conjugated chains. FTIR spectra verified the formation of the polypyrrole backbone and revealed systematic shifts in vibrational bands with variation in the oxidant-to-monomer (O/M) ratio, indicating changes in doping level and structural ordering. UV–Vis studies demonstrated characteristic π–π* transitions and polaron–bipolaron absorption bands, while the calculated optical band gap showed dependence on the O/M ratio, reflecting modifications in the electronic structure and conjugation length.

DC conductivity measurements revealed that electrical conductivity increases with increasing oxidant concentration, attributed to a higher charge-carrier density resulting from increased cation formation. SEM micrographs indicated spherical, agglomerated morphology with grain size variation depending on the O/M ratio.

Compared with the conventional method, the ultrasonication-assisted method produced more uniform and better-performing films, suggesting improved polymer chain growth and enhanced interaction between the monomer and oxidant under ultrasonic irradiation. Overall, the study establishes that synthesis parameters, particularly the O/M ratio and polymerization technique, play a crucial role in tailoring the optoelectronic properties of polypyrrole thin films. The obtained results demonstrate the potential of ultrasonication-assisted PPy films for applications in electronic devices, sensors, and energy-related systems.

**References**

Blinova, N. V., Stejskal, J., Trchová, M., Prokeš, J., & Omastová, M. (2007). Polyaniline and polypyrrole: A comparative study of the preparation. *European Polymer Journal,* 43(6), 2331–2341. https://doi.org/10.1016/j.eurpolymj.2007.03.045

Chitte, H. K., Bhat, N. V., Gore, M. A. V., & Shinde, G. N. (2011). Synthesis of polypyrrole using ammonium peroxydisulfate (APS) as an oxidant, together with some dopants for use in gas sensors. *Materials Sciences and Applications,* 2(10), 1491–1498.

Fulari, V. J., Thombare, J. V., & Kadam, A. B. (2013). Chemical oxidative polymerization and characterization of polypyrrole thin films for supercapacitor application. In the 2013 *International Conference on Energy Efficient Technologies for Sustainability* (pp. 1068–1071). IEEE. https://doi.org/10.1109/ICEETS.2013.6533535

Kamenshchikov, M. V., Solnyshkin, A. V., Bogomolov, A. A., & Pronin, I. P. (2011). Conductivity and current–voltage characteristics of PZT thin-film heterostructures. *Physics of the Solid State,* 53, 2080–2084. https://doi.org/10.1134/S1063783411100155

Sravanthi, M., & Manjunatha, K. G. (2021). Synthesis and characterization of conducting polypyrrole with various dopants. *Materials Today: Proceeding*s, 46, 5964–5968. https://doi.org/10.1016/j.matpr.2020.11.762

Yussuf, A., Al-Saleh, M., Al-Enezi, S., & Abraham, G. (2018). Synthesis and characterization of conductive polypyrrole: The influence of the oxidants and monomer on the electrical, thermal, and morphological properties. *International Journal of Polymer Science,* 2018, Article 4191747. https://doi.org/10.1155/2018/4191747

# Influence of Solar Activity Phases on Seasonal Extreme Precipitation over Kerala

**[1]Elizabeth Thomas and [2]Noble P. Abraham**

[1,2] Mar Thoma College, Kuttapuzha P.O., Tiruvalla, PIN:689103, Kerala, India.
[2] Assistant Professor and Research Guide, Department of Physics, Mar Thoma College, Tiruvalla. E-mail: noblepa@gmail.com

**Abstract:** Global attention has been focused on extreme climatic changes. This paper investigates the relationship between different phases of solar activity and extreme precipitation events in Kerala, India. Sunspot number and rainfall data were analysed over 122 years (1901-2022). The solar phases of Solar Cycles 14-24 were determined for all seasons, and the years with excessive and insufficient rainfall were identified. It was observed that the descending phase impacted excess rainfall events during the winter and pre-monsoon seasons, while the ascending phase notably affected the monsoon and post-monsoon seasons. The study specifically examined the different magnetic polarities of sunspots in alternating solar cycles, focusing on even and odd cycles. It was found that extreme rainfall events were more frequent during the winter and pre-monsoon seasons in even cycles, whereas in odd cycles they were more prevalent during the monsoon and post-monsoon seasons. These findings are presented for the first time and offer new perspectives on how different phases of the cycle affect rainfall. This study identifies a physical link between solar activity and extreme precipitation in Kerala, thereby enhancing predictability.

**Keywords:** Sunspot number, solar phases, extreme rainfall, rainfall over Kerala

## 1. Introduction

The global climate is changing drastically, posing a threat to our very existence. Solar activity, occurring in an 11-year cycle, can be observed through phenomena such as sunspots, solar flares, and coronal mass ejections (Usoskin, 2017). These events interact with Earth's atmosphere, thereby affecting our weather and climate. Sunspot number quantifies sunspots and is a widely used solar index because of its long-term availability. There is minimal evidence suggesting that solar variations significantly contribute

to recent global climate change, but substantial evidence exists for a solar impact on the climate of specific areas as well as across the atmosphere (Wasko & Sharma, 2009; Mauas et al., 2011; Rampelotto et al., 2012; Ermolli et al., 2013). There have been few studies conducted recently on the relationship between solar activity and precipitation in China (Zhai, 2017; Yu et al., 2019; Song et al., 2022), the United States (Nitka & Burnecki, 2019), Europe (Laurenz et al., 2019), Africa (Mohamed & El-Mahdy, 2021), Argentina (Heredia et al., 2019), Nepal (Tiwari et al., 2021; Gautam et al., 2024), and Northeast Asia (Song et al., 2022).

The economy, agriculture, and ecosystem in India could be seriously impacted by changing rainfall patterns (Doranalu Chandrashekar et al., 2017). Many researchers have examined the potential connection between solar activity and rainfall across India and in various regions (Jagannathan & Bhalme, 1973; Hiremath & Mandi, 2004; Badruddin & Aslam, 2015; Warrier et al., 2017; Thomas & Abraham, 2022b). The direct and indirect effects were studied, and the results were often localised and contradicted other authors (Jagannathan & Parthasarathy, 1973; Bhalme et al., 1981; Hiremath, 2006; Bhattacharyya & Narasimha, 2007; Lihua et al., 2007; Selvaraj et al., 2009; Selvaraj & Aditya, 2011; Selvaraj et al., 2013; Hiremath et al., 2015; Malik & Bronnimann, 2018; Thomas et al., 2023).

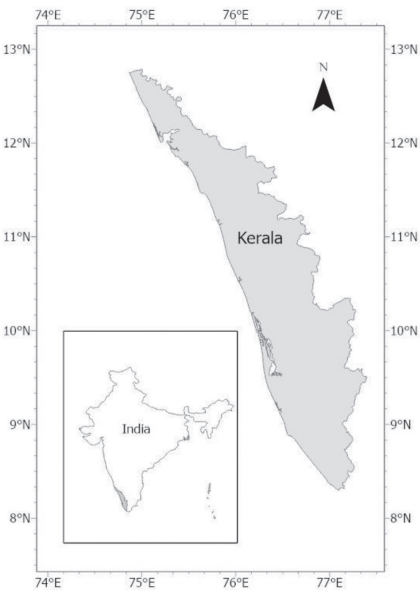

Figure 1. Location map of Kerala

Kerala is located at the southwest tip of India, bordered to the east by the Western Ghats and to the west by the Arabian Sea. Kerala has a wet, tropical climate, with the major contributions from the southwest monsoon and the post-monsoon. Kerala's diverse features make it more susceptible to climate change. It is known as the "Gateway of the summer monsoon". Studies of long-term rainfall variability revealed that rainfall during the southwest monsoon significantly decreased, while rainfall during the post-monsoon period increased (Krishnakumar et al., 2009; Kothawale & Rajeevan, 2017). Recently, a few studies reported the influence of sunspot number on the rainfall over Kerala (Thomas & Abraham, 2022a,b; Thomas et al., 2023).

## 2. Data and Methods

We have used 122 years (1901 – 2022) of rainfall data in Kerala and sunspot numbers, covering eleven complete Solar cycles (SC14 – SC24). Sunspot number (SSN) is the commonly used solar index to measure solar activity and is taken from the World Data Center SILSO, Royal Observatory of Belgium, Brussels. The dataset is available at http://www.sidc.be/silso/datafiles. Rainfall (in mm) over Kerala (RF) is obtained from the India Meteorological Department (IMD) gridded rainfall data ($0.25^\circ \times 0.25^\circ$) (Pai et al., 2014). The IMD data can be accessed from https://www.imdpune.gov.in/lrfindex.php. The location map of Kerala is shown in Figure 1.

India Meteorological Department (IMD) classifies the rainfall seasons of India as Winter (January-February), denoted JF, pre-monsoon (March-May), denoted MAM, monsoon (June-September), denoted JJAS, and post-monsoon (October-December) denoted as OND (Hiremath & Mandi, 2004; Hiremath, 2006; Bankoti et al., 2011). This study divides the rainfall values into four seasons: JF, MAM, JJAS, and OND. The sunspot number values for each season are averaged and used throughout the study.

To study the influence of solar phases on the rainfall over Kerala, sunspot data of each season is considered, and the solar phases corresponding to Solar Cycles (SC14 - SC24) are classified using the technique outlined in Sawadogo et al. (2024). According to it, the maximum sunspot number, S_Nmax, for each solar cycle is first calculated. The different phases are determined as follows: (i) minimum phase: $S\_N(t) < 0.122 \times S\_Nmax$ (ii) increasing phase: $0.122 \times S\_Nmax \leq S\_N(t)$ (iii) maximum phase: $S\_N(t) > 0.73 \times S\_Nmax$ and (iv) decreasing phase: $0.73 \times S\_Nmax \geq S\_N(t) > S\_Nmin$ (next cycle).

The years of excess and deficit rainfall over Kerala are identified to study the relationship between extreme rainfall events and solar activity. For that, the mean ($\mu$) and standard deviation ($\sigma$) of rainfall RF during all the seasons (JF, MAM, JJAS, and OND) are determined. A year i is labelled as an extreme rainfall year when $Ri \geq (\mu + \sigma)$ and a year labelled as a deficit rainfall year when $Ri \leq (\mu + \sigma)$, where Ri is the rainfall of that year, i, $k \in R$ (Azad, 2011). In this study, k is set to 1.

## 3. Results and discussion

Attempts are made to understand the possible relationship between solar phases and extreme precipitation events in Kerala during different seasons (JF, MAM, JJAS, and OND). For that the years of excess and deficit rainfall are first identified, as explained in Section 2 (Azad, 2011). The solar phases of Solar Cycles 14-24 are determined using the criterion given in Section 2 from the sunspot data for all seasons. Tables 1, 2, 3, and 4 show the classification of phases during the JF, MAM, JJAS, and OND seasons. The relative timing of solar activity and extreme rainfall is evaluated across different seasons. Figures 2, 3, 4, and 5 show the extreme rainfall events during JF, MAM, JJAS, and OND seasons, along with the phase classifications. The black circle represents years with excess rainfall, and the red circle represents years with deficient rainfall. The decreasing and minimum phases are combined as the descending phase, and the increasing and maximum phases as the ascending phase.

The present study covers 11 complete solar cycles (Solar cycles 14-24), starting from 1901. On numbering these cycles sequentially from 1 to 11, our study covers six odd and five even cycles. Extreme rainfall events during odd and even cycles are also evaluated.

**JF season**

A total of 16 excess and 12 deficit rainfall years are noted during the JF season and are listed below:

Excess (E) years: 1901, 1909, 1917, 1920, 1922, 1928, 1934, 1938, 1943, 1948, 1952, 1962, 1963, 1984, 2000, 2011.

Deficit (D) years: 1931, 1940, 1949, 1964, 1973, 1976, 1980, 1982, 1983, 1989, 1992, 2009

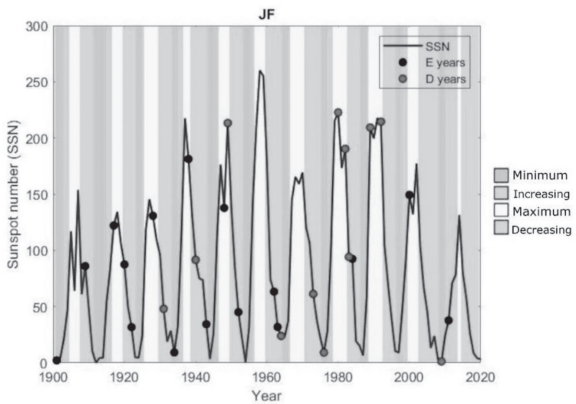


Figure 2. Solar phases during Solar cycles 11-24 along with extreme years of rainfall, during the JF season. E denotes excess rainfall and D denotes deficit rainfall.

Figure 2 denotes the extreme rainfall years during the JF season plotted on the SSN curve. The different phases during the solar cycles 14-24 are also indicated. During this season, excess rainfall events are observed more than deficit ones. Out of 16 excess rainfall years observed, 10 occurred during the descending phase and 6 during the ascending phase of the solar cycles considered. In the case of 12 deficit rainfall years, 7 occurred during the descending phase and 5 during the ascending phases of the solar cycles.

While studying the even and odd cycles, it was observed that even cycles tend to have more extreme rainfall occurrences (excess/deficit) than the odd cycles. Another observation from Figure 2 is that 8 out of 12 deficit years occur when solar activity is at minimum or maximum levels during the solar cycle.

**MAM season**

During the MAM season, 12 excess and 10 deficit rainfall years are observed and listed below:

Excess (E) years: 1909, 1989, 1930, 1933, 1936, 1943, 1955, 1958, 1960, 1999, 2004, 2006

Deficit (D) years: 1906, 1914, 1945, 1979, 1983, 1986, 1987, 1993, 2000, 2019 179

Excess and deficient rainfall years during the MAM season are indicated on the SSN curve in Figure 3, with different solar phases. Out of the 12 excess rainfall years observed in this season, 8 occurred during the decreasing phase and 4 during the ascending phase of different solar cycles. It was observed that even cycles exhibit more extreme rainfall events (excess/deficit) than older cycles, similar to the JF season.

**Table 1: Solar cycles 14-24 classification of phases, during JF season**

| Solar cycle | Minimum | Maximum | Increasing | Decreasing |
|---|---|---|---|---|
| 14 | 1901-1902 | 1905-1907 | 1903-1904 | 1908-1911 |
| 15 | 1912-1914 | 1917-1919 | 1915-1916 | 1920-1923 |
| 16 | 1924 | 1926-1929 | 1925 | 1930-1933 |
| 17 | 1934 | 1937-1938 | 1935-1936 | 1939-1943 |
| 18 | 1944-1945 | 1947-1949 | 1946 | 1950-1953 |
| 19 | 1954-1955 | 1957-1959 | 1956 | 1960-1964 |
| 20 | 1965 | 1967-1970 | 1966 | 1971-1975 |
| 21 | 1976 | 1979-1982 | 1977-1978 | 1983-1986 |
| 22 | 1987 | 1989-1992 | 1988 | 1993-1996 |
| 23 | 1997 | 2000-2002 | 1998-1999 | 2003-2008 |
| 24 | 2009 | 2014 | 2010-2013 | 2015-2019 |

**Table 2: Solar cycles 14-24 classification of phases, during MAM season**

| Solar cycle | Minimum | Maximum | Increasing | Decreasing |
|---|---|---|---|---|
| 14 | 1901-1902 | 1905-1908 | 1903-1904 | 1909-1912 |
| 15 | 1913-1914 | 1916-1918 | 1915 | 1919-1922 |
| 16 | 1923 | 1926-1928 | 1924-1925 | 1929-1932 |
| 17 | 1933-1934 | 1937-1939 | 1935-1936 | 1940-1943 |
| 18 | 1944 | 1947-1948 | 1945-1946 | 1950-1953 |
| 19 | 1954-1955 | 1957-1959 | 1956 | 1960-1963 |
| 20 | 1964-1965 | 1967-1970 | 1966 | 1971-1974 |
| 21 | 1975-1977 | 1979-1982 | 1978 | 1983-1985 |
| 22 | 1986 | 1989-1991 | 1987-1988 | 1992-1995 |
| 23 | 1996-1997 | 2000-2002 | 1998-1999 | 2003-2008 |
| 24 | 2009 | 2012-2014 | 2010-2011 | 2015-2019 |

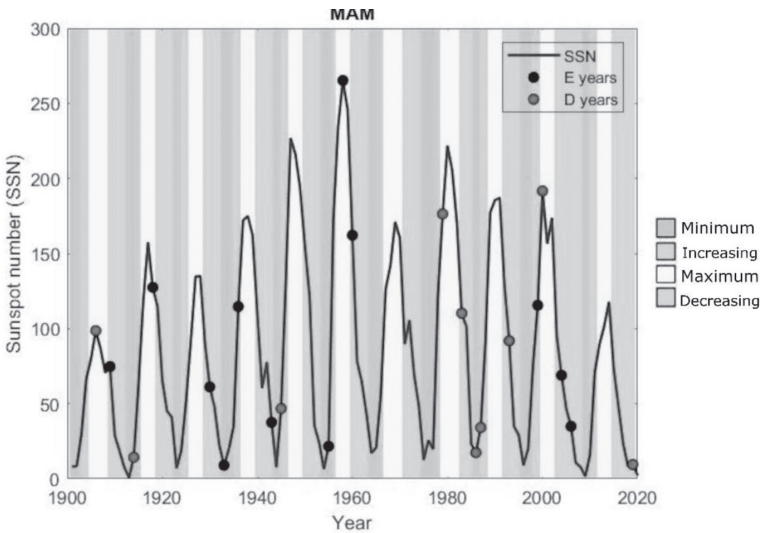


igure 3. Solar phases during Solar cycles 11-24 along with extreme years of rainfall, durir the MAM season. E denotes excess rainfall and D denotes deficit rainfall.

**JJAS season**

In the case of the JJAS season, 13 excess and 7 deficit rainfall events are seen and they are listed below.

Excess (E) years: 1907, 1924, 1931, 1933, 1946, 1950, 1959, 1961, 1968, 1975, 1981, 2007, 2013

Deficit (D) years: 1918, 1952, 1965, 1976, 1987, 2002, 2016

A plot of the extreme rainfall years during the JJAS season is shown in Figure 4. There are also indications of the phases during solar cycles 14-24. During this season, 13 excess rainfall years have been recorded, 6 in the decreasing phase and 7 in the ascending phase. Out of the total 7 deficit years, 4 were visible during the ascending phase and 3 during the descending phase. In this season, the ascending phase appears to have more extreme rainfall events than the descending phase. In contrast to the JF and MAM seasons, the odd cycles experienced more excess and deficit rainfall years than the even cycles.

**Table 3: Solar cycles 14-24 classification of phases, during JJAS season**

| Solar cycle | Minimum | Maximum | Increasing | Decreasing |
|---|---|---|---|---|
| 14 | 1901-1902 | 1905-1908 | 1903-1904 | 1909-1912 |
| 15 | 1913-1914 | 1917-1919 | 1915-1916 | 1920-1922 |
| 16 | 1923 | 1928 | 1924-1927 | 1929-1932 |
| 17 | 1933-1934 | 1937-1939 | 1935-1936 | 1940-1943 |
| 18 | 1944 | 1947-1949 | 1945-1946 | 1950-1953 |
| 19 | 1954-1955 | 1956-1959 | 1955 | 1960-1963 |
| 20 | 1964 | 1967-1970 | 1965-1966 | 1971-1975 |
| 21 | 1976 | 1979-1981 | 1977-1978 | 1982-1985 |
| 22 | 1986 | 1989-1991 | 1987-1988 | 1992-1995 |
| 23 | 1996 | 1999-2002 | 1997-1998 | 2003-2007 |
| 24 | 2008-2009 | 2011-2014 | 2010 | 2015-2018 |

**OND season**

During the OND season, 11 excess and 15 deficit rainfall events are noticed and are listed below 197

Excess (E) years: 1902, 1930, 1932, 1939, 1944, 1946, 1966, 1977, 1997, 2006, 2010 198

Deficit (D) years: 1904, 1908, 1927, 1938, 1947, 1949, 1967, 1974, 1982, 1985, 1988, 1995, 2000, 2012, 2016

Figure 5 illustrates the excess and deficient rainfall years during the OND season with different solar phases. Out of 11 excess rainfall years observed, 5 occurred during the descending phase and 6 during the ascending phase of the solar cycles considered. In the case of 15 deficit rainfall years, 6 occurred during the descending phase and 9 during the ascending phases of the solar cycles.

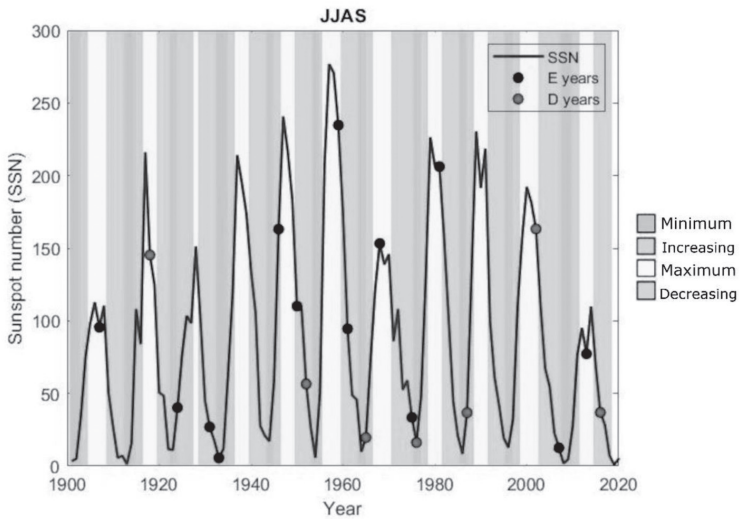


Figure 4. Solar phases during Solar cycles 11-24 along with extreme years of rainfall, during the JJAS season. E denotes excess rainfall and D denotes deficit rainfall.

**Table 4: Solar cycles 14-24 classification of phases, during OND season**

| Solar cycle | Minimum | Maximum | Increasing | Decreasing |
|---|---|---|---|---|
| 14 | 1901-1902 | 1905-1907 | 1903-1904 | 1908-1912 |
| 15 | 1913 | 1917-1918 | 1914-1916 | 1919-1922 |
| 16 | 1923 | 1925-1929 | 1924 | 1930-1932 |
| 17 | 1933-1934 | 1936-1938 | 1935 | 1939-1942 |
| 18 | 1943 | 1946-1949 | 1944-1945 | 1950-1952 |
| 19 | 1953-1954 | 1956-1958 | 1955 | 1959-1963 |
| 20 | 1964 | 1967-1970 | 1965-1966 | 1971-1974 |
| 21 | 1975-1976 | 1979-1981 | 1977-1978 | 1982-1984 |
| 22 | 1986 | 1988-1991 | 1987 | 1992-1995 |
| 23 | 1996 | 1999-2002 | 1997-1998 | 2003-2007 |
| 24 | 2008-2009 | 2011-2014 | 2010 | 2015-2018 |

This study explored how various phases of solar activity may affect extreme rainfall events in Kerala. The descending phase was found to play a significant role in the occurrence of excess rainfall in the JF and MAM seasons, and the ascending phase was found to play a significant role in the occurrence of excess rainfall in the JJAS and OND seasons. Due to the magnetic polarity of the sunspots differing between the alternate solar cycles, the study was carried out for the even and odd cycles. The even cycles witnessed more extreme rainfall events during the JF and MAM seasons, while the odd cycles witnessed more extreme rainfall events during the JJAS and OND seasons. This is the first time the potential relationship between the solar phases and intense rainfall events has been investigated in detail.

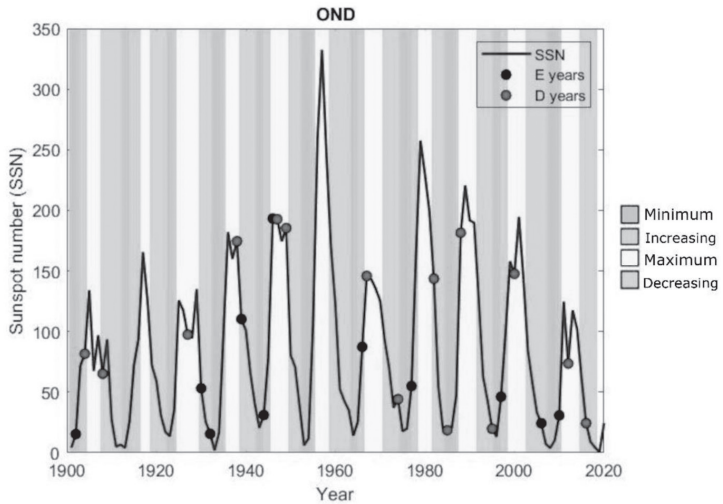


Figure 5. Solar phases during Solar cycles 11-24 along with extreme years of rainfall, during the OND season. E denotes excess rainfall and D denotes deficit rainfall.

Several Indian studies have documented floods and droughts during solar maximum and minimum periods. Bhalme & Mooley (1981) observed that the Flood Area Index over India was associated with the double sunspot cycle. During alternate solar cycles, Ananthakrishnan & Parthasarathy (1984) noted significantly more excess rainfall years during the ascending phase. According to Jain & Tripathy (1997), the periodicity of floods and droughts are well correlated with sunspot main periods and quasi-periods in the Udaipur subtropical region of Rajasthan. Bhattacharyya & Narasimha (2005) have shown that high rainfall correlates with high solar activity, while low rainfall correlates with low solar activity.

## 4. Conclusions

The influence of solar activity on Earth's climate has been an interesting research topic for a long. This work examined the possible impact of sunspot numbers on the rainfall over Kerala using 122 years of data. The association between different phases of solar activity and the extreme precipitation events over Kerala, India, was evaluated in this study. The solar phases (minimum,

increasing, maximum, and decreasing) of Solar Cycles 14-24 were determined for all the seasons. The years when Kerala saw excessive or insufficient rainfall were identified, and their relationship with the different phases was investigated. The descending phase was observed to affect excess rainfall events (excess/deficit) during the winter and pre-monsoon seasons. In contrast, the ascending phase had a notable effect during the monsoon and post-monsoon seasons, i.e., different phases influence different seasons. The study focused on the different magnetic polarities of sunspots across alternating solar cycles, specifically examining even and odd cycles. Extreme rainfall events were more frequent during the winter and pre-monsoon seasons in even cycles, whereas in odd cycles they were more prevalent during the monsoon and post-monsoon seasons. These findings are presented for the first time and may offer fresh insights into how different phases affect rainfall. This study raises the possibility of a physical link between solar activity and extreme precipitation in Kerala, which could improve predictability and future climate change research. Including other natural factors, such as ENSO, in future studies will help clarify the indirect effects of solar activity on rainfall.

**References**

Ananthakrishnan, R., & Parthasarathy, B. (1984). Indian rainfall in relation to the sunspot cycle: 1871-1978. *J. Climatol.,* 4(2), 149–169.

Azad, S. (2011). Extreme Indian Monsoon Rainfall Years and the Sunspot Cycle. *Adv. Sci. Lett.,* 4(1), 159–164.

Badruddin, & Aslam, O. P. (2015). Influence of cosmic-ray variability on the monsoon rainfall and temperature. *J. Atmos. Sol.-Terr. Phys.,* 122, 86–96.

Bankoti, N. S., Joshi, N. C., Pande, S. et al. (2011). Correlative study of different solar activity features with all India homogeneous rainfall during 1963-2006. *Quat. Int,* 229(1-2), 8–15.

Bhalme, H., & Mooley, D. (1981). Cyclic fluctuations in the flood area and relationship with the double (hale) sunspot cycle. *J. Appl. Meteorol.,* 20(9), 1041–1048.

Bhalme, H., Reddy, R., Mooley, D. et al. (1981). Solar activity and Indian weather/climate. *Proc. Indian Acad, Sci. (Earth Planet. Sci.),* 90(3), 245–262.

Bhattacharyya, S., & Narasimha, R. (2005). Possible association between Indian monsoon rainfall and solar activity. *Geophys. Res. Lett.,* 32(5), 1–5.

Bhattacharyya, S., & Narasimha, R. (2007). Regional differentiation in multidecadal connections between Indian monsoon rainfall and solar activity. *J. Geophys. Res. Atmos.,* 112(24), 1–10.

Doranalu Chandrashekar, V., Shetty, A., Singh, B. B. et al. (2017). Spatio-temporal precipitation variability over Western Ghats and Coastal region of Karnataka, envisaged using high resolution observed gridded data. *Model. Earth Syst. Environ.,* 3(4), 1611–1625.

Ermolli, I., Matthes, K., Dudok De Wit, T. et al. (2013). Recent variability of the solar spectral irradiance and its impact on climate modelling. *Atmos. Chem. Phys.,* 13(8), 3945–3977.

Gautam, S. P., Silwal, A., Baral, B. D. et al. (2024). The possible impact of solar activity on rainfall in Nepal: A case study. *Adv. Space Res.,* 74(5), 2133–2143.

Heredia, T., Bazzano, F. M., Cionco, R. G. et al. (2019). Searching for solar-like interannual to bidecadal effects on temperature and precipitation over a southern hemisphere location. *J. Atmos. Sol.-Terr. Phys,* 193, 105094.

Hiremath, K. M. (2006). The Influence of Solar Activity on the Rainfall over India: Cycle-to-Cycle Variations. *J. Astrophys. Astr.,* 27, 367–372.

Hiremath, K. M., & Mandi, P. I. (2004). Influence of the solar activity on the Indian Monsoon rainfall. *New Astron.,* 9(8), 651–662.

Hiremath, K. M., Manjunath, H., & Soon, W. (2015). Indian summer monsoon rainfall: Dancing with the tunes of the sun. *New Astron.,* 35, 8–19.

Jagannathan, P., & Bhalme, H. (1973). Changes in the pattern of distribution of southwest monsoon rainfall over india associated with sunspots. *Mon. Weather Rev.,* 101(9), 691–700.

Jagannathan, P., &Parthasarathy, B. (1973). Trends and Periodicities of 351 Rainfall Over India. *Mon. Weather Rev.,* 101(4), 371–375.

Jain, R., & Tripathy, S. C. (1997). Correlation study between sunspot and rainfall in Udaipur subregion. *Mausam,* 48(3), 405–412.

Kothawale, D. R., & Rajeevan, M. (2017). Monthly, Seasonal and Annual Rainfall Time Series for All-India, Homogeneous Regions and Meteorological Subdivisions: 1871-2016. Indian Institute of Tropical Meteorology (IITM) Earth System Science Organization, Ministry of Earth Sciences, 02, 1–164.

Krishnakumar, K. N., Prasada Rao, G. S., & Gopakumar, C. S. (2009). Rainfall trends in twentieth century over Kerala, *India. Atmos. Environ,* 43(11), 1940–1944.

Laurenz, L., Ludecke, H. J., & Luning, S. (2019). Influence of solar activity changes on European rainfall. *J. Atmos. Sol.-Terr. Phys.,* 185, 29–42.

Lihua, M., Yanben, H., & Zhiqiang, Y. (2007). The possible influence of solar activity on Indian summer monsoon rainfall. *Appl. Geophys.,* 4(3), 231–237.

Malik, A., Bronnimann, S., Stickler, A. et al. (2017). Decadal to multi-decadal scale variability of Indian summer monsoon

rainfall in the coupled ocean-atmosphere chemistry climate model SOCOL-MPIOM. *Clim. Dyn.,* 49(9-10), 3551–3572.

Mauas, P. J., Buccino, A. P., & Flamenco, E. (2011). Long-term solar activity influences on South American rivers. *J. Atmos. Sol.-Terr. Phys.*, 73(2-3), 377–382.

Mohammed, M. A., & El-Mahdy, M. E. S. (2021). Impact of sunspot activity on the rainfall patterns over eastern Africa: A case study of Sudan and South Sudan. *J.Water Clim. Change,* 12(5), 2104–2124.

Nitka,W., & Burnecki, K. (2019). Impact of solar activity on precipitation in the United States. *Physica A: Statistical Mechanics and its Applications,* 527, 121387.

Pai, D. S., Sridhar, L., Rajeevan, M. et al. (2014). Development of a new high spatial resolution (0.25° × 0.25°) long period (1901-2010) daily gridded rainfall dataset over India and its comparison with existing data sets over the region. *Mausam,* 65(1), 1–18.

Rampelotto, P. H., Rigozo, N. R., da Rosa, M. B. et al. (2012). Variability of rainfall and temperature (1912-2008) parameters measured from Santa Maria (29°41'S, 53°48'W) and their connections with ENSO and solar activity. *J. Atmos. Sol.-Terr. Phys.,* 77, 152–160.

Selvaraj, R. S., & Aditya, R. (2011). Study on the correlation between the southwest and northeast monsoon rainfall over Tamil Nadu. Univers. *J. Environ. Res. Technol.,*1(4).

Selvaraj, R. S., Muthuchami, A., & Nancharaiah, M. (2009). Influence of sunspot activity on the annual rainfall of Tamil Nadu, India. *Indian J. Phys.,* 83(9),1251–1258.

Selvaraj, R. S., Umarani, R., Mahalakshmi, N. et al. (2013). Correlative study on Solar activity and all India rainfall : Cycle to Cycle Analysis. *J. Ind. Geophys. Union,* 17(1), 59–63.

Song, Y., Li, Z., Gu, Y. et al. (2022). Impact of solar activity on snow cover variation over the Tibetan plateau and linkage to the summer precipitation in China. *Front. Earth Sci.,* 9, 756762.

Thomas, E., & Abraham, N. P. (2022a). Impact of solar activity on the seasonal rainfall of Kerala, India. India (January 26, 2022).

Thomas, E., & Abraham, N. P. (2022b). Relationship between sunspot number and seasonal rainfall over Kerala using wavelet analysis. *J. Atmos. Sol.-Terr. Phys,* 240, 105943.

Thomas, E., Joseph, I., & Abraham, N. P. (2023). Wavelet analysis of annual rainfall over Kerala and sunspot number. *New Astron,* 98,101944.

Tiwari, B., Xu, J., Adhikari, B. et al. (2021). Wavelet and cross correlation analysis on some climatology parameters of Nepal. *BIBECHANA,* 18, 105–116.

Usoskin, I. G. (2017). A History of Solar Activity over Millennia. Living Rev. *Solar Phys,* 14, 3.

Warrier, A. K., Sandeep, K., & Shankar, R. (2017). Climatic periodicities recorded in lake sediment magnetic susceptibility data: Further evidence for solar forcing on Indian summer monsoon. *Geosci. Front.,* 8(6), 1349–1355.

Wasko, C., & Sharma, A. (2009). Effect of solar variability on atmospheric moisture storage. *Geophys. Res. Lett.,* 36(3).

Yu, X., Wang, Y., Yu, S. et al. (2019). Synchronous droughts and floods in the southern Chinese loess plateau since 1646 CE in phase with decadal solar activities. *Glob. Planet Change,* 183, 103033.

Zhai, Q. (2017). Influence of solar activity on the precipitation in the North-central China. *New Astron.,* 51, 1339–1351.

# Hydrothermal Synthesis, Spectral Characterization and Photocatalytic Activity of Two Cu (II)-Based Coordination Polymers Derived from Aromatic Dicarboxylates

**[1]Karthika V Gopal and [2]Sujesh Baby**

[1] Indira Gandhi College of Arts & Science, Nellikkuzhi, Kothamangalam, Ernakulam

[2]Associate Professor, Department of Chemistry, Christian College, Chengannur

**Abstract:** Two new Cu(II)-based coordination polymers, $\{[Cu(C_6H_{12}N_4)0.5(C_8H_4O_4)]\cdot 5H_2O\}_n$ (1) and $\{[Cu(C_4H_{12}N_2)(C_8H_4O_4)_2]\cdot H_2O\}_n$ (2), have been synthesized through a hydrothermal route employing mixed(1:1)aqueous-dimethyl formamide medium. The compounds were characterized by elemental analysis, infrared spectroscopy, electronic spectroscopy, thermal analysis and magnetic susceptibility measurements. Infrared spectral data indicate monodentate coordination of the carboxylate groups in both the compounds. Electronic spectral and magnetic studies suggest square planar geometry around Cu(II) in compound 1 and distorted octahedral geometry in compound 2. Thermogravimetric analysis reveals the presence of lattice water molecules and good thermal stability of the framework materials. The synthesized coordination polymers also exhibit photocatalytic activity toward degradation of organic dyes under UV irradiation, indicating their potential utility in wastewater purification applications.

**Keywords:** Coordination polymers, hydrothermal synthesis, photocatalytic activity.

## Introduction

Coordination polymers and metal–organic frameworks (MOFs) have emerged as an important class of crystalline materials owing to their fascinating structural diversity and promising applications in gas storage, catalysis, sensing, magnetism and photocatalysis. The structural versatility of these materials arises from the combination of metal ions with multifunctional organic ligands through coordination-driven self-assembly processes.

Among the various organic linkers employed, carboxylate ligands occupy a prominent position because of their rich coordination modes and ability to generate multidimensional architectures. Copper(II)-based coordination polymers are particularly attractive due to the stereochemical flexibility associated with the d9 electronic configuration. The Jahn–Teller distorted coordination environment often results in diverse structural geometries such as square planar, square pyramidal and distorted octahedral arrangements. Aromatic dicarboxylates such as phthalic acid and terephthalic acid are widely utilized as bridging ligands in MOF chemistry because of their rigid structures and efficient coordination abilities. In recent years, considerable attention has been devoted to the development of Cu(II)-carboxylate coordination polymers with auxiliary nitrogen donor ligands. The incorporation of neutral N-donor ligands can significantly influence the dimensionality, topology and functional properties of the resulting frameworks.

In the present study, two Cu(II)-based coordination polymers incorporating isomeric aromatic dicarboxylates and auxiliary nitrogen donor ligands have been synthesized through a hydrothermal method. Their structural features were investigated using elemental, spectral, magnetic and thermal techniques, and their photocatalytic activities toward dye degradation were evaluated.

## Experimental

### Materials and Methods

Copper nitrate, phthalic acid, terephthalic acid, hexamethylenetetramine and 1,4-diaminobutane were obtained commercially and used without further purification. Distilled water and dimethylformamide (DMF) were used as solvents.

Infrared spectra were recorded using a Perkin Elmer IR spectrophotometer operating in the range 4000–400 cm−1 in ATR mode. Electronic spectra were recorded using a Shimadzu UV–160A spectrophotometer. Elemental analyses were carried

out using a Vario EL III elemental analyzer. Thermogravimetric analyses were performed on Perkin Elmer TG-DTA instrument under nitrogen atmosphere with a heating rate of 10 °C min−1. Magnetic susceptibility measurements were carried out at room temperature using a Sherwood Scientific magnetic susceptibility balance.

Synthesis of $\{[Cu(C_6H_{12}N_4)0.5(C_8H_4O_4)]\cdot 5H_2O\}_n$ (1)

Coppernitrate(0.242g),phthalicacid(0.332g)andhexamethylenetetramine (0.140 g) were taken in a Teflon-lined vessel. Distilled water (6 mL) and DMF (6 mL) were added and the mixture was stirred thoroughly. The sealed autoclave was heated at 120 °C for 48 hours and then cooled slowly to room temperature. Light blue crystals obtained were filtered, washed with water and dried in air. Yield: 60%.

Synthesis of $\{[Cu(C_6H_{12}N_2)(C_8H_4O_4)2]\cdot H_2O\}_n$ (2)

Copper nitrate (0.242 g), terephthalic acid (0.332 g) and 1,4-diaminobutane (0.1 mL) were placed in a Teflon-lined vessel containing distilled water (6 mL) and DMF (6 mL). The reaction mixture was heated hydrothermally at 120 °C for 48 h. After gradual cooling, blue needle-shaped crystals were isolated by filtration, washed and dried in air. Yield: 55%.

**Results and Discussion**

Elemental Analysis

The experimentally observed elemental analytical values are in good agreement with the theoretically calculated values, thereby supporting the proposed compositions of the synthesized coordination polymers.

For compound 1, $\{[Cu(C_6H_{12}N_4)0.5\ (C_8H_4O_4)]\cdot 5H_2O\}n$, the experimentally determined carbon, hydrogen and nitrogen contents were 30.77%, 4.51% and 7.27%, respectively, while the corresponding calculated values were 30.94%, 4.64% and 7.22%. Likewise, compound 2, $\{[Cu(C_4H_{12}N_2)(C_8H_4O_4)2]\cdot H_2O\}_n$, showed experimental values of C 48.20%, H 4.06% and N 5.83%, which

are in close agreement with the calculated values of 48.19%, 4.41% and 5.62%, respectively. The close correspondence between the observed and calculated analytical data confirms the purity and stoichiometry of the synthesized coordination polymers.

**Infrared Spectral Studies**

The characteristic IR absorption bands provide significant information regarding the coordination behavior of the ligands and the nature of the coordination environment around the Cu(II) centers. For compound 1, the asymmetric stretching vibration, $\nu as(CO_2)$, and symmetric stretching vibration, $\nu s(CO_2)$, of the carboxylate group were observed at 1594 and 1391 $cm^{-1}$, respectively, giving a $\Delta\nu$ value of 203 $cm^{-1}$. This relatively large separation between $\nu as(CO_2)$ and $\nu s(CO_2)$ indicates the monodentate coordination mode of the carboxylate group of the 1,2-benzenedicarboxylate ligand. An absorption band observed in the region 1000–1100 $cm^{-1}$ corresponds to the characteristic C–N stretching vibration of coordinated hexamethylenetetramine, confirming its involvement in coordination with the Cu(II) ion. The broad absorption band appearing in the region 2900–3050 $cm^{-1}$ is attributed to C–H stretching vibrations, while the broad bands observed around 3400–3460 $cm^{-1}$ are assigned to O–H stretching vibrations of lattice water molecules present in the framework.

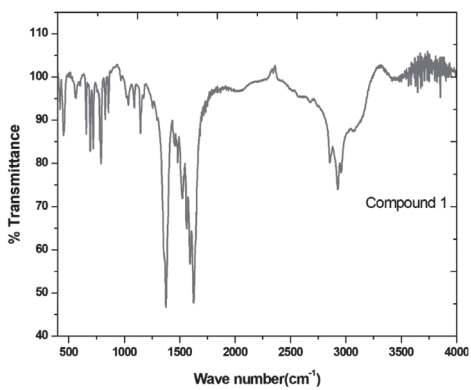


**Fig.3.1** IR Spectra of compound **1**

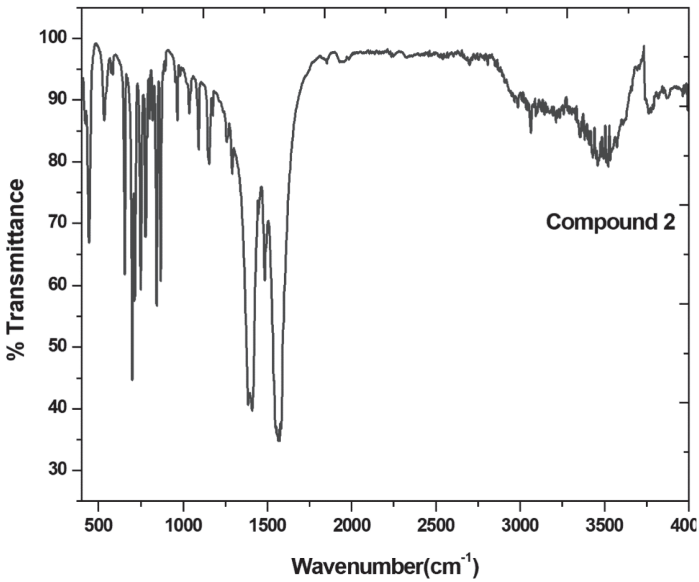


**Fig.3.2 IR Spectra of compound 2**

In compound 2, the $\nu as(CO_2)$ and $\nu s(CO_2)$ vibrations appeared at 1593 and 1394 $cm^{-1}$, respectively, with a $\Delta\nu$ value of 199 $cm^{-1}$, suggesting monodentate coordination of the carboxylate groups of the terephthalate ligand. A broad absorption band observed in the region 3150–3300 $cm^{-1}$ can be attributed to N–H stretching vibrations of the coordinated 1,4-diaminobutane ligand. In addition, broad bands appearing near 3400 $cm^{-1}$ indicate the presence of lattice water molecules in compound 2 as well. The IR spectral features therefore support the proposed coordination modes and compositions of the synthesized coordination polymers. IR spectral details are given in Fig. 3.1 and Fig.3.2.

**Electronic Spectral Studies and Magnetic Measurements**

Electronic spectra of the synthesized Cu(II) coordination polymers were recorded in the solid state due to the insoluble nature of the compounds in common organic solvents. The observed absorption bands are characteristic of d–d transitions associated with Cu(II) centers and provide useful information

regarding the coordination environment around the metal ion. Since Cu(II) possesses a $d^9$ electronic configuration and frequently undergoes Jahn–Teller distortion, the electronic spectra generally appear as broad and unsymmetrical bands. Compound 1 exhibited a broad absorption band centered at 18181 $cm^{-1}$, which can be assigned to the $^2B_1g \rightarrow {}^2A_1g$ transition generally observed for square-planar Cu(II) complexes. The spectral pattern suggests the presence of a tetragonally distorted coordination environment around the Cu(II) ion. In the case of compound 2, the absorption maximum observed at 16949 $cm^{-1}$ may be attributed to the $^2B_1g \rightarrow {}^2B_1g$ transition, characteristic of octahedral or distorted octahedral Cu(II) complexes. The comparatively lower transition energy indicates the influence of ligand field distortion around the Cu(II) center. Although the broad nature of Cu(II) electronic spectra makes exact structural assignment difficult, the observed spectral features, together with elemental, infrared and thermal analytical data, support the proposed square-planar geometry for compound 1 and distorted octahedral geometry for compound 2. The electronic spectral data therefore provide additional evidence for the successful formation of the Cu(II)-based coordination polymers. The electronic spectra of compounds 1 and 2 are shown in Fig. 3.3.

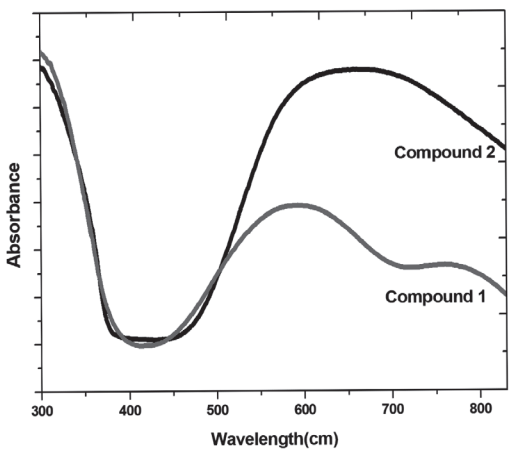


Fig. 3.3 Electronic spectra of compound1&2

The magnetic moments of compounds 1 and 2 were measured at room temperature using a digital Gouy balance. Compound 1 exhibited a magnetic moment value of 1.74 BM, while compound 2 showed a value of 1.72 BM. These values are consistent with the presence of one unpaired electron associated with the Cu(II) ion in both coordination polymers.

**Thermal Analysis**

Thermogravimetric analysis (TGA) was carried out under a nitrogen atmosphere in order to investigate the thermal stability and decomposition behavior of the synthesized coordination polymers. Both compounds exhibited multistep decomposition patterns, indicating the sequential loss of lattice molecules followed by decomposition of the coordination framework. For compound 1, an initial weight loss was observed in the temperature range 92–104 °C, which can be attributed to the removal of lattice water molecules present in the framework. The experimentally observed weight loss was found to be in close agreement with the calculated value, confirming the presence of coordinated or lattice water molecules. A second major decomposition stage occurred between 283 and 356 °C, corresponding to the decomposition of the organic ligands and collapse of the coordination framework, ultimately leading to the formation of CuO as the final residue. Compound 2 also exhibited an initial decomposition stage in the temperature range 90–98 °C due to the loss of lattice water molecules. Further heating resulted in decomposition of the organic framework in the range 276–333 °C, yielding CuO as the final decomposition product. The thermal decomposition pattern indicates that both coordination polymers possess moderate thermal stability before undergoing framework degradation at elevated temperatures. The close agreement between the experimentally observed and theoretically calculated weight losses further supports the proposed compositions of the synthesized coordination polymers.

**Proposed Structures**

Based on the elemental analytical data, infrared spectral studies, electronic spectral analysis, magnetic susceptibility measurements and thermogravimetric investigations, tentative structures have been proposed for the synthesized Cu(II)-based coordination polymers. Compound 1 is proposed to contain square-planar Cu(II) centers coordinated by phthalate and hexamethylenetetramine ligands, together with lattice water molecules stabilized within the framework. The coordination environment around the Cu(II) ion is likely influenced by the nitrogen donor atoms of hexamethylenetetramine and the oxygen donor atoms of the monodentately coordinated phthalate ligands, resulting in the formation of an extended coordination network. Compound 2 is suggested to possess a distorted octahedral coordination geometry around the Cu(II) center, where terephthalate ligands and 1,4-diaminobutane act as bridging units to generate an extended polymeric framework. The terephthalate moieties provide oxygen donor sites, while the diamine ligand contributes nitrogen donor atoms, facilitating the construction of multidimensional coordination architectures. The combined analytical and spectroscopic investigations therefore support the successful formation of two distinct Cu(II)-based coordination polymers with different coordination geometries and structural arrangements.

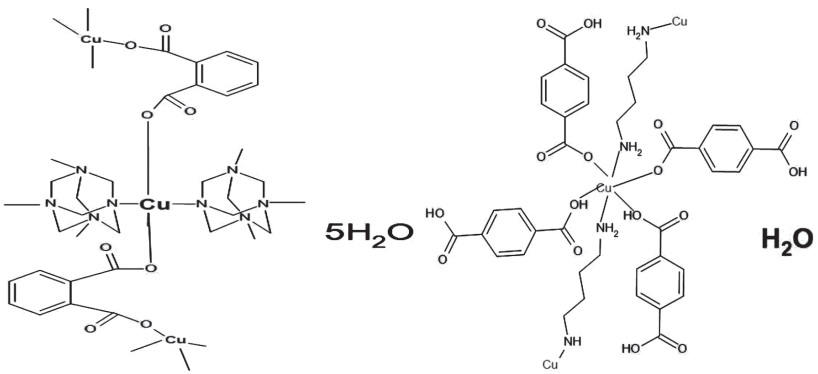


**Photocatalytic Activity**

Organic dyes such as methyl orange (MO), methylene blue (MB) and rhodamine B (RhB) are widely used in textile and dyeing industries and are known for their resistance to biodegradation, thereby posing serious environmental concerns. The degradation of these dye molecules into simpler and less harmful species is therefore of considerable importance in wastewater treatment. In the present study, the photodegradation of these organic dyes was employed as a model reaction to evaluate the photocatalytic activities of compounds 1 and 2. The degradation curves for the photocatalytic studies are shown in Fig. 3.4.

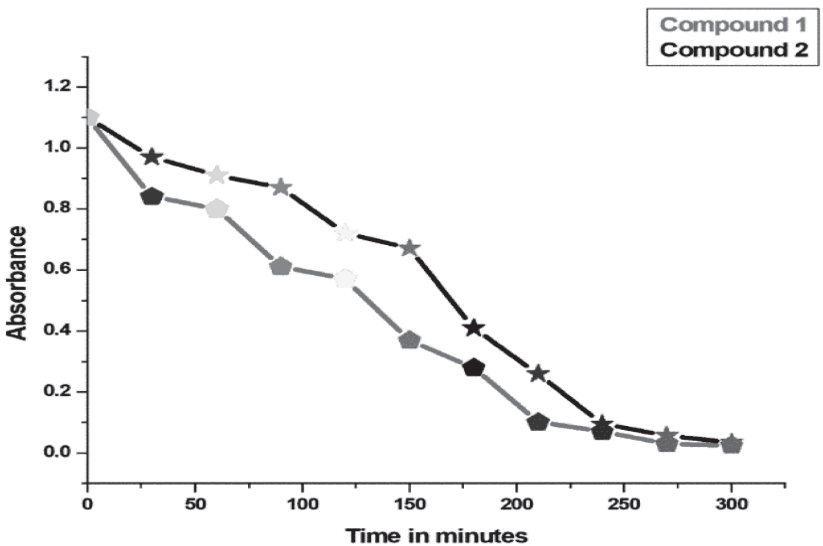


Fig. 3.4. Degradation curves of compound 1 and 2

The degradation of methyl orange was monitored using its characteristic absorption band at 464 nm. Under UV irradiation in the absence of any catalyst, negligible degradation of MO was observed, indicating the poor self-decomposition ability of the dye. In contrast, the presence of the synthesized coordination polymers significantly enhanced the degradation process, demonstrating their photocatalytic efficiency. Methylene blue showed comparatively higher photodegradation under UV irradiation and was almost completely degraded after 5 h even

in the absence of catalyst. However, the degradation efficiency was further improved in the presence of compounds 1 and 2. The enhanced photocatalytic behavior of the synthesized coordination polymers may be attributed to effective photoinduced electron transfer processes occurring within the Cu(II)-based coordination frameworks.\n\nThe degradation profiles clearly indicate that the synthesized polymeric materials can function as efficient photocatalysts for the degradation of organic dyes and may therefore find potential applications in the purification of contaminated wastewater.

**Conclusion**

In conclusion, two new Cu(II)-based coordination polymers containing aromatic dicarboxylate ligands and auxiliary nitrogen donor ligands were successfully synthesized via a hydrothermal route. The synthesized compounds were characterized using elemental analysis, infrared spectroscopy, electronic spectroscopy, magnetic susceptibility measurements and thermogravimetric analysis. The combined analytical and spectroscopic investigations suggest a square-planar coordination geometry around the Cu(II) center in compound 1, whereas compound 2 is proposed to possess a distorted octahedral geometry. Infrared spectral studies revealed monodentate coordination of the carboxylate groups in both coordination polymers. Thermogravimetric analysis demonstrated moderate thermal stability of the frameworks and confirmed the presence of lattice water molecules in the structures. In addition, the synthesized Cu(II)-based coordination polymers exhibited appreciable photocatalytic activity toward the degradation of organic dyes under UV irradiation, indicating their potential application in wastewater purification and environmental remediation.\n\nOverall, the present study demonstrates that aromatic dicarboxylate ligands in combination with auxiliary nitrogen donor ligands provide an effective approach for constructing Cu(II)-based coordination polymers with promising structural and functional properties. Further investigations

involving single-crystal X-ray diffraction studies and detailed photocatalytic evaluations are necessary to establish the exact framework architectures and to better understand the structure–property relationships governing their catalytic behaviour.

**References**

Ahmed, A., Kelly, A., Leonard, D., Saleem, W., Bezrukov, A., Efthymiou, C. G., Zaworotko, M. J., Tiana, D., Boyd, A. & Papatriantafyllopoulou, C. (2024). *Dalton Trans.* 53, 11867–11879.

An, J. & Rosi, N. L. (2010). J. Am. Chem. Soc. 132, 5578–5579.

Banerjee, R., Phan, A., Wang, B., Knobler, C., Furukawa, H., O'Keeffe, M. & Yaghi, O. M. (2008). *Science,* 319, 939–943

Campbell, M. G., Sheberla, D., Liu, S. F., Swager, T. M. & Dinca, M. (2015). *Angew. Chem. Int. Ed.* 54, 4349–4352

Carlucci, L., Ciani, G., Maggini, S., Proserpio, D. M. & Visconti, M. (2010). *Chem. Eur. J.* 16, 12328–12341.

Chen, B., Yang, Y., Zapata, F., Lin, G., Qian, G. & Lobkovsky, E. B. (2007). *Adv. Mater.* 19, 1693–1696

Chen, M., Chen, S. S., Okamura, T., Su, Z., Chen, M. S., Zhao, Y., Sun, W. Y. & Ueyama, N. (2011). *Cryst. Growth Des.* 11, 1901–1908.

Chernikova, V., Yassine, O., Shekhah, O., Eddaoudi, M. & Salama, K. N. (2018). *J. Mater. Chem. A,* 6, 5550–5554.

Chatterjee, T., Hossain, E., Khan, S., Roy, S., Islam, M. A., Alam, S. M. & Mira, M. H. (2022). *J. Mol. Struct.* 1260, 134011.

Dai, J. C., Wu, X. T., Fu, Z. Y., Cui, C. P., Hu, S. M., Du, W. X., Wu, L. M., Zhang, H. H. & Sun, R. Q. (2002). *Inorg. Chem.* 41, 1391–1396.

Dhakshinamoorthy, A., Li, Z. & García, H. (2018). *Chem. Soc. Rev.* 47, 8134–8172.

Dolomanov, O. V., Bourhis, L. J., Gildea, R. J., Howard, J. A. K. & Puschmann, H. (2009). *J. Appl. Cryst.* 42, 339–341.

Drago, R. S. (1971). *Physical Methods in Inorganic Chemistry.* New Delhi: Affiliated East–West Press

Fan, X.-F., Deng, X.-C., Cao, Q.-L., Dong, G.-Y. & Fu, L. (2024). *J. Mol. Struct.* 1295, 136757.

Farahmand Kateshali, A., Gholizadeh Dogaheh, S., Soleimannejad, J. & Blake, A. J. (2020). *Coord. Chem. Rev.* 419, 213392.

Furukawa, H., Cordova, K. E., O'Keeffe, M. & Yaghi, O. M. (2013). *Science,* 341, 1230444.

Furukawa, H., Ko, N., Go, Y. B., Aratani, N., Choi, S. B., Choi, E., Yazaydin, A. O., Snurr, R. Q., O'Keeffe, M., Kim, J. & Yaghi, O. M. (2010). *Science,* 329, 424–428.

Guchhait, S., Baby, S., Padmanabhan, M., Medhi, A. & Nath, R. (2021). *Europhys. Lett.* 133, 57006.

Han, D. L., Liu, X. M. & Wu, S. L. (2022). *Chem. Soc. Rev.* 51, 7138–7169.

Horcajada, P., Serre, C., Vallet-Regi, M., Sebban, M., Taulelle, F. & Férey, G. (2006). *Angew. Chem. Int. Ed.* 45, 5974–5978.

Lever, A. B. P. (1984). *Inorganic Electronic Spectroscopy.* Amsterdam: Elsevier.

Liang, T.-W., Chen, C., Kusaka, S., Siddique, S. K., Chang, C.-Y., Matsuda, R. & Ho, R.-M. (2025). *J. Am. Chem. Soc.* 147, 23608–23616.

Nakamoto, K. (2009). *Infrared and Raman Spectra of Inorganic and Coordination Compounds,* 6th ed. Hoboken: Wiley.

Sathyanarayana, D. N. (2001). *Electronic Absorption Spectroscopy and Related Techniques.* Hyderabad: Universities Press.

Usman, M., Chibuike, M., Patil, D., Rigin, S., Zhang, S., Wu, Y., Lindline, J. & Timofeeva, T. V. (2020). *Inorg. Chem. Commun.* 122, 108261.

Yang, G.-P., Hou, L., Ma, L.-F. & Wang, Y.-Y. (2013). *Cryst Eng Comm,* 15, 2561–2578.

Zhou, H.-C. & Kitagawa, S. (2014). *Chem. Soc. Rev.* 43, 5415–5418.

Zulfiqar, A., Miao, B., Khan, F., Ali, N., Ahmed,S., Rehman, W., Asad, M., Nawaz, M. A., Mir, I. A. & Rasheed, L. (2025). *Langmuir,* 41, 24049–24077.

# Micrometric Evaluation of Human Hair Shaft Diameter: A Comparative Study of Age-Related Morphological Changes.

**[1]Sunitha A Philip**

[1]Associate Professor, Department of Zoology, Mar Thoma College, Thiruvalla-689103, Kerala, India. Email: sunithaphilip@gmail.com

**Abstract:** The present study was conducted to quantitatively analyze and compare variations in human hair width across different age groups and genders. Utilizing a cross-sectional design, hair samples were collected from a balanced cohort of 60 individuals (30 males and 30 females) stratified into six distinct developmental categories: Toddler (2–5 years), Schooler (6–12 years), Adolescence (13–18 years), Adult (20–40 years), Middle Adult (40–55 years), and Older Adult (60+ years). The diameter of individual hair strands was precisely measured using micrometry and statistically evaluated through Mean, Standard Deviation, and ANOVA analyses. The comparative results revealed that females generally exhibit a significantly greater average hair width (Mean = 79.40 µm) than males (Mean = 70.55 µm) across most age groups. The study identified a non-linear trajectory in hair morphology: hair width increases gradually from early childhood, reaches its maximum during adolescence and young adulthood, and subsequently decreases during the aging process. Notably, the most prominent rate of increase in hair diameter occurred during the adolescent stage (13–18 years) for both genders, likely influenced by peak hormonal activity. These findings suggest that while both age and gender independently influence hair shaft diameter, the interaction between these factors remains statistically non-significant. This research provides valuable normative data for applications in dermatology, cosmetology, and forensic science.

**Keywords:** Hair shaft diameter, micrometry, gender dimorphism, ANOVA.

## Introduction

As a defining characteristic of mammals, hair functions as a biological insulator that facilitates thermoregulation by conserving body heat. In humans, hair is categorized into two

primary types: terminal hair—which includes the scalp hair and other androgen-dependent fibers—and vellus hair, alongside specialized structures such as eyelashes and eyebrows. Scalp hair is typically characterized by being long, thick, and highly pigmented. Structurally, hair is a filamentous fiber composed primarily of the fibrous protein keratin, originating from follicles embedded within the dermal layer. With the exception of glabrous skin, hair follicles are distributed across the majority of the human body.

The biological base of the follicle, the hair bulb, contains mitotically active cells that generate the hair shaft. These cells are supported by a complex vascular network that delivers nutrients and regulatory hormones essential for growth. The hair growth cycle proceeds through three distinct phases: Anagen (active growth), Catagen (transition), and Telogen (quiescence/resting). During Anagen, the hair fiber is actively synthesized; in Catagen, growth decelerates; and in the Telogen phase, growth ceases entirely until the hair eventually detaches. Hair pigmentation is determined by melanocytes that produce melanin; however, as these cells undergo age-related apoptosis, the hair fiber loses its color (Alonso & Fuchs, 2006).

The diameter or width of the hair shaft is a variable trait influenced by age, genetics, nutritional status, and chemical treatments. Morphologically, the hair fiber consists of three layers: the innermost medulla, the central cortex, and the outer protective cuticle. The medulla is composed of transparent cells and air spaces, though it is often absent in finer hairs and primarily found in thick terminal fibers (Hutchinson & Thompson, 1999). The cortex constitutes approximately 90% of the hair's mass and contains the melanin responsible for pigmentation, while the cuticle serves as a defensive barrier against environmental damage (Nagase, 2019).

Human hair fibers undergo significant structural and physiological alterations throughout the lifespan. These age-related

changes affect parameters such as hair shaft diameter, density, pigmentation, and tensile strength. Hair quality is influenced by multiple interacting factors, including chronological age, genetic background, ethnicity, hormonal status, and environmental exposure. Research indicates that hair shaft diameter generally increases from childhood through adolescence, reaches its maximum during early adulthood, and gradually declines with advancing age due to intrinsic aging and extrinsic influences (Ebling, 1986; Robbins, 2012). Because tensile strength is positively correlated with shaft diameter, thicker hair fibers typically demonstrate greater mechanical resistance.Hair greying is primarily attributed to oxidative stress within the follicular microenvironment. The accumulation of reactive oxygen species (ROS) contributes to melanocyte dysfunction and apoptosis in the hair follicle, leading to progressive depigmentation (Tobin, 2005). Genetic predisposition plays a more dominant role in hair greying, whereas hair thinning and shaft diameter variation are more strongly associated with hormonal regulation, nutritional status, cosmetic practices, and environmental stressors.

Sex-based differences in hair morphology have been widely documented. Males and females differ in growth patterns, follicular density, and shaft dimensions. Although males exhibit greater body hair growth due to androgenic stimulation, studies suggest that females may have slightly thicker and more uniform scalp hair fibers during certain life stages (Robbins, 2012). Estrogen is believed to prolong the anagen (growth) phase of the hair cycle, contributing to maintained density and shaft integrity, whereas androgens—particularly dihydrotestosterone (DHT)—are implicated in follicular miniaturization in genetically susceptible males (Sawaya & Price, 1997). Age-related thinning is more pronounced in males due to androgenetic alopecia, while females generally experience diffuse thinning, especially after menopause when estrogen levels decline.Genetic variability further contributes to differences in hair shaft dimensions among populations. Molecular studies have demonstrated that genetic

markers influencing hair thickness vary by ethnicity and sex, highlighting the role of hereditary determinants (Peters et. al., 2009). Population-based morphometric analyses have reported that females in early and middle adulthood often show slightly greater mean hair shaft diameters than males; however, these differences may diminish or reverse with aging due to hormonal changes (Takahashi et. al., 2003).

Recent dermatological and forensic investigations continue to emphasize the relevance of hair morphometry. Contemporary imaging and trichoscopic studies confirm that age- and sex-related variations in shaft diameter have diagnostic value in clinical dermatology and population profiling (Kaur & Sinha, 2020; Trüeb, 2021; Birch et. al., 2022). Moreover, emerging research highlights the impact of oxidative stress, endocrine modulation, and follicular stem cell aging in regulating hair fiber characteristics across the lifespan (Paus & Cotsarelis, 2020; Shin et al., 2023).

Recent research has underscored the clinical significance of hair width in diagnosing physiological and pathological states (Bernard et al., 2022). Variations in hair diameter are strongly associated with chronological age, driven by hormonal shifts, genetic predisposition, and environmental stressors. Quantitative changes in hair width provide critical data regarding the aging process and the progression of age-related hair disorders (Loussouarn et al., 2005). While hair width typically increases through development, it eventually decreases during late adulthood, with significant fluctuations observed during puberty and menopause (Pavicic et al., 2009). Specifically, the decline of estrogen levels during menopause is a primary driver of hair thinning in females. Consequently, comparative analysis of hair width across demographics is essential for advancing diagnostic accuracy in dermatology, developing age-targeted cosmeceuticals, and refining forensic evidence analysis.

This study was designed to conduct a comprehensive comparative analysis of human hair shaft diameter across different stages of development. Using precise micrometric measurement techniques, the research aims to quantitatively assess and compare hair shaft width between male and female groups in order to identify significant gender-based morphological differences. The study further seeks to evaluate variations in hair thickness across six distinct age categories, spanning from early childhood to late adulthood, thereby mapping chronological changes in hair fiber characteristics. Additionally, it explores the natural diversity and variability in hair shaft diameter as influenced by biological and environmental factors.

The findings of this investigation contribute to a broader scientific understanding of hair biology and the physiological mechanisms associated with aging. Recent literature indicates that morphological data of this nature are essential for understanding hair follicle miniaturization and the effects of hormonal fluctuations on terminal hair growth. Moreover, the empirical evidence generated from this study has practical implications across multiple disciplines, including clinical dermatology for the diagnosis of hair disorders, cosmetology for the development of age-specific hair care formulations, and forensic science for improved population profiling and sample stratification.

## Materials and Methods

### Study Design

The present study aimed to assess variations in human hair shaft diameter across different age groups and between males and females. Hair samples were obtained from participants spanning early childhood to older adulthood (2–60+ years). Each specimen was carefully stored in a separately labeled collection bag, with clear documentation of the participant's age and gender to ensure accurate categorization and traceability throughout the analysis.

**Sample Size and Grouping**

A total of 60 participants were included in the study, comprising 30 males and 30 females. Participants were equally distributed across six age categories:

- Toddler (2–5 years)
- School-age (6–12 years)
- Adolescents (13–18 years)
- Young Adults (20–40 years)
- Middle-aged Adults (40–55 years)
- Older Adults (60+ years)

**Measurement Technique**

Hair shaft diameter was measured using micrometry under a compound light microscope equipped with an ocular micrometer and a stage micrometer.

**Calibration Procedure**

Before measurement, the microscope was calibrated to determine the calibration factor.

1. The eyepiece (10 × magnification) was removed from the ocular tube.
2. The ocular micrometer was inserted into the eyepiece.
3. The stage micrometer was placed on the microscope stage and brought into focus so that both scales (ocular and stage) were clearly visible.
4. The two scales were aligned such that their zero marks coincided.
5. The stage micrometer was adjusted until the graduations of both scales overlapped precisely.
6. The number of ocular divisions corresponding to a known number of stage micrometer divisions was recorded.
7. The calibration factor was calculated using the formula:

$$\text{“Calibration factor”} = \frac{\text{Stage micrometer divisions”} \times 10}{\text{Ocular micrometer divisions}}$$

8. The value obtained was divided by 10 to estimate the final calibration value per ocular division.

**Measurement of Hair Diameter**

**After calibration:**

1. The stage micrometer was removed from the stage.
2. Individual hair strands were mounted on clean microscopic slides.
3. The breadth (diameter) of each hair shaft was measured using the ocular micrometer.
4. Hair diameter was calculated using:

   Hair shaft diameter = Ocular divisions × Calibration factor

Multiple readings were taken for each strand, and the average diameter per strand was calculated and recorded to minimize measurement error.

**Statistical Analysis**

- Descriptive statistics, including mean and standard deviation, were calculated for each age and gender group.
- Two-way Analysis of Variance (ANOVA) followed by Duncan's post hoc test with interaction effect was performed to determine statistically significant differences in hair shaft diameter across age groups and between genders.

A significance level of $p < 0.05$ was considered statistically significant.

**Results**

For the purpose of analysis, the study participants were divided into six age classes. The frequency and percentage distribution of samples across these age groups are shown in Table 1.

**Table 1. Frequency Distribution of Hair Shaft Diameter Across Age Groups**

| Age Class | Frequency | Percentage (%) |
|---|---|---|
| 1 | 10 | 16.67% |
| 2 | 10 | 16.67% |
| 3 | 10 | 16.67% |
| 4 | 10 | 16.67% |
| 5 | 10 | 16.67% |
| 6 | 10 | 16.67% |
| **Total** | **60** | **100%** |

The frequency distribution table presents the allocation of observations across six defined age categories in the analysis of hair shaft diameter. The dataset demonstrates a perfectly balanced structure, with each age group comprising 10 observations, accounting for 16.67% of the total sample (N = 60).

This equal representation across groups minimizes sampling bias and enhances the reliability of statistical comparisons, ensuring that differences observed in hair width are attributable to age-related variation rather than unequal group sizes.

To ensure balanced representation in the study, participants were grouped based on gender. The frequency and percentage distribution of male and female participants are summarized in Table 2.

**Table 2. Frequency Distribution of Participants by Gender**

| Gender | Frequency | Percentage (%) |
|---|---|---|
| Female | 30 | 50.0% |
| Male | 30 | 50.0% |
| **Total** | **60** | **100%** |

The gender distribution in this study demonstrates a perfectly balanced representation, with 30 observations each for females (50.0%) and males (50.0%), summing to a total sample size of 60 participants. This balanced sampling design reduces potential gender-related bias and strengthens the validity of comparative statistical analyses, particularly when examining differences in hair shaft diameter between males and females.

The analysis of hair shaft diameter revealed noticeable variations between males and females across different age groups. Table 3 presents the mean values and standard deviations of hair width for both genders. Among males, the mean ± standard deviation of hair shaft diameter was 57.55 ± 5.70 μm in the 2–5 years age group, 66.00 ± 11.50 μm in the 6–12 years group, and 85.25 ± 6.15 μm in the 13–18 years group. The 20–40 years group showed a mean value of 79.75 ± 6.15 μm, while the 40–55 years group recorded 63.25 ± 12.30 μm.

In females, the mean ± standard deviation was 60.50 ± 7.53 μm in the 2–5 years age group and 77.65 ± 8.21 μm in the 6–12 years group. The highest mean value was observed in the 13–18 years group (99.00 ± 17.93 μm), followed by the 20–40 years group (96.25 ± 16.84 μm). In the 40–55 years group, the mean diameter was 74.25 ± 7.53 μm, and in the 60+ age group, it was 68.75 ± 13.75 μm.

Overall, the results indicate that hair shaft diameter increased from early childhood to adolescence in both genders, followed by a gradual decline in later age groups. Females demonstrated comparatively higher mean hair shaft diameters than males in most age categories.

**Table 3. Mean (± SD) Hair Shaft Diameter (µm) Across Age Groups and Gender**

| Age Group (Years) | Male (Mean ± SD) | Female (Mean ± SD) |
|---|---|---|
| 2–5 | 57.55 ± 5.70 | 60.50 ± 7.53 |
| 6–12 | 66.00 ± 11.50 | 77.65 ± 8.21 |
| 13–18 | 85.25 ± 6.15 | 99.00 ± 17.93 |
| 20–40 | 79.75 ± 6.15 | 96.25 ± 16.84 |
| 40–55 | 71.50 ± 15.06 | 74.25 ± 7.53 |
| 60+ | 63.25 ± 12.30 | 68.75 ± 13.75 |

The mean hair shaft diameter across different age groups and between genders is illustrated in Figure 1.

**Figure 1. Mean (± SE) Hair Shaft Diameter (µm) Across Age Groups and Gender**

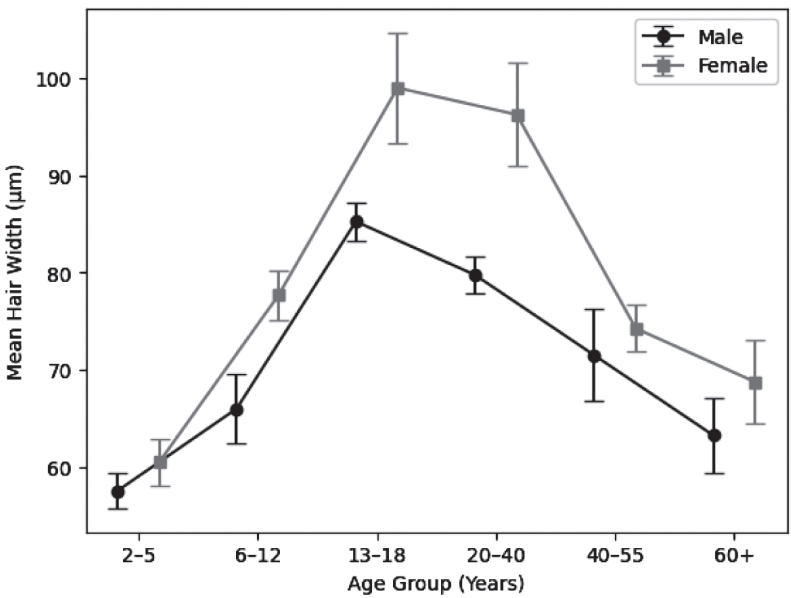

Two-way ANOVA was conducted to examine the main effects of age and gender, as well as to determine whether there was a statistically significant interaction between age and gender on hair shaft diameter.

**Table 4: Two-Way ANOVA for Variation in Hair Shaft Diameter**

| Source of Variation | Sum of Squares | df | Mean Square | F-value | P-value |
|---|---|---|---|---|---|
| Age | 8130.587 | 5 | 1626.117 | 12.246** | <0.001 |
| Gender | 1174.837 | 1 | 1174.837 | 8.847** | 0.005 |
| Age × Gender | 434.038 | 5 | 86.808 | 0.654NS | 0.660 |

***: P<0.01(Significant), NS: P>0.05 (Not Significant)*

The results of the two-way ANOVA demonstrate statistically significant main effects of age ($F(5, 48) = 12.246$, $p < 0.001$) and gender ($F(1, 48) = 8.847$, $p = 0.005$) on hair shaft diameter. These findings indicate that both age and gender independently exert a significant influence on hair width.

However, the interaction effect between age and gender was not statistically significant ($F(5, 48) = 0.654$, $p = 0.660$). This suggests that the pattern of age-related changes in hair shaft diameter is comparable between males and females, and the influence of age on hair width does not significantly differ by gender.

To examine the variation in hair shaft diameter among different age groups, descriptive statistical measures including mean and standard deviation were calculated. The results are summarized in Table 5.

**Table 5. Descriptive Statistics of Hair Shaft Diameter Across Age Groups**

| Age Group | Mean Hair Width | Standard Deviation (SD) |
|---|---|---|
| 2 to 5 | 59.03a | 6.49 |
| 6 to 12 | 71.83b | 11.25 |
| 13 to 19 | 92.13c | 14.57 |
| 20 to 39 | 88.00d | 14.78 |
| 40 to 55 | 72.88e | 11.32 |
| 56+ | 66.00f | 12.64 |
| **Total** | **74.98g** | **16.53** |

Means with different superscripts indicates significant differences by Duncun's test

Duncan's test indicates a progressive increase in hair shaft diameter from early childhood (2–5 years: Mean = 59.03 μm) to adolescence (13–19 years: Mean = 92.13 μm), with values remaining relatively high during young adulthood (20–39 years: Mean = 88.00 μm). A gradual decline is observed in middle adulthood (40–55 years: Mean = 72.88 μm) and older age (56+ years: Mean = 66.00 μm), suggesting age-associated thinning of hair fibers.

Variability in hair width, as reflected by the standard deviation, is highest during adolescence and young adulthood (SD ≈ 14.57–14.78), indicating greater heterogeneity in hair morphology during hormonally active phases. In contrast, early childhood exhibits the lowest variability (SD = 6.49), suggesting relatively uniform hair shaft characteristics at younger ages.

The variation in hair shaft diameter across different age groups is illustrated in Figure 2.

**Figure 2: Hair Shaft Diameter Across Age Groups**

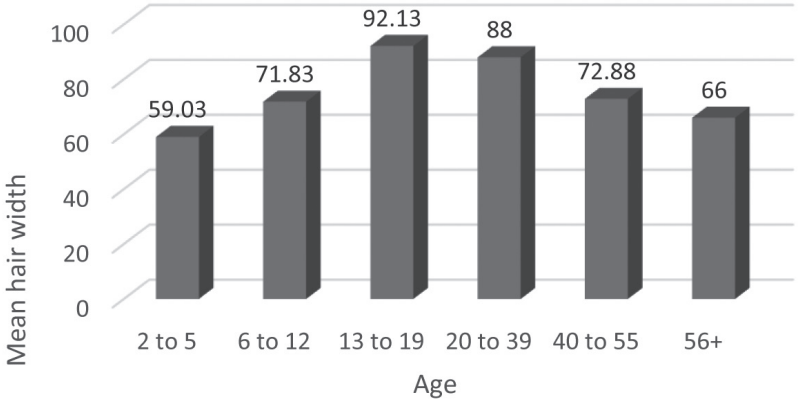


To evaluate gender-based variations in hair shaft diameter, descriptive statistical measures including mean and standard deviation were calculated. The results are summarized in Table 6.

**Table 6. Descriptive Statistics of Hair Shaft Diameter by Gender**

| Gender | Mean Hair Width | Standard Deviation (SD) |
|---|---|---|
| Female | 79.40a | 18.33 |
| Male | 70.55b | 13.39 |
| **Total** | **74.98** | **16.53** |

Means with different superscripts indicates significant differences by Duncun's test

The Duncan's test indicate that females demonstrate a higher mean hair shaft diameter (79.40 μm) compared to males (70.55 μm). This finding suggests the possible influence of biological and hormonal factors on hair morphology between sexes.

Furthermore, females exhibit greater variability in hair width (SD = 18.33) than males (SD = 13.39), indicating a wider range of hair shaft characteristics among female participants.

This increased variation may be attributed to differences in hormonal fluctuations, genetic diversity, and environmental exposures. Overall, the data supports the presence of gender-based differences in hair shaft diameter, with females showing comparatively thicker hair on average.

To examine gender-based differences in hair shaft diameter, the measurements for male and female participants are presented in Figure 3.

**Figure 3: Hair Shaft Diameter by Gender**

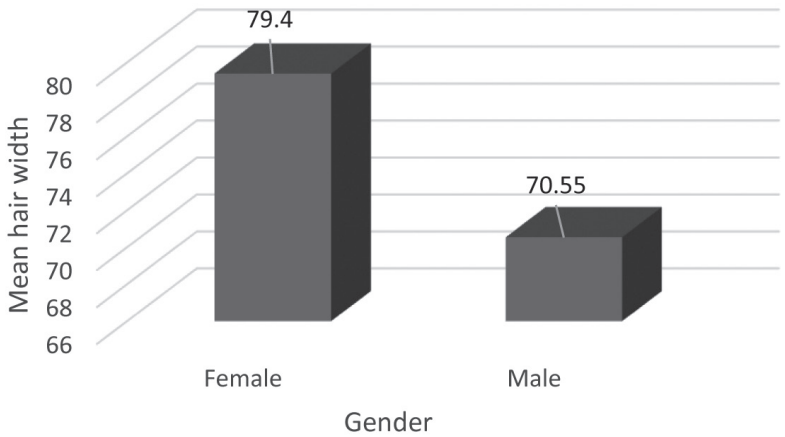


## Discussion

The present study evaluated age-and gender-related variations in hair shaft diameter and demonstrated that hair width increases progressively from childhood, reaches its peak during adolescence and young adulthood, and subsequently declines with advancing age. This pattern reflects the biological dynamics of the hair growth cycle and age-dependent hormonal modulation. The highest mean hair diameter was observed in the 13–19 years age group, with relatively high values maintained during the 20–39 years group. A noticeable reduction in mean hair width was evident after 40 years of age, suggesting age-associated thinning of hair fibers. The elevated variability in later age groups may

reflect individual differences in genetic predisposition, hormonal changes, and environmental influences associated with aging.

Gender-wise observations indicate that the increase in hair width was more pronounced in females during adulthood, whereas in males, hair diameter increased up to adolescence before gradually declining. The reduction in hair width in later years may be associated with hormonal changes and the natural aging process.

Human hair growth occurs in three distinct phases: anagen (growth phase), catagen (transitional phase), and telogen (resting phase). The anagen phase is responsible for active fiber production and determines both hair length and thickness. During adolescence and early adulthood, a higher proportion of follicles remain in the anagen phase, contributing to increased shaft diameter and optimal hair texture. With aging, the duration of the anagen phase gradually shortens, and follicular activity declines, leading to reduced fiber thickness and density (Trüeb, 2021; Shin et al., 2023). This physiological shift may explain the progressive thinning observed in middle-aged and older groups in the present study.

The comparative gender-based analysis revealed that females generally exhibited greater mean hair shaft diameter than males across most age groups, particularly during adolescence and adulthood. These findings are consistent with current endocrinological evidence. Estrogen, the predominant female sex hormone, plays a crucial role in prolonging the anagen phase, enhancing dermal papilla cell survival, and promoting thicker, more resilient hair fibers (tur, testosterone and its more potent metabolite, dihydrotestosterone (DHT), are implicated in follicular miniaturization in genetically predisposed males. DHT shortens the anagen phase and progressively reduces hair shaft diameter, contributing to androgenetic alopecia (Paus & Cotsarelis, 2020).

The minimal differences observed between males and females in the prepubertal age group further support the central role of sex hormones in modulating hair morphology. Prior to puberty, circulating androgen and estrogen levels are relatively low and similar between sexes; therefore, hair shaft characteristics show limited sexual dimorphism. Following puberty, hormonal divergence becomes more pronounced, leading to measurable differences in hair width and density (Grymowicz et al., 2020).

Genetic determinants also substantially influence hair structure and thickness. Variations in genes encoding keratins, keratin-associated proteins, and desmosomal components affect hair fiber integrity and morphology. Additionally, molecular pathways involving lysophosphatidic acid (LPA) signaling have been shown to regulate follicular growth and hair shaft formation (Fujimoto et al., 2007; Birch et al., 2022). Ethnic and hereditary factors may therefore contribute to inter-individual variability observed within age groups.

The decline in hair width observed in older adults aligns with current understanding of follicular aging. Aging is associated with oxidative stress, stem cell exhaustion, reduced melanocyte function, and altered dermal papilla signaling, all of which contribute to follicular miniaturization and decreased fiber production (Shin et al., 2023). The higher variability noted in later age groups may reflect differences in genetic susceptibility, hormonal changes (especially post-menopausal estrogen decline in females), lifestyle factors, nutritional status, and hair care practices.

Environmental influences such as ultraviolet exposure, pollution, chemical treatments, and mechanical stress may further exacerbate structural weakening of the hair shaft over time (Trüeb, 2021). Nutritional deficiencies, particularly in iron, protein, and essential micronutrients, can also impair keratin synthesis and reduce hair thickness.

Overall, the findings of the present study are consistent with existing dermatological and trichological literature, supporting the hypothesis that hair shaft diameter follows a non-linear age-related trajectory and that females generally maintain thicker hair fibers than males during hormonally active phases of life. The observed patterns highlight the combined influence of endocrine regulation, genetic predisposition, and aging mechanisms on hair morphology.

**Conclusion**

The present comparative investigation provides clear evidence that hair shaft diameter varies significantly with both age and gender. The findings indicate that hair width increases progressively from early childhood, reaches its peak during adolescence and young adulthood, and gradually declines with advancing age. This non-linear pattern reflects the biological dynamics of follicular maturation, hormonal activity, and age-related follicular aging.

Gender-based analysis revealed that females generally exhibit greater mean hair shaft diameter than males across most age categories, particularly after puberty. This difference is likely attributable to endocrine influences. Estrogen is known to prolong the anagen (growth) phase of the hair cycle and support follicular integrity, thereby contributing to thicker and more resilient hair fibers. In contrast, androgens—especially dihydrotestosterone (DHT)—may promote follicular miniaturization in genetically predisposed individuals, leading to relatively reduced hair shaft diameter in males over time. The minimal differences observed in prepubertal groups further reinforce the role of hormonal divergence after puberty in shaping hair morphology.

The study also highlights that hair shaft diameter is not determined solely by age and gender. Considerable inter-individual variability was observed, suggesting the influence of additional factors such as genetic predisposition, ethnicity, nutritional status, environmental exposure, hair care practices, and overall health.

Age-related oxidative stress, stem cell depletion, and hormonal fluctuations—particularly during menopause and andropause—may further contribute to progressive thinning in later life.

From a broader perspective, these findings have important implications in dermatology, cosmetology, and forensic science. Understanding normative patterns of hair shaft variation across age and gender can aid in the early detection of pathological thinning, guide age-specific hair care formulations, and enhance the reliability of biological profiling in forensic investigations.

In conclusion, hair shaft diameter demonstrates a dynamic and biologically regulated pattern influenced by hormonal, genetic, and environmental determinants. Future research incorporating larger and more diverse populations, advanced imaging techniques, and molecular analysis would further clarify the mechanisms underlying age- and gender-related variations in hair morphology.

**References**

Alonso, L., & Fuchs, E. (2006). The hair cycle. *Journal of Cell Science,* 119(3), 391–393.

Bernard, B. A., Ouali, F., Moga, A., & Poinsot, R. (2022). Age-associated thin hair displays molecular, structural and mechanical differences. *Journal of Structural Biology,* 214(2), 107888.

Birch, M. P., Messenger, J. F., & Messenger, A. G. (2022). Hair density and diameter variations in women with pattern hair loss. *British Journal of Dermatology,* 186(2), 284–291.

Ebling, F. J. G. (1986). Hair. *Journal of Investigative Dermatology,* 87(1), 3S–5S.

Fujimoto, A., et al. (2007). A scan for genetic determinants of human hair morphology. *Nature Genetics,* 40(5), 523–528.

Grymowicz, M., Rudnicka, E., Podfigurna, A., Napierala, P., Smolarczyk, R., Smolarczyk, K., & Meczekalski, B. (2020). Hormonal effects on hair follicles. *International Journal of Molecular Sciences,* 21(15), 5342.

Hutchinson, P. E., & Thompson, J. M. (1999). The structure and development of hair. *Clinical and Experimental Dermatology,* 24(6), 401–408.

Kaur, M., & Sinha, S. (2020). A forensic approach to analysis of human scalp hair diameter variations in different age and sex groups. *International Journal of Forensic Sciences,* 5(3), 45–52.

Loussouarn, G., El Rawadi, C., & Genain, G. (2005). Diversity of hair growth profiles. *International Journal of Dermatology,* 44(S1), 6–9.

Messenger, A. G., Birch, M. P., & Sinclair, R. D. (2003). The menopausal transition: Is the hair follicle "going through menopause"? *Biomedicines,* 11(11), 3041.

Nagase, S. (2019). The outermost structure of human hair: The cuticle and its protective function. *International Journal of Trichology,* 11(2), 45–49.

Paus, R., & Cotsarelis, G. (2020). The biology of hair follicles. *New England Journal of Medicine,* 341(7), 491–497.

Pavicic, T., Gauglitz, G. G., Lersch, P., Schwichtenberg, U., & Ruzicka, T. (2009). Managing hair loss in midlife women. *Maturitas,* 62(2), 161–164.

Peters, E. M. J., Muller, Y. A., & Kruse, N. (2009). Biological basis of hair shaft variation among populations. *Journal of Dermatological Science,* 55(2), 123–130.

Powell, B. C., & Rogers, G. E. (1986). Hair keratin: Composition, structure, and biogenesis. *Journal of Investigative Dermatology,* 87(1), 52S–56S.

Robbins, C. R. (2012). *Chemical and physical behavior of human hair* (5th ed.). Springer.

Sawaya, M. E., & Price, V. H. (1997). Different levels of 5α-reductase type I and II, aromatase, and androgen receptor in hair follicles of women and men with androgenetic alopecia. *Journal of Investigative Dermatology,* 109(3), 296–300.

Shin, H., Yoo, H. G., & Inui, S. (2023). Advances in understanding hair follicle aging and regeneration. *International Journal of Molecular Sciences,* 24(5), 4123.

Takahashi, T., Kamiya, T., & Tolura, Y. (2003). Comparative analysis of hair diameter across gender and age in Asian populations. *Journal of Cosmetic Science, 5*4(4), 367–376.

Tobin, D. J. (2005). Biochemistry of human hair: Our current understanding. *Clinics in Dermatology,* 23(4), 361–366.

Trüeb, R. M. (2021). Aging of hair. *International Journal of Trichology,* 13(3), 89–99

# A Socioeconomic Analysis of Emigration Trends, Remittance Flows, And Structural Transformation: Kerala Economy

**[1]Liji Samuel, [2]Alen Zachariah, [3]Shalini, [4]Jeena Thankam, [5]Divya and [6]Shilpa**

[1 to 6] Department of Economics, Mar Thoma College, Tiruvalla, Kerala, India

[1]Assistant Professor, Department of Economics, Mar Thoma College, Tiruvalla, Kerala, India

**Abstract:** Kerala, a southern state of India with a population of approximately 35 million, has one of the most distinctive migration histories in the developing world. Since the oil boom of the 1970s, large-scale emigration — primarily to Gulf Cooperation Council (GCC) countries — has fundamentally reshaped the state's economic landscape. This paper examines the historical evolution of Kerala's migration patterns, quantifies the scale of remittance inflows, and critically evaluates the multifaceted impacts of emigration on the state's economy. Drawing on data from the Kerala Migration Survey (KMS), the Centre for Development Studies (CDS), the Reserve Bank of India (RBI), and the World Bank, the paper analyses the dual nature of migration's impact: the short-term economic benefits of remittances that have elevated household consumption, reduced poverty, and financed infrastructure development, alongside the long-term structural challenges including labour shortages, wage inflation, land price distortions, Dutch Disease tendencies, and growing dependency on external income flows. The paper further discusses the implications of return migration, demographic changes, and recent policy responses aimed at sustainable economic development. The findings suggest that while migration has been the engine of Kerala's relative prosperity, the state faces critical imperatives to diversify its economic base and develop productive employment at home.

**Keywords:** Kerala migration, Gulf remittances, Kerala economy, emigration, NRK (Non-Resident Keralite), Dutch Disease, labour market, return migration, development economics, India

## 1. Introduction

Kerala's relationship with migration is both ancient and deeply transformative. Historically, the Malabar Coast served as a trading hub connecting South Asia with the Arab world and East Africa, and this outward orientation continued into the modern era. However, it was the dramatic surge in labour migration to the Gulf Cooperation Council (GCC) countries following the oil price hike of 1973 that set Kerala on a unique developmental trajectory — one that has come to be known internationally as the "Kerala Model" of development.

Unlike the classical developmental pathways driven by industrialisation, Kerala's relative prosperity has been built substantially on human capital export and the consequent inflow of remittances. In 2023, Kerala received an estimated ₹ 1,58,000 crore (approximately USD 19 billion) in remittances, accounting for nearly 36 percent of the state's Gross State Domestic Product (GSDP) — one of the highest ratios for any sub-national entity globally (Centre for Development Studies, 2023). This extraordinary dependence on external income flows raises fundamental questions about sustainability, structural transformation, and the resilience of Kerala's economy.

This paper is structured as follows: Section 2 reviews the historical evolution of Kerala's migration; Section 3 presents an analysis of contemporary migration data; Section 4 examines remittance trends and their macroeconomic implications; Section 5 analyses the socioeconomic impacts; Section 6 discusses structural vulnerabilities and challenges; Section 7 reviews policy responses; and Section 8 offers conclusions and recommendations.

## 2. Historical Background and Evolution of Migration

### 2.1 Pre-Gulf Era Migration

Migration from Kerala predates the modern state, with documented movement to Sri Lanka, Malaya, and Fiji during the British colonial period, primarily as plantation labourers and administrative staff. Following Indian independence in 1947,

educated Keralites particularly nurses, teachers, and government officials -migrated within India and to countries such as the United Kingdom, the United States, and Canada.

### 2.2 The Gulf Migration Wave (1970s–1990s)

The first and most consequential wave of Gulf migration began in earnest following the 1973 OPEC oil embargo, which dramatically increased revenues for oil-exporting GCC nations and created an enormous demand for construction workers, domestic helpers, drivers, and semi-skilled technicians. Kerala, with its relatively high literacy rates and surplus rural labour force, was exceptionally well-positioned to supply this demand. By the 1980s, remittances had become the single largest source of foreign exchange for Kerala.

The Kerala Migration Survey (KMS), first conducted by the Centre for Development Studies in 1998, documented approximately 1.36 million emigrants at that time. Subsequent waves (2003, 2007, 2011, 2016, and 2023) have tracked the growth, composition, and changing nature of this diaspora, making Kerala one of the most empirically well-studied migration systems in the world.

### 2.3 Diversification of Destinations (2000s–Present)

While the Gulf region continues to dominate, the 21st century has seen significant diversification in destination countries and migrant profiles. Increasingly, highly educated Keralites - software engineers, medical professionals, academics, and entrepreneurs - have emigrated to the United States, Australia, Canada, the United Kingdom, and Western Europe. This second-generation migration has different implications for the Kerala economy, including a more permanent character, reduced remittance flows per household, and a more severe form of brain drain.

## 3. Contemporary Migration Data and Trends

Based on the Kerala Migration Survey 2023 and supplementary data from the Ministry of External Affairs, Government

of India, the following key statistics characterise the current migration landscape:

**Table 1: Key Migration Indicators for Kerala, 2011–2023**

| Indicator | 2011 | 2018 | 2023 |
|---|---|---|---|
| Total emigrants (in millions) | 2.28 | 2.10 | 1.72* |
| Share in Gulf countries (%) | 89.2 | 85.7 | 79.4 |
| Female emigrants (%) | 12.4 | 14.8 | 17.3 |
| Return migrants (in millions) | 0.73 | 1.20 | 1.60 |
| Remittances received (₹ crore) | 43,128 | 85,092 | 1,58,000 |
| Remittances as % of GSDP | 18.6 | 26.4 | 35.8 |
| Emigrant households (%) | 17.3 | 19.1 | 18.9 |

** Decline in stock partly attributed to COVID-19 related return migration and stricter Kafala system enforcement in GCC countries.*

*Sources: Kerala Migration Survey 2023, Centre for Development Studies; RBI Remittance Data 2023.*

A noteworthy trend is the decline in total emigrant stock between 2011 and 2023, driven largely by the mass return of workers during the COVID-19 pandemic (2020–2021), subsequent regularisation of immigration policies in Saudi Arabia, UAE, and Kuwait under Kafala reform [The Kafala system is a sponsorship model that governs the employment of foreign workers. It has faced criticism for creating conditions of labor exploitation and abuse. The government introduced new laws aimed at enhancing workers' rights and protections. Revisions include allowing workers to change employers without prior consent from sponsors. Enhanced mobility for workers may lead to better job opportunities and improved working conditions. Advocacy groups highlight the need for continuous monitoring to ensure compliance with reforms. Potential challenges may arise as the reforms are implemented and tested in real-world scenarios], and the automation of certain semi-skilled job categories in Gulf

economies under their respective Vision plans (Saudi Vision 2030, UAE Vision 2031).

### 3.1 Socio-Demographic Profile of Emigrants

Contemporary Keralite emigrants are younger, more educated, and increasingly diversified by gender compared to earlier cohorts. The proportion of emigrants with tertiary education has risen from 22 percent in 1998 to over 41 percent in 2023, indicating a qualitative shift from semi-skilled to skilled emigration. Female emigration, historically concentrated in nursing and domestic work, has expanded to include teaching, allied health, and IT-enabled services.

## 4. Remittance Flows and Macroeconomic Implications

### 4.1 Scale and Significance

Kerala accounts for approximately 19–21 percent of India's total inward remittances, a remarkable share given the state constitutes only 2.8 percent of the national population. Remittances have consistently exceeded the state's own tax revenues, foreign direct investment inflows, and central government grants, making them the most important external resource for the Kerala economy.

**Table 2: Kerala Remittances as a Share of GSDP, 2000–01 to 2022–23**

| Year | Remittances (₹ Crore) | GSDP (₹ Crore) | Remittances/GSDP (%) |
|---|---|---|---|
| 2000–01 | 14,510 | 1,05,200 | 13.8 |
| 2005–06 | 24,890 | 1,68,400 | 14.8 |
| 2010–11 | 43,128 | 2,31,700 | 18.6 |
| 2015–16 | 72,543 | 3,12,800 | 23.2 |
| 2020–21 | 88,200 | 2,98,100 | 29.6 |
| 2022–23 | 1,58,000 | 4,41,600 | 35.8 |

*Sources: RBI Handbook of Statistics on Indian Economy; Kerala Economic Review 2023; CDS Migration Survey.*

### 4.2 Channels and Distribution

Remittances are predominantly transmitted through formal banking channels, with over 78 percent arriving via SWIFT transfers, NRE/NRO accounts, or money transfer operators partnered with scheduled commercial banks. The remaining 22 percent utilises informal Hawala networks, particularly for smaller amounts in rural areas. Remittances are geographically concentrated in Malappuram, Thrissur, Kannur, and Kozhikode districts, which together account for over 60 percent of the total inflow.

### 4.3 Utilisation Patterns

Research consistently shows that remittance utilisation in Kerala follows a predictable pattern: the majority of funds are directed towards household consumption (food, clothing, education of children), construction of residential houses, repayment of migration-related debt, and purchase of land and gold. A comparatively smaller proportion is channelled into productive investment, entrepreneurship, or financial assets a pattern that has significant implications for the multiplier effect of remittances in the local economy.

**Table 3: Pattern of Remittance Utilisation in Kerala (2023)**

| Category of Expenditure | Share of Remittances (%) |
|---|---|
| Household consumption | 38.4 |
| Construction / Renovation of house | 24.7 |
| Education and Healthcare | 12.3 |
| Repayment of migration debt | 9.6 |
| Purchase of land | 8.2 |
| Business investment | 4.1 |
| Savings and financial instruments | 2.7 |

*Source: Kerala Migration Survey 2023; authors' calculations.*

## 5. Socioeconomic Impacts of Migration

### 5.1 Poverty Reduction and Human Development

The most celebrated impact of migration on Kerala's economy has been the dramatic reduction in poverty and the advancement of human development indicators. The poverty headcount ratio declined from approximately 59 percent in 1973–74 to 7.1 percent in 2019–20 (NFHS-5), a pace considerably faster than the national average. Emigrant households consistently exhibit higher per-capita expenditure, lower malnutrition rates, and greater school enrolment than comparable non-emigrant households.

Kerala's human development achievements — including a literacy rate of 94 percent, an Infant Mortality Rate of 6 per 1,000 live births, and a life expectancy of 74.9 years — are partially attributed to the social investment financed through remittance income. The healthcare and education sectors have benefited enormously from remittance-financed private expenditure, giving rise to a large network of private hospitals, engineering colleges, and nursing institutions.

### 5.2 Labour Market Transformation

Migration has profoundly transformed Kerala's labour market. The emigration of working-age males has created significant labour shortages in agriculture, construction, traditional industries (coir, handloom, fisheries), and even the informal service sector. Ironically, Kerala now imports millions of inter-state migrant workers — estimated at 3.5 to 4 million in 2023, primarily from Odisha, West Bengal, Assam, Jharkhand, and Bihar — to fill gaps left by Keralite emigrants. This phenomenon, studied extensively by the Gulati Institute of Finance and Taxation, represents a fundamental restructuring of the state's labour supply.

### 5.3 Real Estate and Land Markets

Remittance inflows have been a primary driver of Kerala's notoriously high land prices. The demand for residential land in

coastal and peri-urban areas, financed by Gulf remittances, has generated speculative bubbles in districts such as Malappuram, Thrissur, and Ernakulam. For non-emigrant families, rising land costs represent a significant welfare loss, limiting access to affordable housing and making productive agricultural investment increasingly uneconomical.

### 5.4 Gender and Social Dynamics

The migration of male members has altered household power structures, in some cases empowering women as de facto heads of household managing remittance income, investment decisions, and children's education. However, the literature also identifies negative consequences including psychological stress among "Gulf wives," disruption of family bonds, vulnerability to domestic financial mismanagement, and social isolation. Female emigration — particularly of nurses has generated its own set of social implications, including delayed marriages and the "care drain" phenomenon documented by scholars such as Irudaya Rajan and Bindhulakshmi Pattadath.

## 6. Structural Vulnerabilities and Challenges

### 6.1 Dutch Disease Effects

Economists have identified symptoms consistent with the Dutch Disease in Kerala's economy. The abundance of remittance income has appreciated the purchasing power of remittance-receiving households, driven up wages in the non-tradeable sector (services, construction), and made Kerala's traditional export industries cashew processing, coir, handloom, spices increasingly uncompetitive. Agricultural output per worker and cultivated land area have both declined steadily since the 1980s, creating a structural shift away from productive sectors.

### 6.2 Remittance Dependency and Vulnerability

Kerala's heavy dependence on remittances exposes the state economy to shocks originating in the Gulf region. The fall in global oil prices (2014–2016), the Saudi Nitaqat or Iqama

crackdowns, COVID-19 pandemic restrictions (2020–2021), and escalating geopolitical tensions in West Asia have all produced sharp, if temporary, declines in remittance inflows. The absence of a diversified industrial base means that such external shocks directly translate into household income losses, reduced consumption, and rising unemployment — with limited automatic stabilisers available.

### 6.3 Return Migration Challenges

The return of large cohorts of migrants — estimated at over 1.6 million by 2023 presents both an opportunity and a crisis. Return migrants possess valuable skills, international experience, and in some cases, capital savings. However, the absence of adequate entrepreneurship ecosystems, the skill mismatch between Gulf-acquired competencies and domestic market demands, and the social stigma of "failed migration" have limited the productive reintegration of return migrants. Studies by the Kerala Non-Resident Keralites' Welfare Board (NORKA) indicate that a significant proportion of return migrants are unable to find employment commensurate with their skills and remain economically inactive or underemployed.

### 6.4 Demographic Ageing and Brain Drain

Sustained emigration of young adults has accelerated Kerala's already rapid demographic ageing. Kerala is projected to have the highest dependency ratio among Indian states by 2031, with significant implications for the sustainability of the public pension system, healthcare expenditure, and the productive labour force. The emigration of highly educated professionals — doctors, engineers, academics — represents a substantial loss of human capital that Kerala's public educational system has financed, without receiving commensurate productivity returns within the state.

## 7. Policy Responses

The Government of Kerala has initiated a range of institutional and policy responses to manage migration and harness its developmental potential:

The Non-Resident Keralites' Affairs (NORKA) department and the NORKA Roots programme have been established to facilitate re-integration of return migrants through skill re-training, entrepreneurship funding, and welfare services. The Pravasi Welfare Fund provides emergency financial assistance, insurance, and pension benefits to registered emigrants and their families.

Several initiatives including the ODEPC (Overseas Development and Employment Promotion Consultants), the Kerala Financial Corporation's NRK schemes, and the Start-Up Mission aim to channel migrant savings into productive investment within Kerala. The state's Industrial and Commercial Policy 2023 explicitly targets the NRK community as a potential investor class.

At the national level, the Emigration Act (currently under revision as the Emigration Bill 2021) and the e-Migrate system are aimed at regularising and protecting the rights of low-skilled emigrant workers. Kerala has been an active advocate for stronger bilateral labour agreements between India and GCC nations to protect worker rights and welfare.

Despite these efforts, critics argue that Kerala lacks a coherent long-term economic diversification strategy that is not predicated on continued emigration. The state's GSDP growth rate, while positive, remains heavily services-oriented, with manufacturing accounting for barely 10 percent of the lowest shares among comparable Indian states.

**8. Conclusions and Recommendations**

The migration of Keralites, primarily to the Gulf and increasingly to Western economies, has been the single most transformative economic force in Kerala's post-independence history. Remittances have undeniably financed poverty reduction, human development, and infrastructure, producing social outcomes that surpass what the state's productive domestic economy alone could have generated. In this sense, Kerala's

migration model represents a genuine, if fragile, development success story.

However, the very success of this model has generated structural distortions and remittance dependency, Dutch Disease tendencies, labour market dualization, speculative real estate inflation, and demographic ageing that threaten long-term economic sustainability. The declining trend in emigrant stock, combined with an accelerating return migration flow, suggests that Kerala may be approaching a critical inflection point where the migration dividend begins to diminish.

The following policy recommendations emerge from this analysis:

First, Kerala must urgently develop a productive domestic economic base through targeted industrial policy, special economic zones, and investment in high-value manufacturing and knowledge industries that leverage the state's comparatively educated workforce. Second, the state should develop robust financial instruments including diaspora bonds, NRK investment funds, and co-investment schemes to productively channel migrant savings. Third, comprehensive return migrant reintegration programmes, with specific skill-matching, mentorship, and entrepreneurship support, must be scaled up. Fourth, Kerala should advocate for multilateral frameworks to protect the rights and welfare of its emigrant workers while actively negotiating bilateral social security agreements with key destination countries. Fifth, demographic policies must address the implications of rapid ageing, including expansion of old-age social protection and increased female labour force participation.

In summary, Kerala's migration story is a testament to human resilience and enterprise, but the state now stands at a crossroads. The transition from a remittance-dependent economy to a self-sustaining, diversified economy will require both visionary policy and the collective investment of the Keralite diaspora in the state's future.

**References**

Centre for Development Studies. (2023). *Kerala migration survey 2023: Key results.* Centre for Development Studies.

Gulati Institute of Finance and Taxation. (2022). *Interstate migrant workers in Kerala: Scale, sectors and policy implications.* GIFT.

Irudaya Rajan, S. (Ed.). (2022). India migration report 2022: *Labour migration and remittances.* Routledge.

Kerala State Planning Board. (2023). *Kerala economic review 2023: Annual report on the state economy.* Government of Kerala.

Ministry of External Affairs. (2023). *Annual report* 2022–23. Government of India.

NORKA Roots. (2023). *Return migrant status report* 2023. Government of Kerala.

Reserve Bank of India. (2023). *Handbook of statistics on Indian economy* 2022–23. RBI.

Rajan, S. I., & Percot, M. (2011). *Dynamics of Indian migration: Historical and current perspectives.* Routledge India.

Sreelekha, N. (2020). Remittances and development in Kerala: Empirical evidence and policy implications. *Economic and Political Weekly,* 55(12), 45–53.

United Nations Development Programme. (2023). *Human development report 2023/24.* UNDP.

World Bank. (2023). *Migration and development brief 39: Remittances brave global headwinds.* World Bank Group.

Zachariah, K. C., & Irudaya Rajan, S. (2012). *Kerala's Gulf connection: CDS studies on international labour migration from Kerala State in India.* Orient Blackswan.

Bain & Company. (2022, July 13). *The trillion-dollar manufacturing exports opportunity for India.* https://www.bain.com/insights/the-trillion-dollar-manufacturing-exports-opportunity-for-india/

India: An engine for global economic growth through manpower exports. (2023, October 31). *The Financial Express*. https://www.financialexpress.com/

Mandha, B. R. (2022, September 22). India, the largest exporter of manpower, does not have a migration policy. *The Siasat Daily.* https://www.siasat.com/india-the-largest-exporter-of-manpower-does-not-have-a-migration-policy-2418492/

Fang, T., & Wells, A. (2023). *Diaspora economics*. In SpringerLink. https://doi.org/10.1007/978-3-319-57365-6_105-1

Mazumdar, D., & Sarkar, S. (n.d.). *Globalization, labor markets and inequality in India.* https://idrc-crdi.ca/sites/default/files/openebooks/373-7/

*Circular migration between the North and the South: Effects on the source southern economies*. (2014). Procedia - Social and Behavioral Sciences. https://doi.org/10.1016/j.sbspro.2014.06.004

Koczan, Z., Pinat, M., & Rozhkov, D. L. (2021). The impact of international migration on inclusive growth: A review. *IMF eLibrary.* https://doi.org/10.5089/9781513571966.001.A001

Bortolazzi, O., & Khan, N. (2023). *From 'brain drain' to 'capital gain': Indian skilled migration to the UAE*. In SpringerLink. https://doi.org/10.1007/978-981-19-7796-1_14

Oxford University Press. (n.d.). https://academic.oup.com/book/27510/chapter-abstract/197457438

Giordano, A., & Terranova, G. (2012). The Indian policy of skilled migration: Brain return versus diaspora benefits. *Journal of Global Policy and Governance.* https://doi.org/10.1007/s40320-012-0002-

# Effect Of Annealing And Doping On Zinc Sulphide Thin Films

**[1]Swathy Satheesh, [2]Betty Elsa Joseph and [3]Angel Susan Cherian**

[1, 2, 3] Department of Physics, Mar Thoma College, Kuttapuzha P.O, Tiruvalla, Kerala, India.

[1]E-mail: swathysatheesh572@gmail.com

[3]Assistant Professor and HOD, Department of Physics, Mar Thoma College, Tiruvalla. E-mail: angel@mtct.ac.in

**Abstract :** Zinc sulphide (ZnS) thin films were synthesized on glass substrates via chemical bath deposition (CBD). The study evaluated the influence of annealing (100-250°C) and magnesium (Mg)doping (10-25%) on structural and optical characteristics using XRD and UV-Visible spectroscopy. Results indicate that films annealed at100°C possess superior crystallinity, where higher temperatures induce amorphization. Mg incorporation 5formation These findings confirms that controlled annealing and Mg doping effectively tune ZnS properties, optimizing their performance for advance optoelectronic applications.

**Keywords:** ZnS thin films, Chemical bath deposition, Annealing, Magnesium doping, XRD, UV-V is spectroscopy.

## 1. Introduction

Zinc sulphide (ZnS) is II–VI compound semiconductor with wide band gap and excellent optical transparency, making it suitable for applications in optoelectronics, sensors, and solar cells. ZnS is a white to yellow solid with diverse properties, including high melting and boiling points, high surface area, and unique optical and photocatalytic characteristics. It is widely used as a pigment, in phosphorescent materials, and in various optical and electronic applications.

Zinc sulphide (ZnS) thin films are semiconductor materials with diverse applications, particularly in optoelectronics and as buffer layers in solar cells as reported by Arsad et al [4]. They are known for their wide bandgap (around 3.7 eV), high refractive index, and good transparency in the visible spectrum ZnS thin films

can be fabricated using various methods, including chemical bath deposition (CBD), sputtering, and electrodeposition. The wide bandgap of ZnS makes it suitable for applications in blue and UV light-emitting diodes and as a window layer in solar cells, helping to reduce absorption losses. ZnS's high refractive index allows it to be used as a reflector or dielectric filter in optical devices. ZnS thin films also find use in electroluminescence devices, field emission devices, sensors, and as a coating material. Thin film forms of ZnS are particularly attractive due to size-dependent properties and compatibility with device fabrication. Among the various deposition techniques, chemical bath deposition (CBD) offers advantages such as low cost, low temperature processing, simplicity, and large-area deposition capability. Important solution properties are the pH and the concentrations of the metal salts, as well as the additives. The most significant process parameters are temperature, deposition time and stirring rate.

The physical properties of ZnS thin films strongly depend on deposition parameters, post- deposition annealing, and doping. Annealing improves crystallinity and removes residual stresses and defects, while doping with suitable elements modifies electronic band structure and optical response. Magnesium is an attractive dopant due to its ionic radius comparable to $Zn^{2+}$ and its ability to tune the band gap. Mg acts as a band gap engineer, often widening the gap, which is beneficial for optoelectronic devices and increasing photocatalytic activity. The tunability of bandgap helps ZnS thin films to be used as a buffer layer in thin film solar cells and as gate insulator and channel in TFT devices [1]. Chawla et al claimed that Zn1-xMgxO films can be deposited by using triethanolamine and hydrochloric acid 30 mol% Mg. [2]. Ravi et al reported flower-shaped Zn1-xMgxO with incorporated Mg content of 1.5 mol% [2]. Zinc sulphide can be easily doped with magnesium (Mg) due to its comparable ionic radius with zinc. Ryo Inoue, and his groups have investigated the structural, optical and luminescent properties of Mg doped ZnS thin films[3]

This work focuses on the preparation of ZnS thin films using CBD, optimization of deposition parameters, investigation of annealing effects, and systematic study of Mg doping on structural and optical properties.

The chemical bath deposition (CBD) method is one of the most cost-effective techniques for preparing thin films and nanomaterials, as it requires only simple solution containers and substrate holders rather than expensive equipment. It is scalable for large-area or continuous deposition. The process involves two main steps: nucleation and particle growth, where a solid phase forms from solution as substrates are immersed in an alkaline bath containing precursors.

CBD offers advantages such as producing uniform, adherent, and reproducible films at low temperatures. However, a drawback is the wastage of solution after each deposition. Film growth depends strongly on conditions like deposition time, solution composition, temperature, and substrate properties. Historically, Bruckman first deposited ZnS thin films by CBD in 1933. Compared to physical deposition, which requires high energies, CBD is a soft, low-temperature method capable of producing stoichiometrically accurate crystalline phases.

Doping in semiconductors is the intentional introduction of impurities to modify electrical properties, producing extrinsic semiconductors. At very high doping levels, the material behaves like a conductor and is termed a degenerate semiconductor. Doped semiconductors remain electrically neutral, with n-type and p-type designations referring only to the majority charge carriers

In this work, magnesium doping is applied to ZnS thin films. Metal doping in ZnS is known to significantly alter structural, morphological, and optoelectronic properties, enhancing their suitability for thin-film devices. Thin films of pure and Mg-doped ZnS nanoparticles were prepared on soda lime glass substrates using the chemical bath deposition technique, with varying Mg

concentrations to study their effects on crystallinity and transport properties.

## 2. Materials and Methods

### 2.1. Material deposition

The magnesium acetate [Mg $(CH_3COO)_2$], Zinc acetate dihydrate [Zn $(CH_3COO)_2$-2H2O)] and thiourea [$(NH_2)_2CS$] were used as the precursor for the preparation of the Mg-doped ZnS films. Ammonia solution was used as a complexing agent. The ZnS films were deposited by chemical bath deposition by varying the Mg doping concentration on the glass substrates.

Glass substrates were cleaned thoroughly using detergent and distilled water. Aqueous solutions of zinc acetate (0.3 M), thiourea (0.2 M), and ammonia (0.04 M) were prepared separately. The chemical bath was prepared by first adding zinc acetate solution, followed by thiourea, and finally ammonia to form a precipitated solution. The total volume of the bath was maintained at 50 ml. Cleaned glass substrates were vertically immersed in the bath, and deposition was carried out at a bath temperature of 80 °C for 50–60 minutes.

### 2.2 Importance of order of mixing

The order of mixing was very important for obtaining good films. After mixing Zinc acetate and thiourea, the complexing agent NH3 was added. First a white precipitated solution was formed. The volume of each reactant needed was now calculated in 10 ml. They are added in the order given above and the volume of water needed to make up to 50 ml was calculated and added; then the substrate was immersed. The resulting films were found to be more adhesive.

### 2.3 Annealing Treatment

The deposited ZnS thin films were annealed in air at different temperatures: 100 °C, 200 °C and 250 °C for 1 hour to study the effect of annealing on crystallinity. Mohammed et al reported that to investigate the influence of annealing on crystallinity, the

ZnS thin films were subjected to heat treatment in air at different temperature for one hour, following procedures reported in earlier studies [5]

### 2.4 Preparation of Mg-Doped ZnS Thin Films

Mg-doped ZnS thin films were prepared by adding magnesium nitrate solution to the optimized chemical bath. Mg doping concentrations of 10%, 15%, 20%, and 25% (with respect to Zn molar concentration) were introduced. According to Ashokkumar and Boopathyraja, Mg-doped ZnS thin films were obtained by adding magnesium nitrate solution to the optimized chemical bath [6]. The deposition conditions were kept identical to those of pristine ZnS films. All doped samples were annealed at 100 °C, which was identified as the optimal annealing temperature.

## 3. Effect of annealing

### 3.1 X-Ray Diffraction (XRD)

Structural characterization was carried out using X-ray diffraction with Cu Kα radiation (λ = 1.5406 Å). The diffraction patterns were recorded in the 2θ range of 10°–70°. Annealed samples were investigated using X-ray analysis. The broad "hills" between 30° and 40° with no sharp peaks confirms the lack of long-range order of the films, which is common in low-temperature chemical depositions. On further annealing, the films become amorphous.

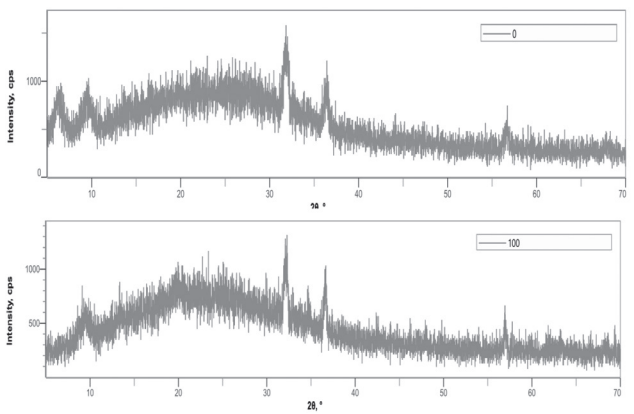

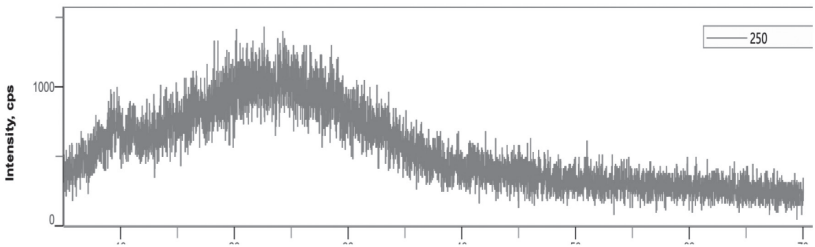


**Fig 1: XRD plots of unannealed and annealed samples**

The improved crystallinity at 100 °C is attributed to defect reduction and rearrangement of atoms, whereas higher temperatures may cause sulphur loss and structural disorder. It is decided to anneal the Mg doped sample at 100 °C for 1 hour so that surface remnants on the film can be removed by slight annealing.

## 4. Effect of Mg Doping

### 4.1. X-Ray Diffraction (XRD)

Structural characterization was carried out using X-ray diffraction with Cu Kα radiation (λ = 1.5406 Å). The diffraction patterns were recorded in the 2θ range of 10°–70°. Phase identification was performed using standard JCPDS data. Doped samples were investigated using X-ray analysis.

From the XRD pattern of pristine sample, we can infer that the peaks obtained at 6.0664°, 9.51°, 31.93°, 36.34° and 56.62° corresponds to reflections from (100), (002), (101), (102) and (110) planes of the ZnS phase with cubic structure.

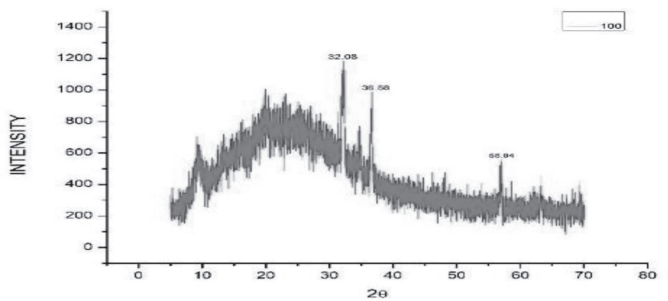


**Fig 2: XRD pattern of pristine ZnS thin film**

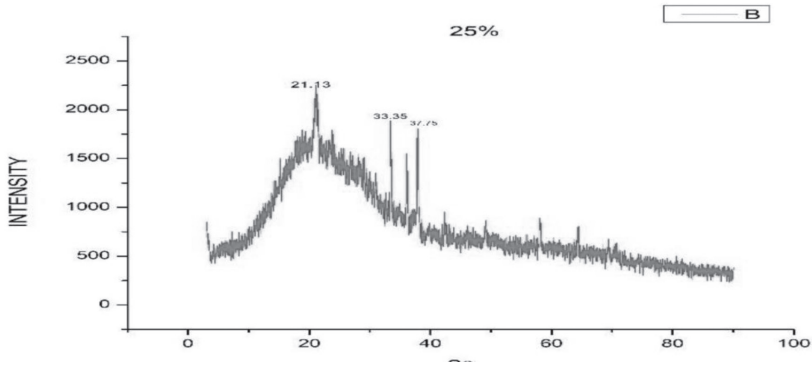


**Fig 3: XRD pattern of 25% Mg doped ZnS thin film**

XRD analysis of Mg-doped ZnS thin films revealed suppression of characteristic ZnS peaks with increasing Mg concentration. A new peak at $2\theta \approx 21.25°$ was observed, corresponding to the (003) plane of rhombohedral MgO, indicating partial phase segregation and increased long range order in the ZnS lattice due to Mg incorporation.

### 4.2. Optical Properties

Optical properties were analysed using a UV–Visible spectrophotometer in the wavelength range of 200–800 nm. The optical band gap was determined using Tauc plots assuming direct allowed transitions.

The optical band gap values were extracted from Tauc plots. The pristine ZnS film exhibited a band gap of 4.0885 eV. With increasing Mg doping concentration, the band gap decreased systematically. The pristine ZnS film exhibited an optical band gap (Eg) of 4.09 eV, which is characteristic of the wide-bandgap nature of Zinc Sulphide. Upon increasing the Mg doping concentration from 10% to 25%, a systematic red-shift in the absorption edge was observed, resulting in a consistent reduction of the band gap to 3.74 eV.

**Table 1: Variation of Optical Band Gap with Mg Doping**

| Mg Doping Concentration (%) | Optical Band Gap Eg (eV) |
|---|---|
| 0% (Pristine) | 4.0885 |
| 10% | 4.0551 |
| 15% | 3.9493 |
| 20% | 3.8838 |
| 25% | 3.7376 |

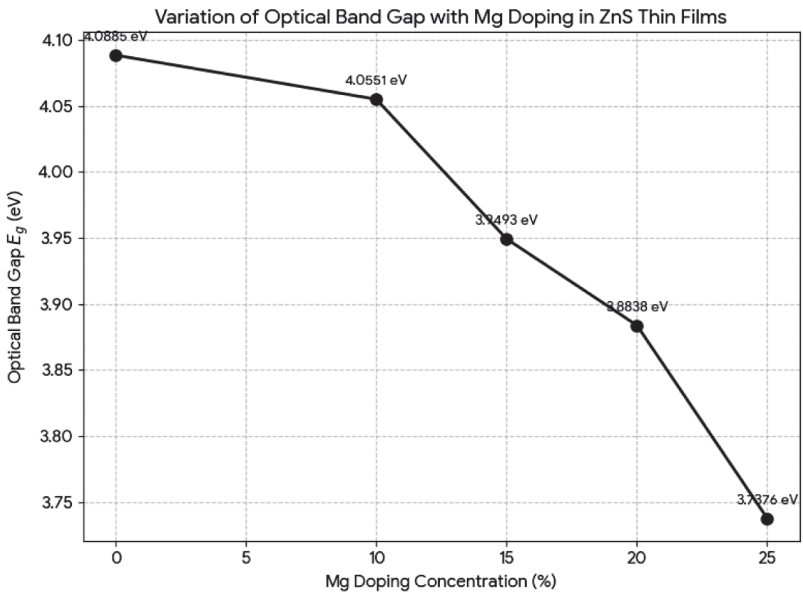


**Fig 4: Variation of Optical Band Gap with Mg Doping**

The plot illustrates the band gap engineering of ZnS thin films. As the magnesium doping concentration increases from 0% to 25%, the optical band gap (Eg) decreases linearly from 4.09 eV to 3.74 eV. This trend, as discussed in the paper, is attributed to grain growth, lattice distortion, and the formation of defect states. This tunability is a key finding of the research, confirming that

Mg doping is a highly effective parameter for tailoring the optical properties of ZnS for specific optoelectronic applications such as solar cell buffer layers and TFT devices.

## 5. Conclusion

ZnS thin films were successfully synthesized via the chemical bath deposition (CBD) technique. Thermal treatment at 100°C was identified as the optimal annealing temperature to enhance long-range structural order and eliminate surface impurities; conversely, higher temperatures induced amorphization. The incorporation of Magnesium (Mg) dopants served as a critical tuning parameter, systematically reducing the optical band gap from 4.09eV to 3.74 eV. These findings demonstrate that precise control over annealing and Mg-doping levels provides a robust framework for tailoring the structural and optical characteristics of ZnS films, facilitating their integration into high-performance optoelectronic devices, sensors, and solar cells.

## References

Arsad, A. Z., Zuhdi, A. W. M., Abdullah, S. F., Chau, C. F., Ghazali, A., Ahmad, I., & Wan Abdullah, W. S. (2023). Effect of chemical bath deposition variables on the properties of zinc sulphide thin films: A review. *Molecules,* 28(6), 2780. [4]

Ashokkumar, M., & Boopathyraja, A. (2018). Structural and optical properties of Mg doped ZnS quantum dots and biological applications. *Superlattices and Microstructures,* 113, 236–243[6]

Chawla S, Jayanthi K, Chander H (2008) Enhancement of luminescence in ZnMgO thin-film nanophosphors and application for white light generation. *Phys Status Solidi A* 205:271–274. [1]

Mohammed, R. Y. (2021). Annealing effect on the structure and optical properties of CBD-ZnS thin films for windscreen coating. *Materials,* 14(22), 6748. [5]

Ravi G, Vijayaprasath G, Manikandan M et al (2013) A comparative study on pure and Mg doped ZnO nano structured thin films. *Asian J Chem* 25:258–260 [2]

Ryo Inoue, Masahiko Kitagawa, Yoshinori Horii, Setsuya Kinba, Takayoshi Nishigaki, Kunio Ichino, Shosaku Tanaka, Hiroshi Kobayashi, Luminescent properties of ZnxMg1−xS: Mn thin film electroluminescent devices, *Journal of Crystal Growth,* Volumes 214–215, 2 June 2000, Pages 931-934 [3]

# A Multi-Faceted Review on the Pharmacology, Phytoremediation Capabilities, Global Market Trends, and Conservation of *Withania somnifera* (L.) Dunal

**[1]Merin John, [2]Jincy P. Abraham and [3]Sonia Anna Zachariah**

[1,2, 3] Postgraduate and Research Department of Botany, Mar Thoma College, Tiruvalla, Kuttapuzha PO, 689103

[2, 3] Assistant Professor, Department of Botany, Mar Thoma College, Tiruvalla

[3] Email: sonia@mtct.ac.in

**Abstract:** Environmental pollution, particularly from heavy metals, agrochemicals, and industrial waste, poses a serious threat to ecosystem health and human well-being. Conventional remediation methods are often expensive, energy-intensive, and ecologically disruptive. Phytoremediation—a nature-based solution utilising plants to detoxify polluted environments—offers a sustainable, cost-effective, and environmentally sound alternative. In recent years, attention has turned toward medicinal plants as dual-purpose agents, capable of both restoring polluted ecosystems and offering therapeutic value. This review explores the potential of *Withania somnifera* (L.) Dunal, widely known as Ashwagandha, as a phytoremediator alongside its well-established pharmacological roles. Although few studies have directly assessed *W. somnifera* for phytoremediation, preliminary findings and its physiological traits suggest promise for this application. The dual-use challenge—balancing the plant's role in environmental cleanup with its use in herbal medicine—is also examined, with emphasis on ensuring medicinal safety and avoiding bioaccumulation of toxins in harvested plant material. This review ultimately advocates for expanded interdisciplinary research and regulatory support to explore medicinal plants as multifunctional resources in sustainable development.

**Keywords:** Phytoremediation, *Withania somnifera,* environmental pollution, medicinal plants, sustainable development.

## Introduction

Environmental pollution has escalated into a pressing global issue, primarily due to intensified industrialisation, rapid urban growth, and extensive use of agrochemicals. Contaminants such as heavy metals, synthetic pesticides, and industrial discharge severely impact soil and water ecosystems, posing significant ecological and public health threats (de Vries et al., 2012). Traditional remediation methods—like physical extraction, chemical processing, and excavation—are frequently cost-prohibitive, environmentally disruptive, and not sustainable over time (Ali et al., 2019). Consequently, phytoremediation, an environmentally friendly approach that utilises plants to remove or neutralise environmental pollutants, has gained prominence as a practical and sustainable alternative (Dushenkov et al., 1995).

Medicinal plants, recognised for their therapeutic efficacy, are increasingly explored for phytoremediation due to their ecological adaptability and ability to produce stress-mitigating secondary metabolites (Ali et al., 2019; Yadav et al., 2024). One such plant, *Withania somnifera* (L.) Dunal—commonly referred to as Ashwagandha—has longstanding importance in traditional medicinal systems including Ayurveda, Siddha, and Unani (Singh et al., 2011). The pharmacological properties of Ashwagandha, particularly its adaptogenic and anti-inflammatory effects, are largely attributed to a class of compounds known as withanolides (Mirjalili et al., 2009).

In addition to its medicinal attributes, emerging studies indicate that *W. somnifera* can withstand and accumulate heavy metals in contaminated soils, rendering it a potential phytoremediation agent (Maharia et al., 2010; Garg, 2014). Its deep-rooted growth habit and tolerance to harsh soil conditions enable it to grow in polluted environments unsuitable for food crops, thereby offering a dual benefit of land remediation and non-competitive resource use (Jangleppanavar, 2010). However, this also necessitates scrutiny regarding the safety of herbal

products derived from plants grown in polluted areas, warranting continuous monitoring of metal levels in harvested plant materials (Maharia et al., 2010).

This review consolidates current scientific insights into the phytoremediation abilities of *W. somnifera,* exploring its mechanisms of metal uptake and stress tolerance, and discusses broader implications for sustainable environmental cleanup and safe medicinal usage. The paper integrates interdisciplinary viewpoints spanning environmental science, plant physiology, and pharmacology to highlight the holistic value of *W. somnifera* in ecological restoration and herbal medicine production.

**Cultivation Practices and Conservation Strategies**

The cultivation of *W. somnifera* plays a critical role in meeting the increasing global demand for its medicinal roots while ensuring sustainable utilisation and conservation of this valuable herbal resource. Native to the dry regions of India, the Middle East, and parts of Africa, *W. somnifera* is a hardy plant adapted to semi-arid climates (Morya, 2022). It thrives in sandy loam soils with neutral to slightly alkaline pH and moderate rainfall, making it suitable for low-input agriculture on degraded lands (Mulay et al., 2025). These traits support sustainable agricultural practices and rural livelihood development (Umadevi et al., 2012). It is typically cultivated during the Rabi season (October to March) with optimal temperatures ranging between 20°C to 35°C and annual rainfall between 500 to 750 mm (Singh et al., 2025).

Propagation is predominantly through seeds, which require pre-treatment like soaking or scarification to enhance germination rates that typically range from 60% to 75% (Richa et al., 2023). Seed propagation is standard, although germination rates are affected by soil type, moisture, and seed viability (Niyaz and Siddiqui, 2014). The crop requires moderate fertilisation, with nitrogen, phosphorus, and potassium applied according to soil fertility status, promoting root biomass and phytochemical content (Manohar et al., 2012). Weed management and pest control are

crucial during the early growth stages to reduce competition and maximise yield. Key pests include leaf miners and aphids, which can be managed using integrated pest management (IPM) techniques emphasising biological control agents (Meshram et al., 2015). Agronomic factors such as plant spacing, irrigation schedules, and nutrient inputs influence both biomass production and the synthesis of therapeutic withanolides (Ankad et al., 2020). Recent advancements in micropropagation have made it possible to propagate elite genotypes with consistent phytochemical profiles and improved yield potential (Singh et al., 2016).

Due to overharvesting from wild populations to meet market demand, *W. somnifera* faces threats of genetic erosion and habitat loss (Kumar et al., 2023). Conservation strategies therefore include in situ approaches like protecting natural habitats and ex situ methods such as seed banks, tissue culture, and micropropagation to preserve genetic diversity (Rajpurohit and Jhang, 2016). Biotechnological interventions like somaclonal variation and elicitation have also been explored to enhance withanolide production and reduce pressure on wild populations (Ahmad et al., 2024).

Sustainable harvesting and cultivation guidelines are essential to protect natural populations from depletion caused by land use change and climatic pressures (Zaman et al., 2025). Promoting cultivation among smallholder farmers through extension services and awareness programmes about sustainable harvesting and quality standards can ensure a steady supply of authentic raw material for herbal industries while conserving biodiversity (Rajeswara et al., 2012). Furthermore, certification schemes like Good Agricultural and Collection Practices (GACP) for medicinal plants are essential to maintain quality, traceability, and sustainable use of *W. somnifera*.

Integrating *W. somnifera* cultivation with conservation initiatives offers multiple benefits—from biodiversity protection and climate resilience to enhancing the supply chain for herbal

medicine. Continued research and policy support are vital for optimising cultivation practices and conserving valuable germplasm for future generations.

**Phytochemistry and Bioactive Compounds**

*W. somnifera* is rich in a diverse array of phytochemicals responsible for its pharmacological activities. The most notable class of compounds are withanolides, a group of steroidal lactones primarily concentrated in the roots, leaves, and berries (Mirjalili et al., 2009). These withanolides, such as withaferin A and withanolide D, exhibit anti-inflammatory, anticancer, neuroprotective, and immunomodulatory effects (Mishra et al., 2000).

In addition to withanolides, *W. somnifera* contains alkaloids, sitoindosides, flavonoids, and phenolic acids that contribute synergistically to its therapeutic potential (Bhattacharya et al., 2000). Alkaloids like somniferine and tropine have been reported to provide calming effects, aligning with the traditional use of *W. somnifera* as a nervine tonic. The presence of sitoindosides VII and VIII, glycosides of withanolides, further enhance antioxidative and adaptogenic properties (Singh et al., 2011).

Extraction methods significantly affect the yield and profile of bioactive compounds. Hydromethanolic and ethanol extracts are commonly used to obtain concentrated withanolides, with advances in supercritical fluid extraction improving purity and sustainability (Kulkarni and Dhir, 2008). Analytical techniques like high-performance liquid chromatography (HPLC), gas chromatography-mass spectrometry (GC-MS), and nuclear magnetic resonance (NMR) spectroscopy have been employed to characterise and quantify these compounds, facilitating standardisation (Kumar et al., 2018).

The concentration of bioactive compounds varies with factors such as plant age, part used, geographic location, and cultivation conditions (Tiwari et al., 2024). This variability underscores the need for stringent quality control and standardisation in herbal

preparations to ensure efficacy and safety (Srivastava and Misra, 2018). Overall, the rich phytochemical profile of *W. somnifera* forms the biochemical basis for its widespread use in traditional and modern herbal medicine.

**Pharmacological Activities and Therapeutic Potential**

*W. somnifera* has been extensively studied for its broad spectrum of pharmacological properties, which justify its traditional use in Ayurvedic medicine and growing acceptance in modern therapeutics. The major bioactive compounds, particularly withanolides, are responsible for its adaptogenic, anti-inflammatory, immunomodulatory, neuroprotective, anticancer, and cardioprotective effects (Choudhary et al., 2017).

Adaptogenic activity of *W. somnifera* helps the body resist physiological and psychological stress by regulating cortisol levels and enhancing stress tolerance (Della et al., 2023). Clinical studies have demonstrated its efficacy in reducing anxiety, depression, and improving sleep quality in both healthy individuals and patients with chronic stress disorders (Pratte et al., 2014). Its anti-inflammatory properties are attributed to inhibition of pro-inflammatory cytokines such as TNF-α and IL-6, which plays a vital role in managing chronic inflammatory diseases like arthritis (Kulkarni and Dhir, 2008).

In cancer research, *W. somnifera* extracts have shown promising cytotoxic effects against various cancer cell lines, including breast, lung, and prostate cancers, by inducing apoptosis and inhibiting metastasis (Sivasankarapillai, 2020). Additionally, the plant exhibits neuroprotective effects by enhancing antioxidant defenses and promoting regeneration of neuronal cells, making it a potential adjunct therapy for neurodegenerative diseases such as Alzheimer's and Parkinson's disease (Singh et al., 2017).

The immunomodulatory role of *W. somnifera* involves stimulation of both cellular and humoral immune responses, which improves resistance to infections and enhances overall immune health (Singha et al., 2024). Cardioprotective effects

have also been documented, including reduction of cholesterol levels and prevention of oxidative damage to heart tissues (Tiwari and Patel, 2012).

Despite these promising findings, more well-designed clinical trials are required to confirm efficacy and establish standardised dosages. Nonetheless, *W. somnifera* remains a cornerstone herb in integrative medicine, valued for its multi-targeted therapeutic potential and minimal adverse effects.

**Phytoremediation Potential and Mechanisms**

Phytoremediation refers to the use of plants to clean contaminated environments by absorbing, stabilising, or transforming harmful substances from soil, water, or air (Salt et al., 1998). *W. somnifera* has emerged as a compelling candidate in this context, thanks to its dual capacity for environmental tolerance and medicinal value.

The species' well-developed root architecture facilitates the uptake of heavy metals such as lead (Pb), cadmium (Cd), and arsenic (As), with partial translocation to aerial tissues (Garg, 2014). This process is mediated by environmental factors like soil pH, the bioavailability of metals, and intrinsic metabolic functions of the plant. To combat metal-induced stress, *W. somnifera* activates several detoxification strategies, including chelation by phytochelatins and compartmentalisation of metals into vacuoles (Clemens, 2006). Empirical findings reveal that the plant can accumulate substantial metal loads without exhibiting marked growth reduction, affirming its potential for both phytostabilisation and phytoextraction (Richa et al., 2023). Additionally, its withanolides and other secondary metabolites may contribute to oxidative stress mitigation by boosting antioxidant enzyme activity, including superoxide dismutase (SOD), catalase (CAT), and peroxidases (POD) (Mirjalili et al., 2009).

Nonetheless, the accumulation of hazardous elements in medicinally valuable tissues underscores the importance of

balancing environmental remediation with consumer safety. Rigorous research is required to refine cultivation techniques, establish safe harvesting protocols, and monitor contaminant levels in finished herbal products to protect public health (Pratte et al., 2014).

**Global Relevance and Market Potential**

*W. somnifera* has gained significant global attention due to its wide-ranging therapeutic properties, including adaptogenic, anti-inflammatory, antioxidant, and neuroprotective effects (Dipankar et al., 2025). India remains the largest producer and exporter of Ashwagandha, accounting for nearly 70% of global supply, with cultivation concentrated in states such as Madhya Pradesh, Rajasthan, and Gujarat (Singh et al., 2025). The increase in exports to regions like North America, Europe, and Asia-Pacific is propelled by growing awareness of Ashwagandha's health benefits, backed by clinical research and integration into complementary and alternative medicine systems (Ghosh, 2013). This surge is driven by increasing consumer preference for natural and holistic health supplements and the growing scientific validation of its pharmacological benefits.

The global market for *W. somnifera* is projected to expand at a compound annual growth rate (CAGR) exceeding 9% between 2023 and 2030, fuelled by rising awareness of stress management, cognitive health, and immune support (Soni et al., 2026). Commercial cultivation has extended beyond traditional regions to include countries such as the United States, Canada, and Australia, supported by improved cultivation protocols and standardisation practices to ensure consistent withanolide content (Singh et al., 2025). Regulatory approvals and certifications from international bodies like the US FDA and the European Medicines Agency have further facilitated market penetration.

However, challenges such as adulteration, lack of standardised quality control, and sustainability concerns persist. These issues necessitate strict quality assurance protocols,

including Good Agricultural and Collection Practices (GACP) and Good Manufacturing Practices (GMP), to safeguard consumer safety and maintain efficacy (Sharma et al., 2026). Additionally, sustainable sourcing is critical to prevent overharvesting from wild populations, which threatens genetic diversity and ecological balance (Shafi et al., 2021). The increasing trend towards sustainable sourcing and biodiversity conservation aligns with global environmental goals, encouraging the cultivation of *W. somnifera* through eco-friendly practices and community-based models. The integration of Ashwagandha into modern functional foods, beverages, and personalised medicine platforms represents a future growth avenue, emphasising its role not only as a traditional herbal remedy but also as a key component of the global herbal medicine industry. With continued research, cultivation improvement, and market regulation, its global relevance as a sustainable herbal resource is set to strengthen, offering economic opportunities for farmers and health benefits for consumers.

**Challenges and Future Perspectives**

Despite the growing global recognition and expanding applications of *W. somnifera*, several challenges impede its full potential in sustainable herbal medicine and commercial utilisation. One major concern is the inconsistency in phytochemical profiles across different geographic regions, cultivars, and cultivation conditions, which affects the quality, efficacy, and safety of Ashwagandha products (Sharma et al., 2026). Standardisation of raw materials and finished products remains a critical issue, requiring rigorous quality control measures and adoption of internationally accepted pharmacopeial standards.

Another challenge is the overexploitation of wild populations, leading to genetic erosion and threats to biodiversity. Conservation efforts are still inadequate in many regions, and sustainable harvesting practices need to be promoted alongside large-scale cultivation. Moreover, adulteration and substitution

with inferior species or plant parts pose serious risks to consumer health and industry credibility (Rajeswara, 2015).

Research gaps also exist in fully elucidating the mechanisms of action of bioactive compounds, optimal dosage regimens, and long-term safety profiles, necessitating more comprehensive clinical trials and pharmacokinetic studies (Choudhary et al., 2017). Advances in biotechnology, such as genetic engineering and metabolic pathway manipulation, offer promising tools for enhancing withanolide content and ensuring sustainable production but require further exploration and regulatory approval.

Future perspectives emphasise integrating traditional knowledge with modern scientific approaches to develop novel formulations, improve bioavailability, and personalise Ashwagandha-based therapies (Patwardhan, 2026). Digital agriculture and precision farming could enhance cultivation efficiency and traceability, while collaborations between academia, industry, and policymakers are essential for establishing robust supply chains and regulatory frameworks.

Addressing these challenges through multidisciplinary efforts will unlock the full therapeutic and economic potential of *W. somnifera* while safeguarding its conservation, thus reinforcing its role in sustainable herbal medicine globally.

## Conclusion

*W. somnifera* has emerged as a highly valued medicinal plant with a rich history in traditional Ayurvedic and other indigenous medical systems. Its wide spectrum of pharmacological activities—ranging from adaptogenic, anti-inflammatory, neuroprotective to immunomodulatory effects—has been increasingly supported by rigorous scientific research in recent decades. This convergence of traditional knowledge with modern science has propelled Ashwagandha to the forefront of global herbal medicine markets and natural health product industries.

The sustainable cultivation of *W. somnifera* is critical to meet the ever-increasing global demand while preserving wild genetic resources and biodiversity. Adoption of Good Agricultural and Collection Practices (GACP), alongside biotechnological interventions, can enhance the yield and consistency of valuable bioactive compounds such as withanolides. Furthermore, conservation strategies must prioritise in situ and ex situ approaches to prevent genetic erosion and habitat loss, which threaten the long-term availability of this vital resource.

Despite its promise, the Ashwagandha industry faces several challenges, including variability in phytochemical composition, adulteration issues, and a lack of uniform regulatory standards internationally. These challenges necessitate stringent quality control protocols, comprehensive phytochemical profiling, and adherence to regulatory guidelines to ensure product safety, efficacy, and consumer confidence.

In addition, gaps remain in clinical evidence regarding optimal dosing, mechanisms of action, and potential drug interactions, underscoring the need for well-designed clinical trials and pharmacological studies. Emerging technologies such as metabolomics, genomics, and nanotechnology hold promise for advancing product development, enhancing bioavailability, and tailoring personalised herbal therapies.

Looking forward, integrated efforts involving researchers, cultivators, industry stakeholders, and policymakers are essential to promote sustainable production, ensure equitable benefit sharing, and harness *W. somnifera's* full potential as a globally relevant herbal medicine. By balancing commercial expansion with ecological stewardship and scientific validation, Ashwagandha can continue to serve as a model for sustainable and effective herbal therapeutics in the 21st century and beyond.

**References**

Ahmad, Z., Shareen, Ganie, I. B., Firdaus, F., Ramakrishnan, M., Shahzad, A., & Ding, Y. (2024). Enhancing withanolide

production in the *Withania species:* advances in in vitro culture and synthetic biology approaches. *Plants,* 13(15), 2171.

Ali, H., Khan, E., & Ilahi, I. (2019). Environmental chemistry and ecotoxicology of hazardous heavy metals: environmental persistence, toxicity, and bioaccumulation. *Journal of chemistry,* 2019(1), 6730305.

Ankad, G. M., Pai, S. R., Hiremath, J., & Hegde, H. V. (2020). Traditional Horticulture Practices Increase the Production of Selected Withanolides in *Withania somnifera* (L.) Dunal—A RP-UFLC Analysis. *Journal of Chromatographic Science,* 58(10), 899-906.

Bhattacharya, S. K., Bhattacharya, A., Sairam, K., & Ghosal, S. (2000). Anxiolytic-antidepressant activity of *Withania somnifera* glycowithanolides: An experimental study. *Phytomedicine,* 7(6), 463-469.

Choudhary, D., Bhattacharyya, S., & Bose, S. (2017). Efficacy and safety of Ashwagandha *(Withania somnifera)* root extract in improving memory and cognitive functions. *Journal of Dietary Supplements,* 14(6), 599-612.

Clemens, S. (2006). Toxic metal accumulation, responses to exposure and mechanisms of tolerance in plants. *Biochimie,* 88(11), 1707–1719.

de Vries, W., Groenenberg, J. E., Lofts, S., Tipping, E., & Posch, M. (2012). Critical loads of heavy metals for soils. *In Heavy metals in soils: trace metals and metalloids in soils and their bioavailability* (pp. 211-237). Dordrecht: Springer Netherlands.

Della Porta, M., Maier, J. A., & Cazzola, R. (2023). Effects of *Withania somnifera* on cortisol levels in stressed human subjects: a systematic review. *Nutrients,* 15(24), 5015.

Dipankar, S. P., Dani, M. M., Anirudhan, R., Tripathi, D., Mishra, C., Devi, S. H., & Dani Sr, M. M. (2025). Pharmacological insights into ashwagandha *(Withania somnifera):* a review

of its immunomodulatory and neuroprotective properties. *Cureus,* 17(8), e89856.

Dushenkov, V., Kumar, P. N., Motto, H., & Raskin, I. (1995). Rhizofiltration: the use of plants to remove heavy metals from aqueous streams. *Environmental Science & Technology,* 29(5), 1239-1245.

Garg, M. (2014). Screening of Indian Withania plant and marketed products for trace elements, heavy metals for quality and efficacy. *Journal of Pharmacognosy and Phytochemistry,* 2(5), 66-68.

Ghosh, S. P. (2013). Promotion of medicinal and aromatic plants in the Asia-Pacific region. Expert Consultation on Promotion of Medicinal and Aromatic Plants in the Asia-Pacific Region: Proceedings, 33.

Jangleppanavar, R. F. (2010). Studies on Seed Dormancy and Invigouration in Ashwagandha *(Withania somnifera)* (Doctoral Dissertation, University Of Agricultural Sciences, Dharwad).

Kulkarni, S. K., & Dhir, A. (2008). *Withania somnifera:* An Indian ginseng. *Progress in Neuro-Psychopharmacology & Biological Psychiatry,* 32(5), 1093-1105.

Kumar, A., Husain, D., Lal, R. K., Singh, S., Singh, V., & Gupta, A. K. (2023). Genetic diversity and future prospects in *Withania somnifera* (L.) Dunal: an assessment based on quantitative traits in different accessions of Ashwagandha. *The Nucleus,* 66(2), 151-159.

Kumar, S., Singh, R., Gajbhiye, N., & Dhanani, T. (2018). Extraction Optimization for Phenolic-and Withanolide-rich fractions from *Withania somnifera* roots: identification and quantification of Withaferin A, 12-deoxywithastromonolide, and withanolide a in plant materials and marketed formulations using a reversed-phase HPLC–photodiode array detection method. *Journal of Aoac International,* 101(6), 1773-1780.

Maharia, R. S., Dutta, R. K., Acharya, R., & Reddy, A. V. R. (2010). Heavy metal bioaccumulation in selected medicinal plants collected from Khetri copper mines and comparison with those collected from fertile soil in Haridwar, India. *Journal of Environmental Science and Health,* 45(2), 174-181.

Manohar, S., Choudhary, M. R., Yadav, B. L., Dadheech, S., & Singh, S. P. (2012). Analyzing the efficacy of organic and inorganic sources of nitrogen and phosphorus on growth of ashwagandha (*Withania somnifera* Dunal.). *Journal of Horticultural Sciences,* 7(2), 161-165.

Meshram, P. B., Mawai, S., & Malviya, R. (2015). Biological control of insect pests of medicinal plants: *Abelmoschus moschatus, Gloriosa superba* and *Withania somnifera* in forest nursery and plantation in Madhya Pradesh, India. *American Journal of Agriculture and Forestry,* 3(2), 47-53.

Mirjalili, M. H., Moyano, E., Bonfill, M., Cusido, R. M., & Palazón, J. (2009). Steroidal lactones from *Withania somnifera*, an ancient plant for novel medicine. *Molecules,* 14(7), 2373-2393.

Mishra, L. C., Singh, B. B., & Dagenais, S. (2000). Scientific basis for the therapeutic use of *Withania somnifera* (Ashwagandha): A review. *Alternative Medicine Review,* 5(4), 334-346.

Morya, K. (2022). Effect of Different Nutrient Management Practices on Growth, Yield, Quality and Economics of Ashwagandha (*Withania somnifera* L.). *The Pharma Innovation Journal,* 11(12), 318–320.

Mulay, V., Nandikar, M., Surwade, P., Karmakar, M., Saste, G., & Hingorani, L. (2025). Ashwagandha: An Overview of Cultivation, Propagation, Extraction, and its Phytochemistry. *Ashwagandha,* 33-47.

Niyaz, A., & Siddiqui, E. N. (2014). Seed germination of *Withania somnifera* (L.) Dunal. *European Journal of Medicinal Plants,* 4(8), 920.

Patwardhan, B. (2026). Ashwagandha: A Promising Immunomodulatory Therapeutic Drug. In *Ashwagandha* (pp. 137-143). CRC Press.

Pratte, M. A., Nanavati, K. B., Young, V., & Morley, C. P. (2014). An alternative treatment for anxiety: a systematic review of human trial results reported for the Ayurvedic herb ashwagandha *(Withania somnifera). The Journal of Alternative and Complementary Medicine: Paradigm, Practice, and Policy Advancing Integrative Health,* 20(12), 901-908.

Rajeswara Rao, B. R. (2015). Genetic diversity, genetic erosion, conservation of genetic resources, and cultivation of medicinal plants. *In Genetic diversity and erosion in plants: case histories* (pp. 357-407). Cham: Springer International Publishing.

Rajeswara Rao, B. R., Rajput, D. K., Nagaraju, G., & Adinarayana, G. (2012). Opportunities and challenges in the cultivation of Ashwagandha {*Withania somnifera* (L.) Dunal}. *Journal of Pharmacognosy,* 3, 88-91.

Rajpurohit, D., & Jhang, T. (2016). In situ and ex situ conservation of plant genetic resources and traditional knowledge. *In Plant genetic resources and traditional knowledge for food security* (pp. 137-162). Singapore: Springer Singapore.

Richa, P. S., Parveen, Z., & Pandey, N. (2023). Study on phytoremediation potential of *Withania somnifera* grown in soil contaminated with tannery effluent. *International Journal of Advanced Scientific Research,* 8(1), 44-50

Salt, D. E., Smith, R. D., & Raskin, I. (1998). Phytoremediation. *Annual Review of Plant Biology,* 49(1), 643-668.

Shafi, A., Hassan, F., Zahoor, I., Majeed, U., & Khanday, F. A. (2021). Biodiversity, management and sustainable use of medicinal and aromatic plant resources. *In Medicinal and aromatic plants: Healthcare and industrial applications* (pp. 85-111). Cham: Springer International Publishing.

Sharma, S., Naman, S., Kaur, R., Dwivedi, J., Ashawat, M. S., Chandan, A., ... & Baldi, A. (2026). Quality Cultivation and Standardization of *Withania somnifera*: Comprehensive Agro-Practices and Regulatory Approach. *Pharmacognosy Research,* 18(2):555-567.

Singh, A., Singh, S., Kumar Singh, A., Shasany, P. K., & Verma, R. K. (2025). Influence of environmental conditions on yield and quality of different cultivars of Ashwagandha (*Withania somnifera* (L.) Dunal). *Natural Product Research,* 1-6.

Singh, H. P., Choudhri, D. K., Sharma, R. S., & Kumar, S. (2025). Comprehensive Analysis of Economics, Marketing, and Trade Performance of Ashwagandha: Indian Prospective. *Plant Archives,* 25(1), 2838-2845.

Singh, N., Bhalla, M., de Jager, P., & Gilca, M. (2011). An overview on ashwagandha: a Rasayana (rejuvenator) of Ayurveda. *African Journal of Traditional, Complementary, and Alternative Medicines,* 8(5 Suppl), 208.

Singh, P., Guleri, R., & Pati, P. K. (2016). In vitro propagation of *Withania somnifera* (L.) Dunal. *In Protocols for In Vitro Cultures and Secondary Metabolite Analysis of Aromatic and Medicinal Plants, Second Edition* (pp. 201-213). New York, NY: Springer New York.

Singh, V., Shah, H. H., & Guillemin, G. J. (2017). Neuroprotective effect of Ashwagandha (roots of *Withania somnifera*): the rejuvenator. *The Canadian Journal of Clinical Nutrition,* 5(2), 34-51.

Singha, P. S., Ghosh, R., & Ghosh, D. (2024). Immunomodulatory phytocompounds from *Withania somnifera* (L.Dunal (Ashwagandha) against COVID-19. *Trends in Immuno-therapy,* 8(1), 2703.

Sivasankarapillai, V. S., Madhu Kumar Nair, R., Rahdar, A., Bungau, S., Zaha, D. C., Aleya, L., & Tit, D. M. (2020). Overview of the anticancer activity of withaferin A, an active constituent of the Indian ginseng *Withania somnifera*.

*Environmental Science and Pollution Research,* 27(21), 26025-26035.

Soni, S., Rathee, S., Tekade, M., Bharti, A., Gupta, R., & Tekade, R. K. (2026). Translational Case Studies on Marketed Phytomedicines: From Traditional Knowledge to Global Therapeutics. *In Biomolecular and Safety Considerations of Phytopharmaceuticals* (pp. 387-407). CRC Press.

Srivastava, S., & Misra, A. (2018). Quality control of herbal drugs: Advancements and challenges. *In New age herbals: resource, quality and pharmacognosy* (pp. 189-209). Singapore: Springer Singapore.

Tiwari, P., & Patel, R. K. (2012). Cardioprotective activity of Ashwagandharishta on Isoproterenol Induced Myocardial Infarction. *Research Journal of Pharmacology and Pharmacodynamics,* 4(5), 294–298.

Tiwari, S., Shukla, P. K., Chauhan, D., & Khatoon, S. (2024). Variability study of active metabolites and identification of elite chemotype of *Withania somnifera* (L.) Dunal collected from Central India. *Journal of Planar Chromatography–Modern TLC,* 37(2), 189-198.

Umadevi, M., Rajeswari, R., Rahale, C. S., Selvavenkadesh, S., Pushpa, R., Kumar, K. S., & Bhowmik, D. (2012). Traditional and medicinal uses of *Withania somnifera*. *The Pharma Innovation,* 1(9, Part A), 102.

Yadav, P., Ansari, M. W., Saini, S., Punia, S., Kaula, B. C., Rani, V., ... & Tuteja, N. (2024). Review and future prospects on the impact of abiotic stresses and tolerance strategies in medicinal and aromatic plants. *Brazilian Journal of Botany,* 47(3), 683-701.

Zaman, W., Ayaz, A., & Park, S. (2025). Climate change and medicinal plant biodiversity: conservation strategies for sustainable use and genetic resource preservation. *Genetic Resources and Crop Evolution,* 72(6), 6275-6308.

# Felled Trees and Silenced Voices: An Ecofeminist Reading of Anton Chekhov's *The Cherry Orchard*

**[1]Remi Cherian George**

[1]Associate Professor, Department of English, Mar Thoma College, Tiruvalla, Kerala, India. E-mail: remi1510@gmail.com

**Abstract:** Anton Chekhov's *The Cherry Orchard* offers a valuable text for ecofeminist interpretation. The play, centred on the sale of a once-glorious estate and its symbolic orchard, reflects a period of social transition in Russia as aristocratic authority gives way to capitalist structures. Through an ecofeminist lens, the orchard can be read as a representation of nature subjected to economic exploitation, while the experiences of characters such as Lyubov Ranevsky reveal the limited agency of women within patriarchal society. The narrative, therefore, exposes the interconnected marginalisation of women and the natural world. This study argues that Chekhov's drama reveals how gender hierarchy, class transformation, and environmental loss operate within the same structures of power.

**Keywords:** Ecofeminism; gender; patriarchy; environment; capitalism.

Anton Chekhov's *The Cherry Orchard* provides a significant literary space for examining the complex relationship between gender, environmental consciousness, and social transformation. Ecofeminist literary criticism explores how the domination of women and the exploitation of nature often emerge from the same patriarchal structures of power. Within such systems, both women and the natural environment are frequently treated as passive entities that can be controlled, owned, or commodified. When Chekhov's play is interpreted through this ecofeminist framework, it reveals important insights into the intersection of gender hierarchy, environmental degradation, and economic change. Although the drama is commonly read as a representation of the decline of the Russian aristocracy and the rise of capitalist modernity, it also offers a powerful reflection on humanity's

relationship with nature. The threatened destruction of the cherry orchard symbolizes not only the collapse of an aristocratic lifestyle but also the transformation of the natural world into a commodity within a rapidly changing economic system.

From an ecofeminist standpoint, the orchard can also be interpreted as a representation of the natural world that exists beyond human economic calculations. Its seasonal blossoming reflects cycles of renewal that operate independently of social structures. However, within the logic of capitalist modernisation, these ecological rhythms are ignored in favour of financial efficiency. The decision to cut down the orchard, therefore, represents a larger cultural shift in which nature is valued only for its economic productivity. Ecofeminist critics argue that such attitudes reveal how patriarchal systems frequently reduce both women and the natural environment to objects of utility.

Written at the beginning of the twentieth century and first performed in 1904, *The Cherry Orchard* portrays a society undergoing dramatic social and economic transformation. Russia during this period witnessed the gradual decline of the feudal aristocratic order and the emergence of new capitalist structures that redefined wealth, labour, and property. The play focuses on the Ranevsky family, members of the once-privileged aristocracy whose estate is burdened by debt and faces imminent sale. The estate's cherry orchard functions as a central symbol throughout the narrative. On one level, it represents inherited wealth and social prestige, reflecting the long history of aristocratic landownership in Russia. On another level, however, it embodies cultural memory and emotional attachment to the land. The orchard links the characters to their past, serving as a reminder of childhood experiences, family traditions, and the stability of a social order that is now disappearing.

Lyubov Ranevskaya, the owner of the estate, emerges as the emotional centre of the play. Her return to the property after several years abroad confronts her with the painful possibility that

the orchard, which shaped her identity and memories, may soon vanish. Her attachment to the orchard reveals how landscapes can carry deep personal and cultural significance. When she recalls her childhood experiences connected to the orchard, she expresses a sense of nostalgia that reflects the human tendency to associate nature with memory and belonging. Yet despite her emotional connection to the land, she remains unable to prevent its loss. Her financial mismanagement and inability to adapt to the economic realities of modern Russia illustrate the vulnerability of individuals who remain attached to a fading social system.

The emotional language used by Ranevskaya when speaking about the orchard also reflects the symbolic connection between women and the natural world that ecofeminist scholars frequently examine. In many literary traditions, landscapes are associated with fertility, nurturing, and continuity—qualities historically attributed to femininity. While such associations can reinforce stereotypes, they also highlight how women's identities have been culturally linked to nature. In Chekhov's play, Ranevskaya's attachment to the orchard represents an attempt to preserve these emotional and cultural connections at a moment when modern economic forces threaten to erase them.

Ecofeminist theory provides a useful lens through which these developments can be understood. Val Plumwood argues that Western philosophical traditions have historically structured social thought through hierarchical dualisms such as man and woman, culture and nature, and reason and emotion (Plumwood, 1993). Within these conceptual hierarchies, men and culture are associated with power and rationality, while women and nature are linked with passivity and emotionality. These assumptions create ideological structures that justify the domination of both women and the natural environment. Ecofeminism challenges these hierarchies by emphasising the interconnectedness of ecological systems and human societies. Rather than viewing nature as a passive resource to be exploited, ecofeminist thinkers

encourage a holistic perspective that recognises the intrinsic value of nonhuman life and the ethical responsibility humans have toward ecological systems.

The fate of the cherry orchard in Chekhov's play reflects the consequences of the hierarchical worldview that ecofeminism critiques. The orchard initially appears as a landscape of beauty and natural vitality, admired by multiple characters. Its blossoms symbolise renewal, continuity, and the cyclical rhythms of nature. Yet as the narrative progresses, the orchard is increasingly defined in economic terms. Instead of being appreciated for its ecological or cultural value, it becomes an asset whose worth lies in its potential for commercial development. This transformation reflects the broader economic shift occurring in Russian society during the period in which the play is set.

The character Lopakhin represents this emerging capitalist mentality. As the son of former serfs who has risen to financial success through business, Lopakhin embodies the new social mobility made possible by capitalist development. Unlike the aristocratic characters, who view the orchard primarily as a symbol of heritage, Lopakhin approaches the land from a pragmatic economic perspective. His solution to the family's financial crisis is to cut down the orchard and divide the property into plots for summer cottages. This proposal illustrates how capitalist logic converts natural landscapes into commodities. From Lopakhin's perspective, the orchard's beauty and historical significance are irrelevant if the land can generate greater profit through development.

Ecofeminist scholars have often criticised economic systems that prioritise growth and profit at the expense of environmental sustainability. Alicia Puleo argues that modern capitalist development encourages competition, material accumulation, and the relentless exploitation of natural resources (Puleo, 2017). Within such systems, ecological concerns are frequently ignored in favour of economic expansion. Chekhov's

portrayal of Lopakhin's proposal reflects this critique. Although his plan appears practical and financially beneficial, it results in the destruction of a landscape that holds immense cultural and emotional value.

The gender dynamics within the play further reinforce ecofeminist interpretations. Despite being the legal owner of the estate, Ranevskaya lacks the authority to protect it. Her position illustrates how women in patriarchal societies may possess symbolic responsibility while lacking real decision-making power. Other female characters in the play experience similar limitations. Varya, who manages the household, performs significant labour but holds little social authority. Anya, the younger generation, expresses hope for change but remains uncertain about her future within the emerging social order.

Karen Warren argues that patriarchal conceptual frameworks link the domination of women with the domination of nature (Warren, 2000). According to Warren, these systems operate through hierarchical thinking that associates women and nature with inferiority and dependence. In Chekhov's play, Ranevskaya's inability to prevent the destruction of the orchard mirrors the broader marginalisation of women within patriarchal economic structures. Although she deeply values the land and recognises its cultural significance, she lacks the power to influence its fate.

The orchard itself functions as a powerful symbol of cultural identity and historical continuity. For the Ranevsky family, it represents a living connection to the past. Landscapes often serve as repositories of memory, linking individuals to their cultural heritage and communal identity. Vandana Shiva argues that modern development frequently disrupts these traditional relationships between communities and the natural world by transforming ecosystems into economic resources (Shiva, 1988). When this transformation occurs, the cultural meanings associated with natural landscapes are often erased. The destruction of the orchard in Chekhov's play therefore signifies both ecological loss and the disappearance of a cultural way of life.

The play also reveals how social class influences attitudes toward the environment. Aristocratic characters often appear detached from the practical realities of agricultural labour. Their relationship with the land is shaped primarily by inheritance and status rather than by direct interaction with nature. This distance from the land's physical realities also demonstrates how social privilege can weaken ecological awareness. Aristocratic characters inherit ownership of the estate without directly engaging in the labour that sustains it. Their detachment from agricultural life contributes to their inability to recognise the environmental consequences of their decisions. Ecofeminist scholars often argue that meaningful ecological responsibility requires a closer relationship between communities and their environments. When this relationship is disrupted by systems of hierarchy and property ownership, environmental exploitation becomes easier to justify. In contrast, peasants and workers possess a closer relationship with the natural environment because their livelihoods depend upon it. Yet despite this ecological familiarity, they lack the political and economic authority to determine the fate of the land. Maria Mies and Vandana Shiva argue that capitalist systems frequently marginalize communities that possess the deepest ecological knowledge (Mies & Shiva, 1993). In *The Cherry Orchard,* decisions about the orchard's future are made not by those who understand the land but by those who control financial resources.

This imbalance of power also reflects broader patterns of environmental injustice. Communities that maintain intimate relationships with local ecosystems often lack the political authority to protect those environments from exploitation. In *The Cherry Orchard,* the voices of workers and servants rarely influence the final outcome of events, even though they possess practical knowledge of the land. The destruction of the orchard, therefore, illustrates how economic power can silence perspectives that prioritise ecological sustainability.

Ecofeminist literary criticism seeks to uncover how literary narratives reflect systems of domination that affect both human and

nonhuman worlds. Greta Gaard argues that literature can reveal the cultural assumptions that permit environmental exploitation and social inequality (Gaard, 1993). Chekhov's portrayal of the orchard's destruction also invites reflection on the cultural meaning of loss. The sound of axes cutting down the trees at the end of the play functions as a powerful auditory symbol of irreversible change. This moment emphasises the emotional consequences of environmental destruction. The loss of the orchard is not merely a financial transaction but a rupture in the relationship between human memory and the natural landscape. Ecofeminist critics often emphasise that environmental degradation involves cultural and psychological loss as well as ecological damage. Chekhov's play illustrates these assumptions by showing how economic modernisation gradually erodes the emotional and cultural relationships that connect individuals to the land.

Carol Adams similarly observes that cultural narratives often normalise exploitation by portraying nature as an object to be controlled, consumed, or commodified (Adams, 2015). The destruction of the orchard reflects this process of objectification. Once the land is redefined in economic terms, its ecological and cultural significance becomes secondary to its market value.

When viewed from an ecofeminist perspective, *The Cherry Orchard* therefore becomes more than a historical drama about the decline of aristocratic privilege. It emerges as a reflection on the fragile relationship between human societies and the natural environment. The play reveals how systems of economic and patriarchal power shape attitudes toward both women and nature. Through the symbolic destruction of the orchard, Chekhov exposes the cultural values that permit environmental degradation in the pursuit of economic progress. In this sense, *The Cherry Orchard* anticipates many contemporary debates about sustainable development and environmental responsibility. Modern societies continue to confront the challenge of balancing economic growth with ecological preservation. Chekhov's play reminds readers that decisions about land and resources are never

purely economic; they are also ethical and cultural choices that shape the future of communities and ecosystems. By highlighting the interconnected fate of women, nature, and social power, the play encourages a reconsideration of the values that guide human relationships with the environment.

Ultimately, an ecofeminist reading highlights the interconnected nature of gender inequality, environmental exploitation, and social transformation. The play suggests that societies structured around hierarchical systems of power often disregard ecological sustainability and social justice. By portraying the destruction of the orchard alongside the decline of the aristocratic family, Chekhov invites readers to reflect on the broader consequences of modernisation. The continuing relevance of *The Cherry Orchard* lies in its ability to illuminate the tensions between tradition and progress, cultural identity and economic development, and human ambition and environmental responsibility.

**References**

Adams, C. J. (2015). *The Sexual Politics of Meat: A Feminist-Vegetarian Critical Theory* (25th Anniversary ed.). Bloomsbury Academic.

Apte, N. H., & Drumi, S. (2016). Analysing Elaine Showalter's Essay "Towards a Feminist Poetics." *International Journal of English Language, Literature and Humanities,* 4(6), 89–96.

Chekhov, A. (1904). *The Cherry Orchard* (J. Hingley, Trans.). Oxford University Press.

Gaard, G. (1993). *Ecofeminism: Women, Animals, Nature*. Temple University Press.

Mies, M., & Shiva, V. (1993). *Ecofeminism*. Zed Books.

Plumwood, V. (1993). *Feminism and the Mastery of Nature*. Routledge.

Puleo, A. H. (2017). What is Ecofeminism? *Quaderns de la Mediterrània,* 26, 27–33.

Sharnappa, P. S. (2018). Reconstructing Ecofeminism: A Study of Kamala Markandaya's Nectar in a Sieve. *International Journal of English Language, Literature and Humanities,* 6(5), 1–10.

Warren, K. J. (2000). *Ecofeminist Philosophy: A Western Perspective on What it is and Why it Matters*. Rowman & Littlefield.